NASA CR-120980
BAC Report No. 8654-953003

FINAL REPORT

NONDESTRUCTIVE TESTS OF REGENERATIVE CHAMBERS

By

G. A. MALONE
R. STAUFFIS
R. WOOD

Prepared For

NATIONAL AERONAUTICS AND SPACE ADMINISTRATION

JULY 1972

CONTRACT NAS 3-14376

Bell Aerospace Company DIVISION OF textron

POST OFFICE BOX ONE • BUFFALO, NEW YORK 14240

NOTICE

This report was prepared as an account of Government-sponsored work. Neither the Unites States, nor the National Aeronautics and Space Administration (NASA), nor any person acting on behalf of NASA:

A.) Makes any warranty or representation, expressed or implied, with respect to the accuracy, completeness, or usefulness of the information contained in this report, or that the use of any information, apparatus, method, or process disclosed in this report may not infringe privately-owned rights; or

B.) Assumes any liabilities with respect to the use of, or for damages resulting from the use of, any information, apparatus, method or process disclosed in this report.

As used above, "person acting on behalf of NASA" includes any employee or contractor of NASA, or employee of such contractor, to the extent that such employee or contractor of NASA or employee of such contractor prepares, disseminates, or provides access to any information pursuant to his employment or contract with NASA, or his employment with such contractor.

1. Report No.	2. Government Accession No.	3. Recipient's Catalog No.
NASA CR-120980		

4. Title and Subtitle	5. Report Date
NONDESTRUCTIVE TESTS OF REGENERATIVE CHAMBERS	July 1972
	6. Performing Organization Code

7. Author(s)	8. Performing Organization Report No.
G. A. Malone, R. Stauffis and R. Wood	BAC 8654-953003
	10. Work Unit No.

9. Performing Organization Name and Address	11. Contract or Grant No.
Bell Aerospace Company Division of Textron P.O. Box 1 Buffalo, New York 14240	NAS 3-14376
	13. Type of Report and Period Covered
12. Sponsoring Agency Name and Address	Contractor Report
National Aeronautics and Space Administration Washington, D. C. 20546	14. Sponsoring Agency Code

15. Supplementary Notes

Project Manager, Rudolph A. Duscha, Chemical and Nuclear Rocket Procurement Section,
NASA Lewis Research Center, Cleveland Ohio

16. Abstract

Flat test panels simulating internally cooled regenerative thrust chamber walls were fabricated by electroforming, brazing and diffusion bonding to evaluate the feasibility of nondestructive evaluation techniques to detect bonds of various strength integrities. Ultrasonics, holography, and acoustic emission were investigated and found to yield useful and informative data regarding the presence of bond defects in these structures.

17. Key Words (Suggested by Author(s))	18. Distribution Statement
Nondestructive tests Regenerative chambers Metal bond integrity	Unclassified - Unlimited

19. Security Classif. (of this report)	20. Security Classif. (of this page)	21. No. of Pages	22. Price*
Unclassified	Unclassified	202	$3.75 ~~$3.00~~

* For sale by the National Technical Information Service, Springfield, Virginia 22151

I

NASA CR-120980
BAC Report No. 8654-953003

FINAL REPORT

NONDESTRUCTIVE TESTS OF REGENERATIVE CHAMBERS

By

G. A. Malone
R. Stauffis
R. Wood

Prepared for

National Aeronautics and Space Administration

July 1972

Technical Management
NASA, Lewis Research Center
Cleveland, Ohio

Chemical Propulsion Division

Rudolph A. Duscha

Bell Aerospace Company
P. O. Box 1
Buffalo, New York 14240

FOREWORD

The work reported herein was performed for NASA/LeRC under Contract NAS 3-14376 titled "Nondestructive Tests of Regenerative Chambers." Mr. R. A. Duscha was the NASA/LeRC project manager.

The authors wish to acknowledge important contributions to this report by several individuals. These include the treatment of brazing and diffusion bonding by F. Pruett, electroforming assistance by J. Nowak, nondestructive evaluation assistance by L. Vecchies, and metallographic analysis by C. Wright.

Mr. G. A. Malone, co-author of this report, was Program Manager. Messers, R. Stauffis and R. Woods were responsible for the nondestructive evaluation work conducted.

(c

ABSTRACT

Flat test panels simulating internally cooled regenerative thrust chamber walls were fabricated by electroforming, brazing, and diffusion bonding to evaluate the feasibility of nondestructive evaluation techniques to detect bonds of various strength integrities. Ultrasonics, holography, and acoustic emission were investigated and found to yield useful and informative data regarding the presence of bond defects in these structures.

CONTENTS

ILLUSTRATIONS

ILLUSTRATIONS (CONTD)

ILLUSTRATIONS (CONTD)

TABLES

I. SUMMARY

Flat test panels were fabricated to contain nickel 200 baseplates with integral manifolding and coolant passages enclosed by means of bonded coverplates. The bonding methods used were electroforming, brazing, and diffusion bonding. Inconel 600 composed the coverplates in the latter two methods. Of the fifteen panels bonded by each method, three groups of panels were produced to contain planned bond integrities of full, weak, and nonbond. In addition, the effect of thermal diffusion after electroforming was investigated on separate specimens.

Bond strengths were verified by testing lap-shear specimens prior to fabrication of nondestructive evaluation test panels.

Potential nondestructive evaluation techniques were screened to determine those methods of greater promise in detecting bond defects in chamber wall bondlines. Ultrasonics, holography, acoustic emission, and spectrum analysis were ultimately selected. The bonded panels were subjected to these evaluation techniques and rated on ability to evaluate bond integrity. The identity of the test panels as to bond integrity was concealed by code numbering so that personnel performing the nondestructive evaluation would have no prior knowledge of planned bond patterns or types.

The test panels were later tested to verify achieved bond strength by destructive testing and metallographic analysis. Ultrasonics, holography, and acoustic emission were each useful in differentiating the various bond types. It was found that these evaluation techniques could be employed most advantageously to ascertain bond types when applied sequentially, rather than as completely independent methods.

II. INTRODUCTION

A conventional regeneratively cooled rocket thrust chamber is usually constructed by bonding a liner (inner wall) to a shell (outer wall) by means of electroforming the shell to the liner, brazing, or diffusion bonding. Integral coolant passages are introduced by milling or electric discharge machining the required configuration into the liner or shell material before bonding. In the case of electroforming, these passages may be introduced by a variation in which the channel lands are electroformed on the liner.

Fabrication of such devices is critical from a standpoint that detection of inferior bonds or leakage paths for the coolant must be detected as early as possible in the fabrication process. Otherwise, expensive and time consuming manifold joining, flow, proof, and hot fire testing will be uneconomically expended on a possibly defective piece of hardware.

Several nondestructive evaluation techniques appeared feasible for detecting these flaws or potential failure areas before completion of fabrication.

Since the hardware is capable of being pressurized, introduction of controlled hydrostatic stresses can be utilized to produce strains or finite bond movements possibly detectable by other less common nondestructive means such as holography or acoustic emission. Using this philosophy, the subject program was conducted to determine and demonstrate the usefulness of these nondestructive methods in evaluating the integrity of a metal to metal bond.

III. TEST PANEL FABRICATION

Flat test panels were fabricated containing Nickel 200 baseplates with integral cooling passages. Coverplates of electroformed nickel or Inconel 600 were bonded over these baseplates to enclose the cooling passages. Bond defect patterns were introduced on selected panels and full bonds applied to the remainder for subsequent evaluation nondestructively and destructively as discussed in this and later sections of the report.

A. TEST PANEL DESIGN AND BOND PATTERNS

The test panel design shown in Figure 1 was selected on the basis that the structure closely simulated production type regeneratively cooled chamber walls and provided sufficient bonding surfaces for variation of bond defect sizes and patterns. In this design, space was provided for location of pressure fittings and transducers, necessary in the performance of some tests, without interference with data acquisition.

Pressurization manifolds were included at each end of the panel to allow passage of fluids through the panel to assure passages were not completely blocked by inadvertent braze runout, to remove channel filler materials necessary in the electroform method of bonding, and to purge air from the passages during hydrostatic pressurization work.

Material thickness selection was based on mechanical properties of the materials of construction, the channel land width, and the ratio of channel width to land width. The coverplate and baseplate were both designed to a thickness of one-eighth inch, which corresponds to the land width. The channel width was purposely made twice that of the land in order to introduce peel, in addition to normal shear, as a mode of failure in final destructive testing. With this design, it was anticipated that thermally bonded panels with full bonds would fail in destructive test at approximately 6,000 psi pressure (41.37×10^6 N/m.^{2})

Table I lists the test panels to be fabricated by method of bonding and type of bond required (i.e. - full, weak, and nonbond). Each method of bonding, except the electroform-thermal diffusion combination, requires fifteen panels. Of these, five panels are of each bond type.

TABLE I
TEST PANELS TO BE FABRICATED

No. of Panels	Type of Fabrication	Type of Bond	Materials of Construction
5	Diffusion Bonding	Full	Inconel 600/Nickel 200
5	Diffusion Bonding	Controlled Nonbond	Inconel 600/Nickel 200
5	Diffusion Bonding	Controlled Weak Bond	Inconel 600/Nickel 200
5	Braze Bonding	Full	Inconel 600/Nickel 200
5	Braze Bonding	Controlled Nonbond	Inconel 600/Nickel 200
5	Braze Bonding	Controlled Weak Bond	Inconel 600/Nickel 200
5	Electroforming	Full	EF Nickel/Nickel 200
5	Electroforming	Controlled Nonbond	EF Nickel/Nickel 200
5	Electroforming	Controlled Weak Bond	EF Nickel/Nickel 200
2	Electroforming and Thermal Diffusion	Full	EF Nickel/Nickel 200
2	Electroforming and Thermal Diffusion	Controlled Nonbond	EF Nickel/Nickel 200
2	Electroforming and Thermal Diffusion	Controlled Weak Bond	EF Nickel/Nickel 200

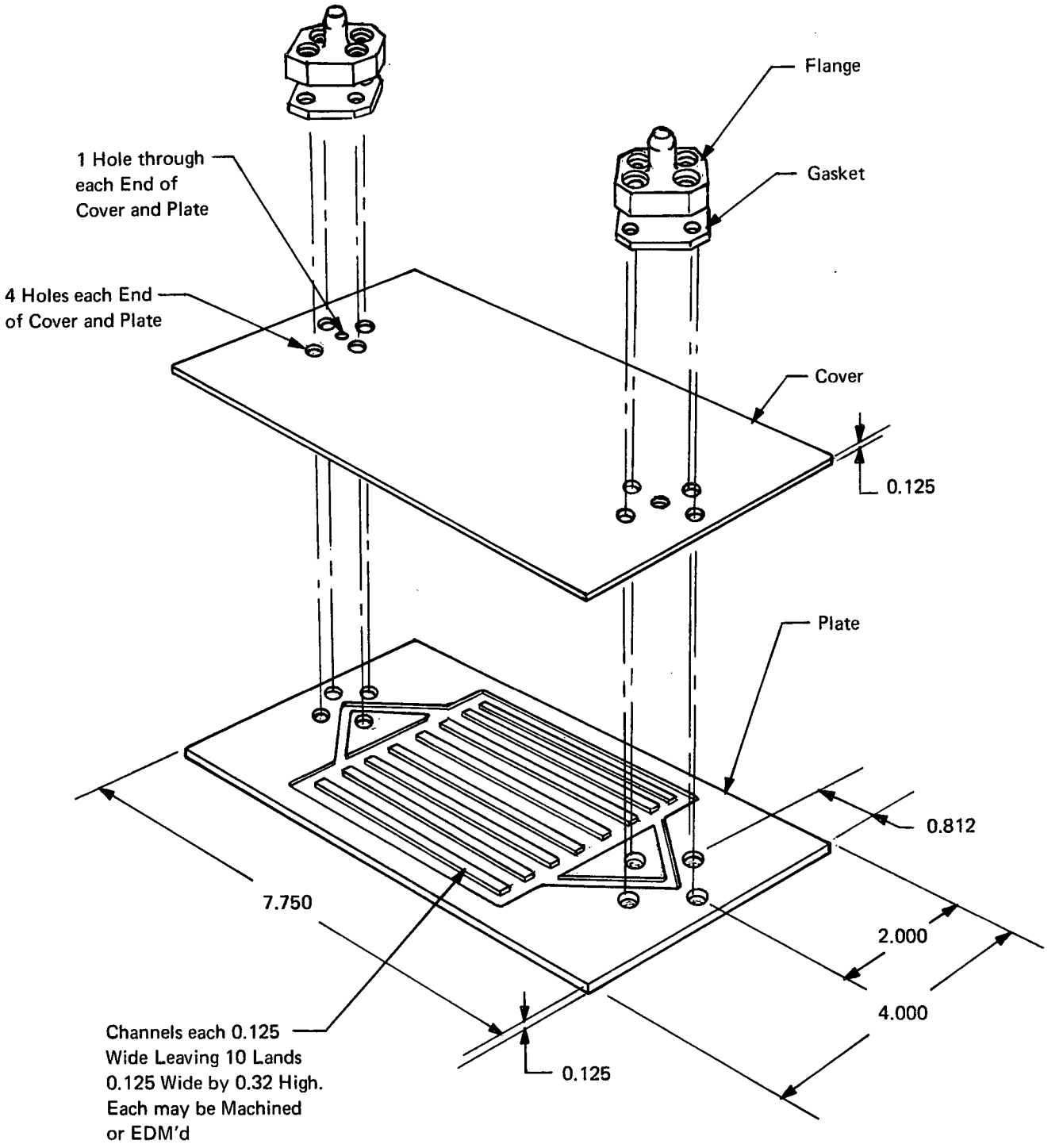

Figure 1. Panel Assembly Designs (Values in Inches; to Convert to Meters, Multiply by 0.0254)

Rather than utilize one bond defect pattern on each group of five panels for a particular bond type, it was determined that more useful information would be possible if two or more patterns were used. By this procedure, bond defect size and ratio of defect to full bond were varied within a bond type panel group.

The patterns approved for electroformed bonds appear in Figures 2, 3, and 4. Two full bond panels were purposely planned to contain small reference defects to determine nondestructive evaluation sensitivity in locating small isolated flaws and confirming the bond line position in such techniques as ultrasonics. Three weak bond patterns were used to provide different total areas of weak bond and various sizes of individual defects. These same patterns were applied to the nonbond panel group in order to enable planned direct correlation of defect size, shape, and area between weak and nonbonds. This was possible in the electroforming method of bonding due to the fact that electrodeposit bond strength can be varied while maintaining complete bond coverage over a given surface.

Braze bond patterns are shown in Figures 5, 6, and 7. With the exception of the nonbond group, a reference defect (Figure 8) was applied to selected test panels to provide a means of accurately detecting the bond line and determining the nondestructive method sensitivity in defining small defect patterns. Patterns were varied on panels in the weak bond group to provide differing defect sizes, shapes, and total defect area. The weak bond patterns and non-bond patterns are not similar because the bond type is achieved by planned control of full bond area. The use of brazing stop-off compounds was not employed because of possible interference with the nondestructive evaluation methods. Planned weak and non-bond regions were purposely designed large to accommodate some expected braze flow.

The diffusion bond patterns, Figures 9, 10, and 11, are similar to the braze patterns in that reference defects are provided on selected panels and bond strength is controlled by the area of planned full bonds.

B. MATERIALS

The materials of construction required for fabricating the test panels consisted of Nickel 200 for baseplates, Inconel 600 for thermally bonded coverplates, and nickel anodes for electroformed coverplates. The nickel anodes obtained were rolled, depolarized and of a sufficient purity for the intended application. Properties obtained from the electrodeposits are discussed later in this section of the report.

The Nickel 200 and Inconel 600 sheets were purchased to appropriate commercial or military specifications and certified analyses obtained to assure conformance. Metallographic sections indicated no defects which would influence the test data or performance of contractual requirements. The certifications supplied the information shown in Table II.

C. PRELIMINARY BOND STRENGTH EVALUATION

To establish and verify the electroforming, brazing, and diffusion bonding process capabilities for fabricating full size test panels, preliminary test pieces were fabricated for bond strength evaluation. Test results demonstrated that the desired bond integrities could be obtained.

1. Electroformed Test Specimens

Lap-shear test specimens as shown in Figure 12 were produced to evaluate the effect of nickel surface activation treatments on the bond strengths achieved after subsequent electroforming. Since the mechanical strength of electroformed nickel as used in the project was much greater than that of the Nickel 200 alloy making up the baseplates, all electroforming to determine bond strength was conducted on 0.250-inch (6.35×10^{-3} m.) thick Nickel 200 stock. This was done to assure that failure in the lap-shear test would occur in the vicinity of the bond line. Certified analyses on the 0.250-inch (6.35×10^{-3} m.) thick Nickel 200 stock confirmed that this material was of acceptable quality and similar to the Nickel 200 to be used in the full-size test panels. Table III provides the certified test data.

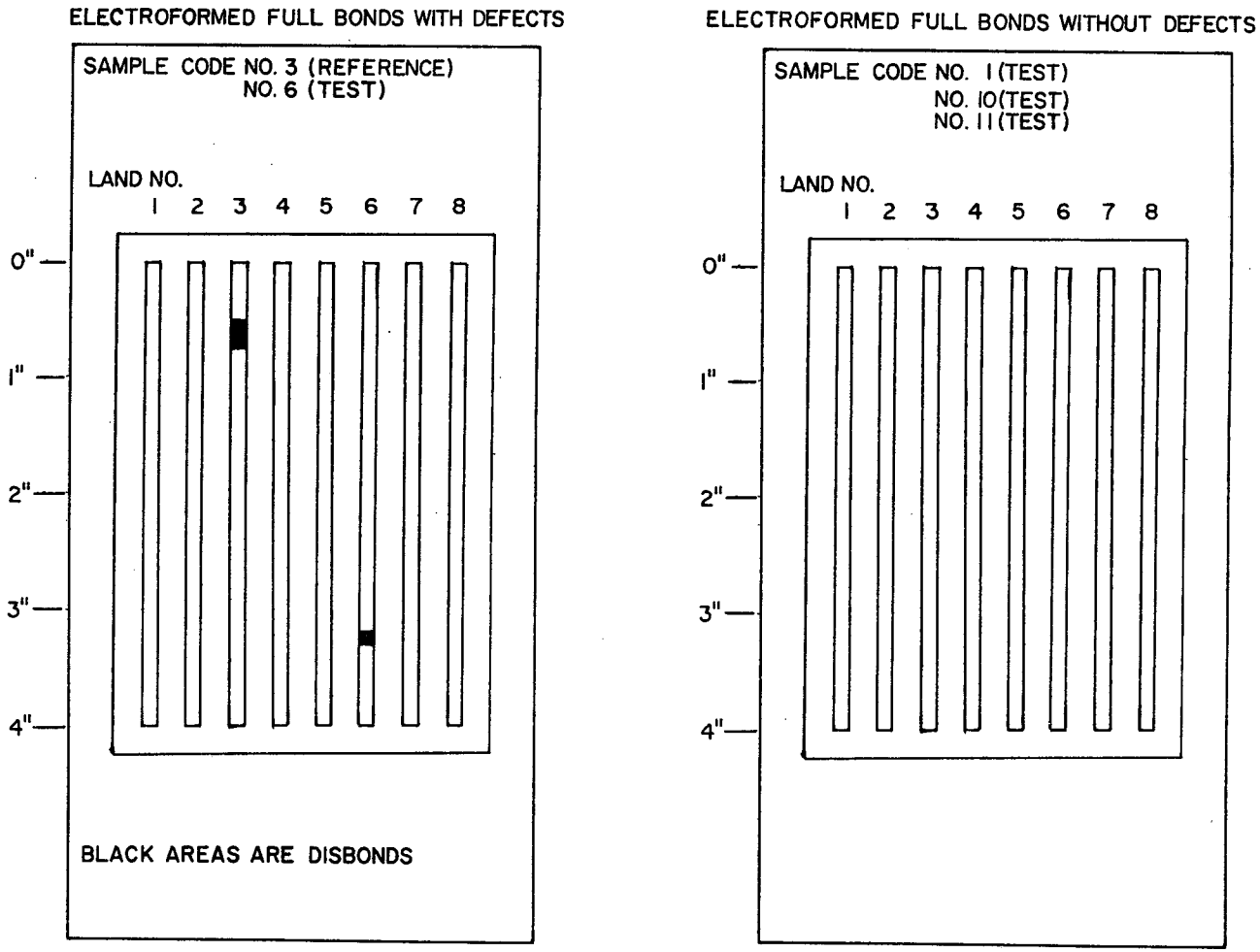

Figure 2. Electroformed Full Bond Patterns

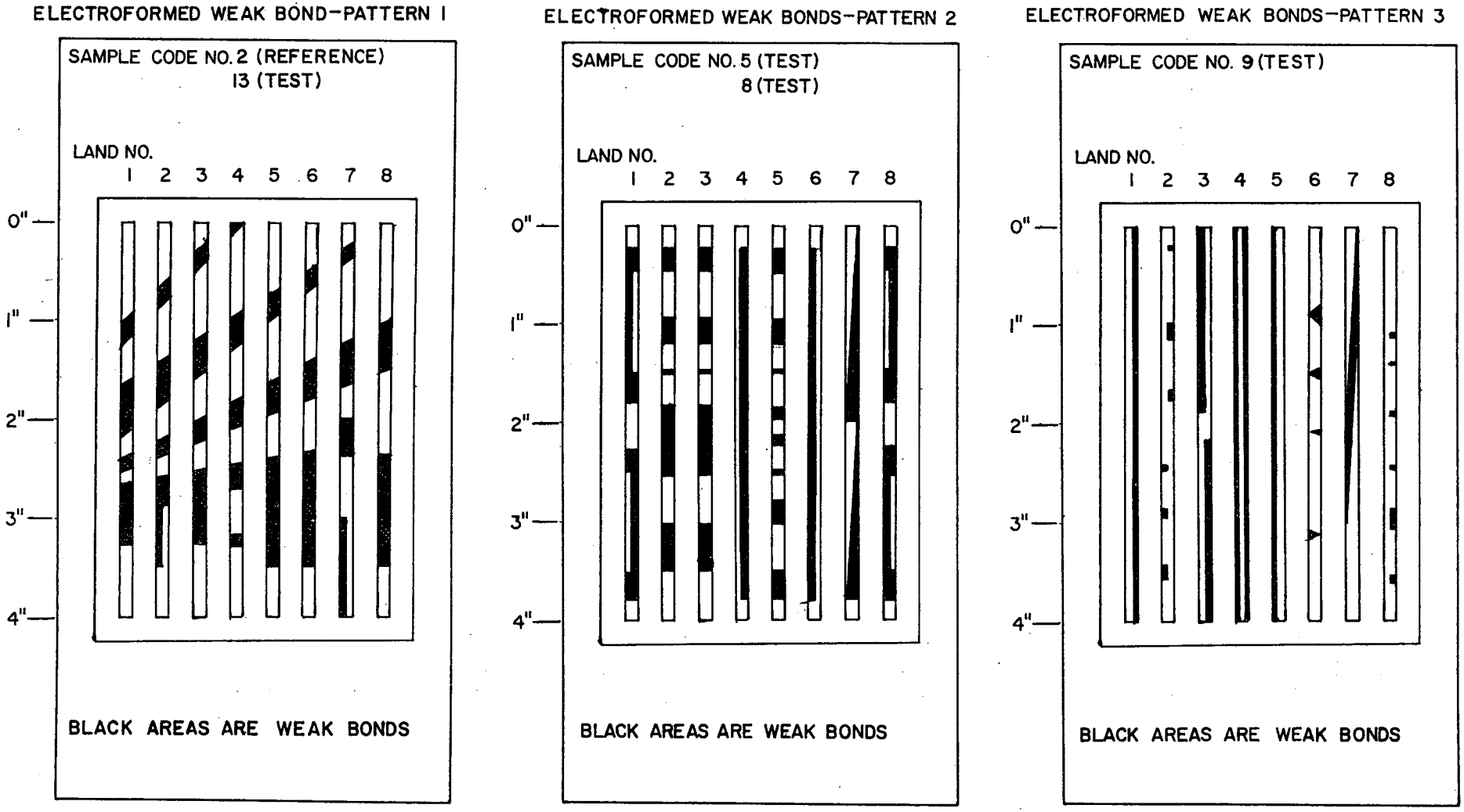

Figure 3. Electroformed Weak Bond Patterns

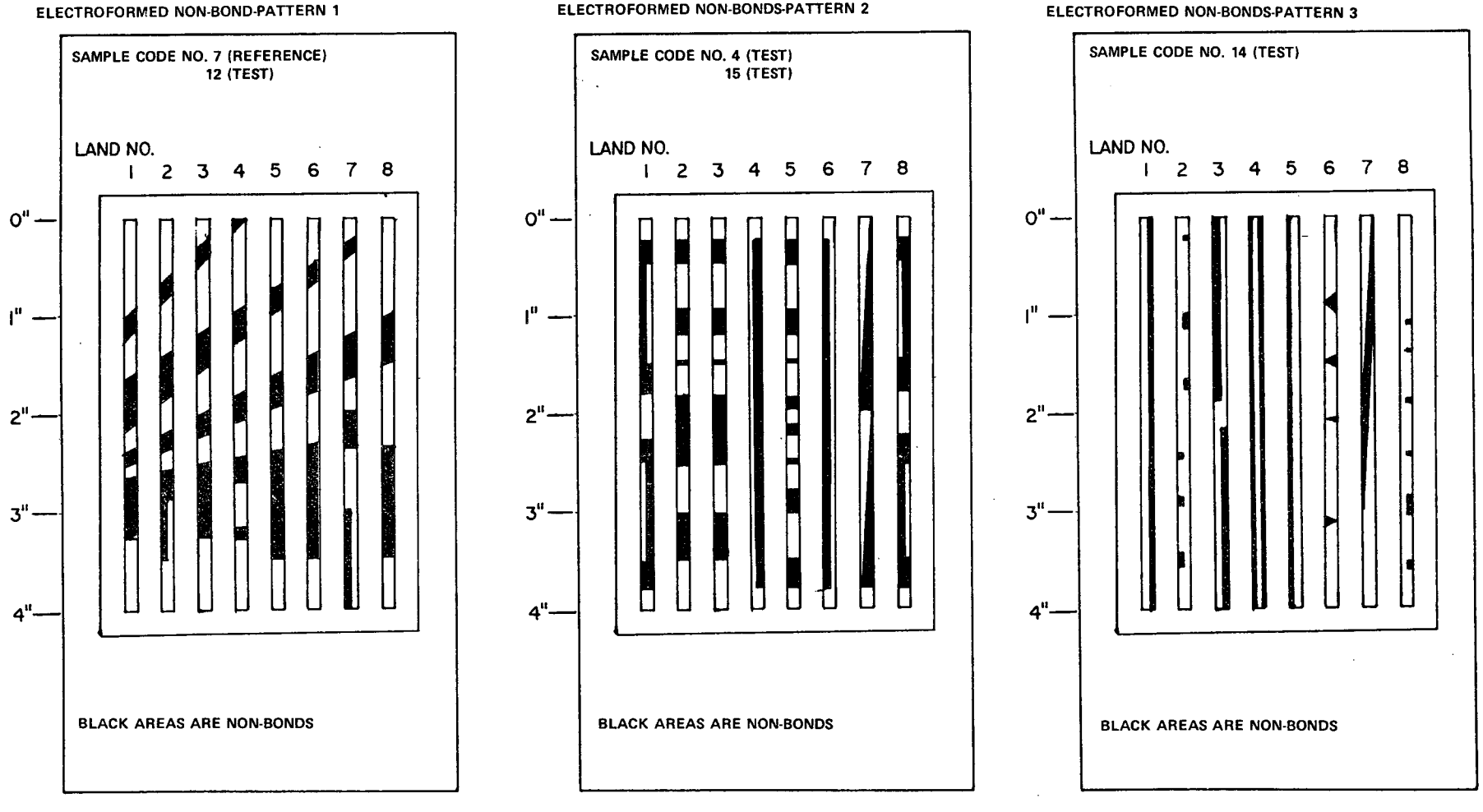

Figure 4. Electroformed Non-Bond Patterns

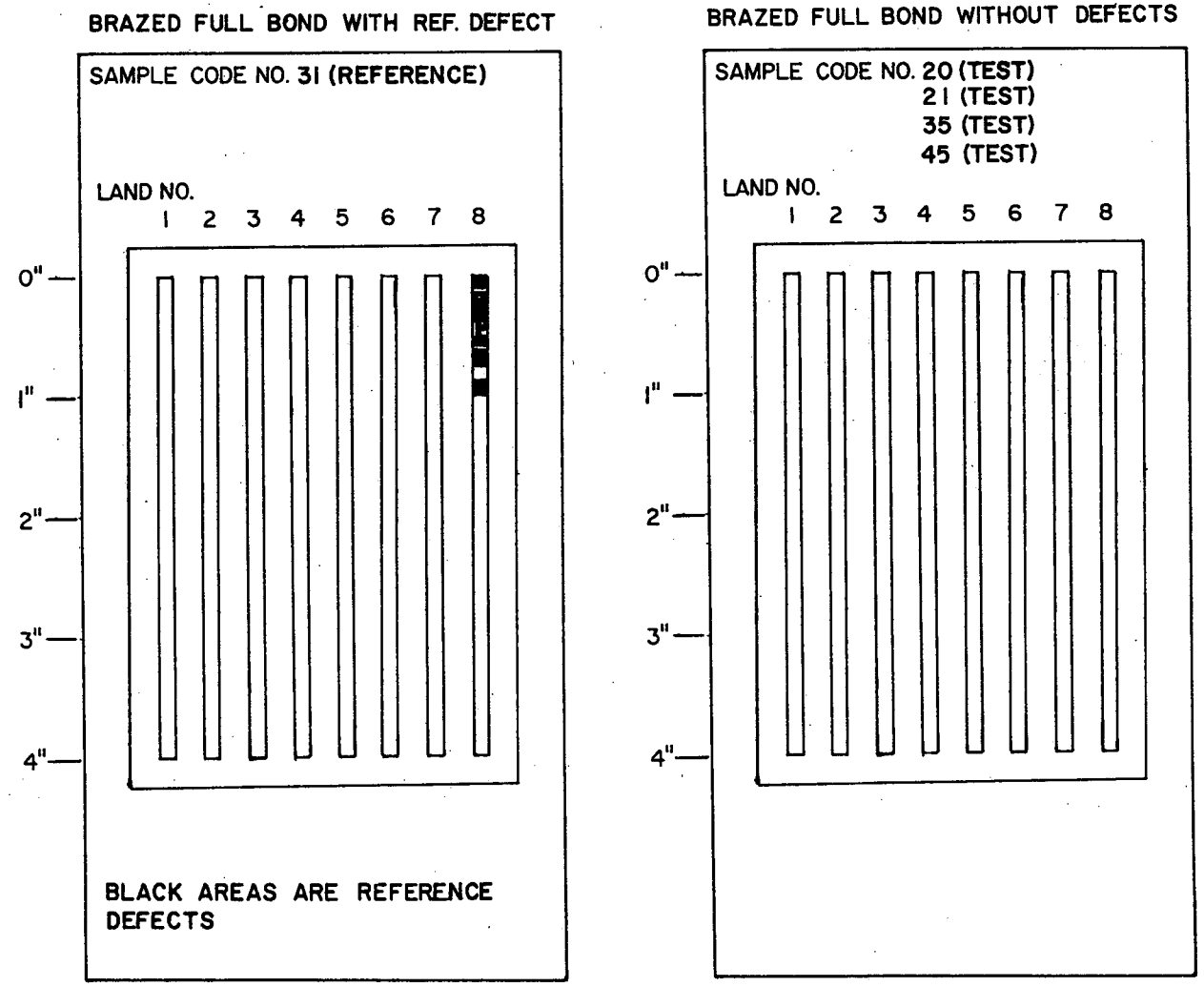

Figure 5. Brazed Full Bond Patterns

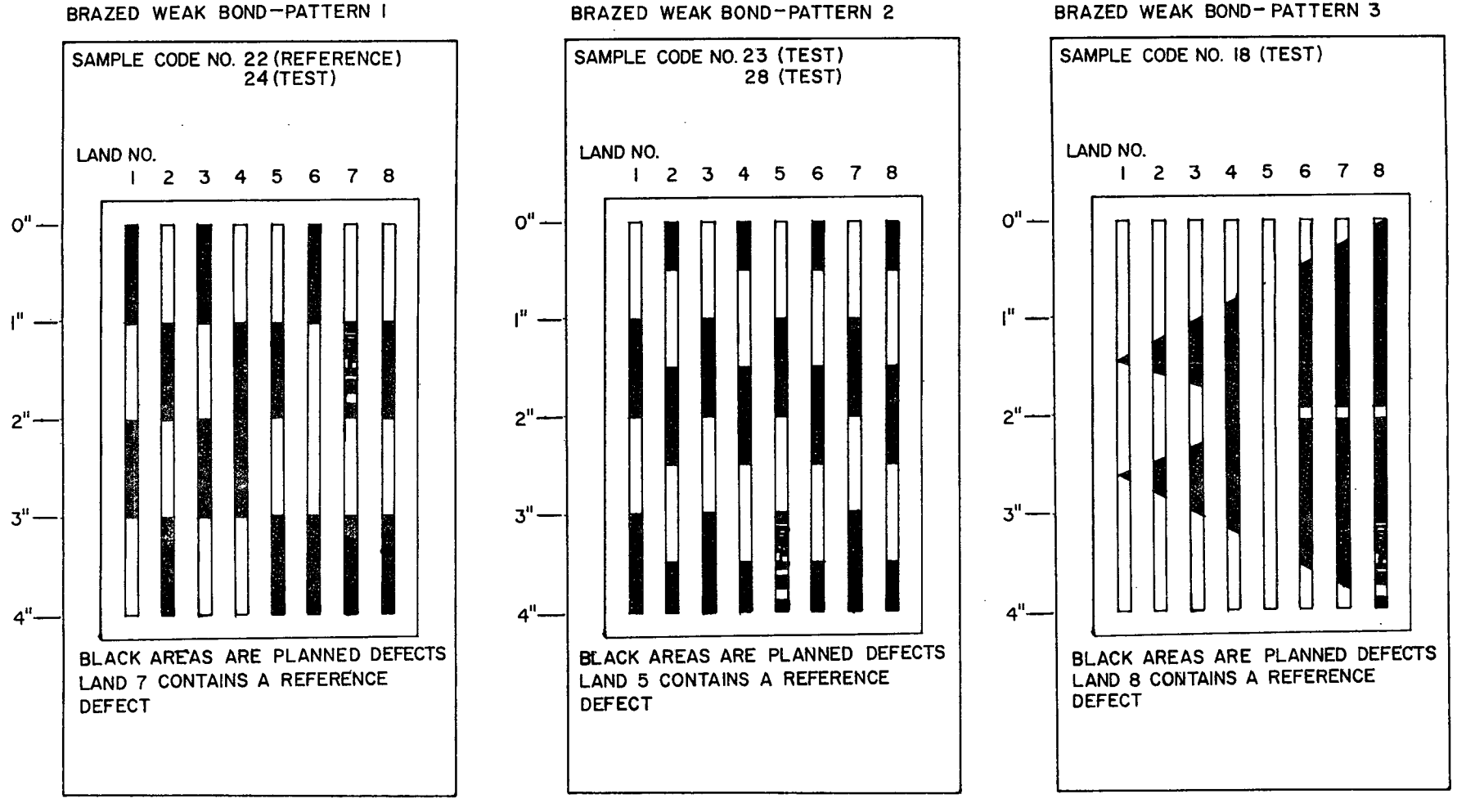

Figure 6. Brazed Weak Bond Patterns

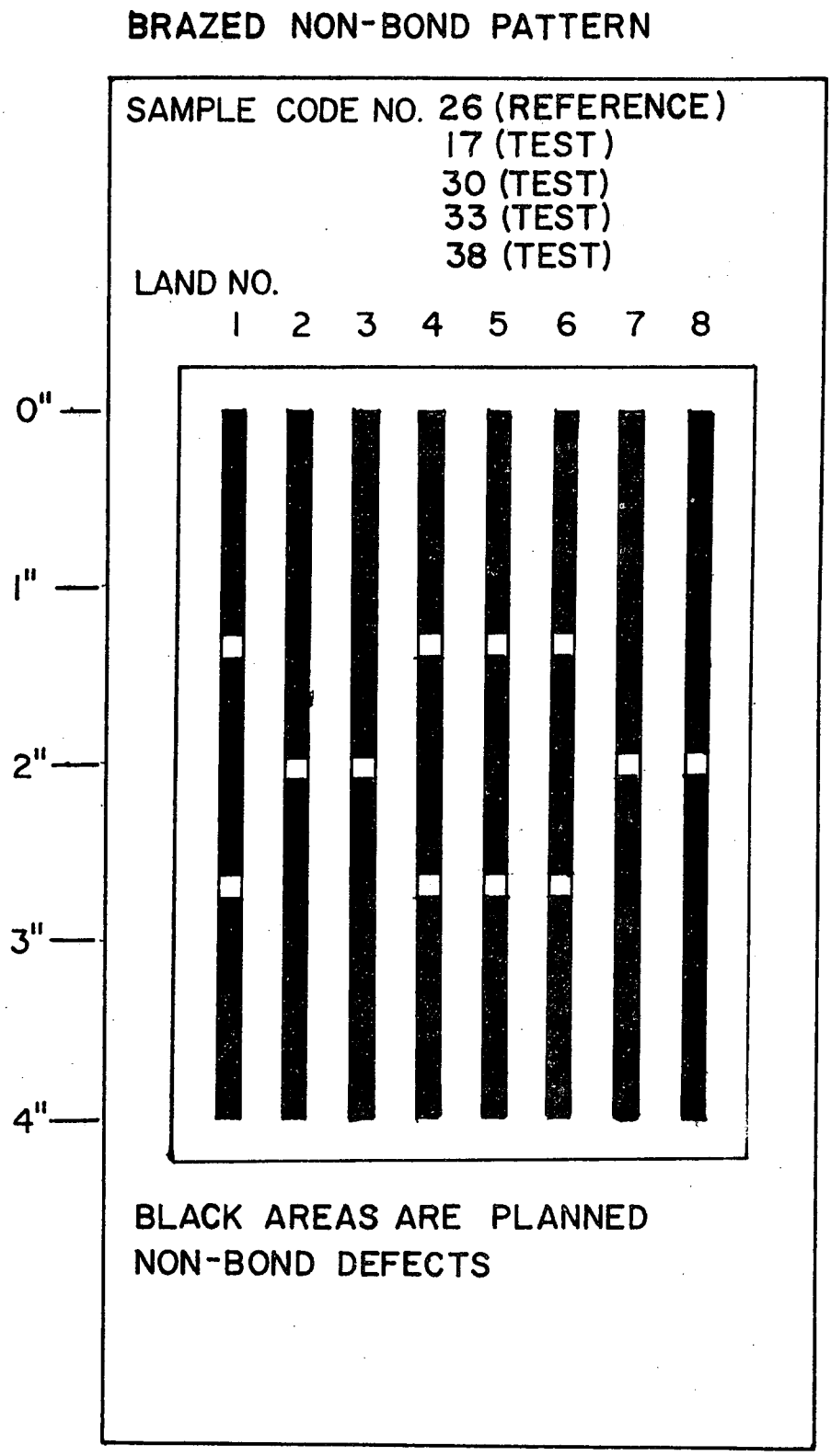

Figure 7. Brazed Non-Bond Patterns

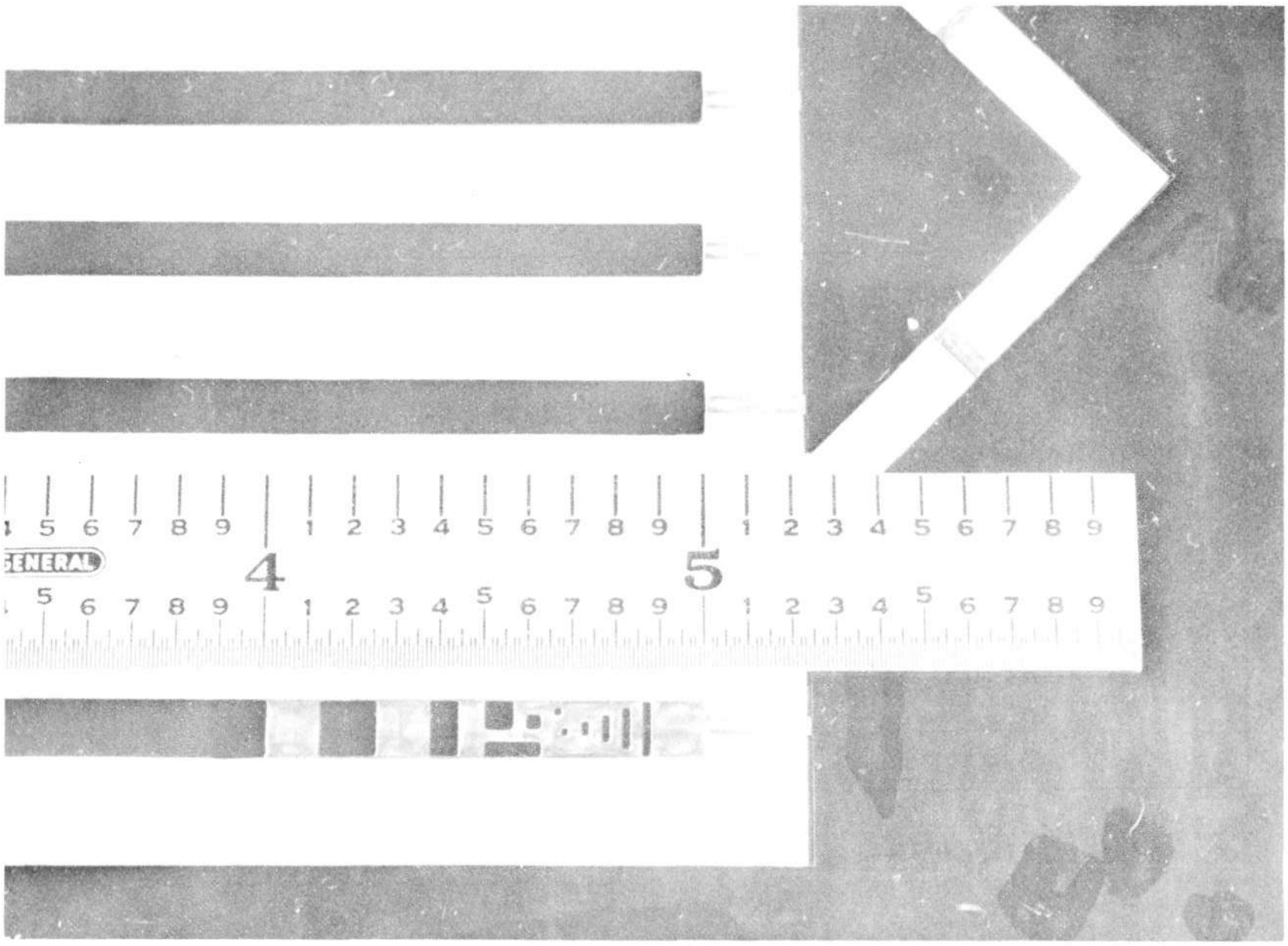

Figure 8. Reference Bond Defect Applied to Selected Brazed and Diffusion Bonded Test Panels (Scale in Inches)

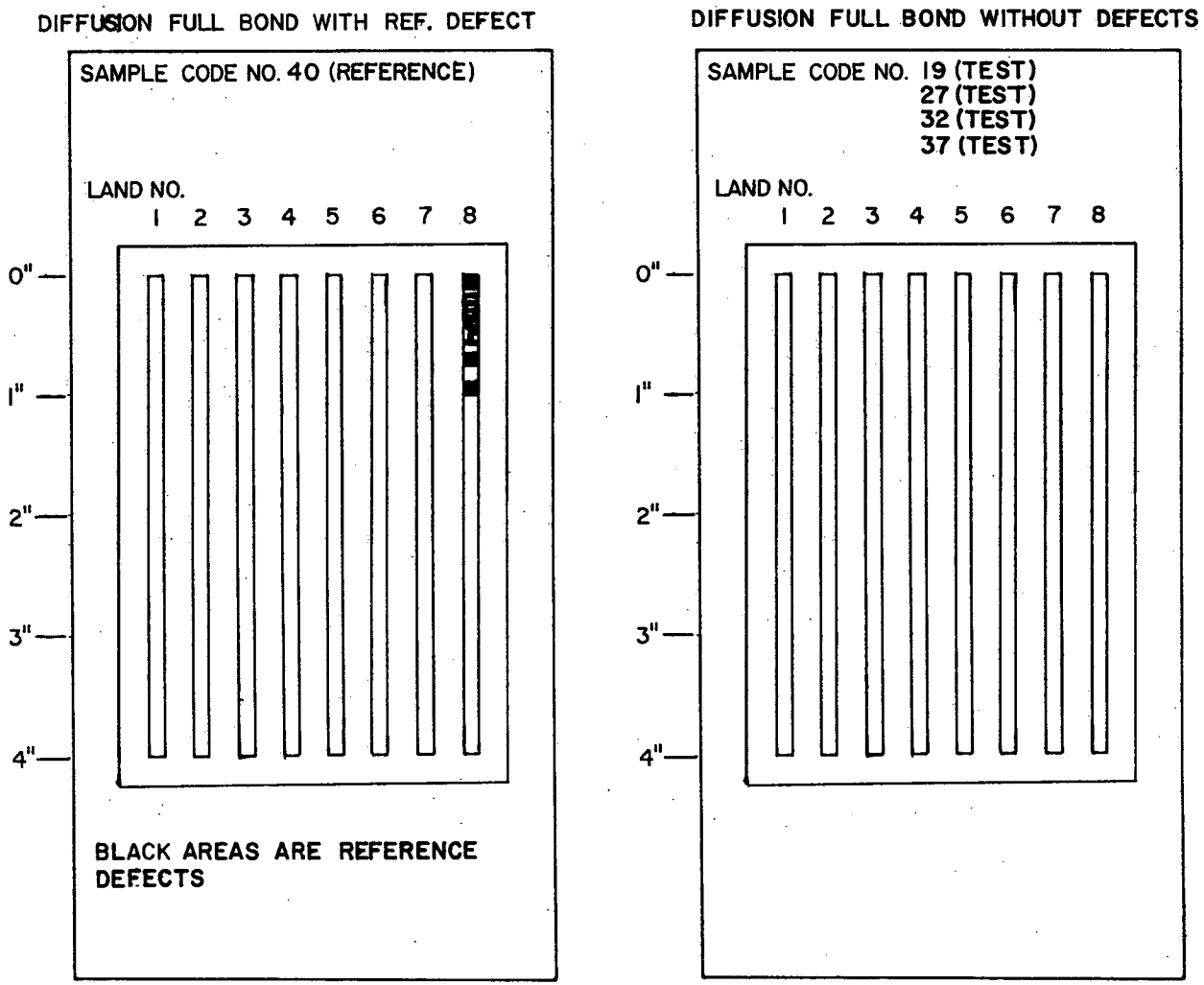

Figure 9. Diffusion Full Bond Patterns

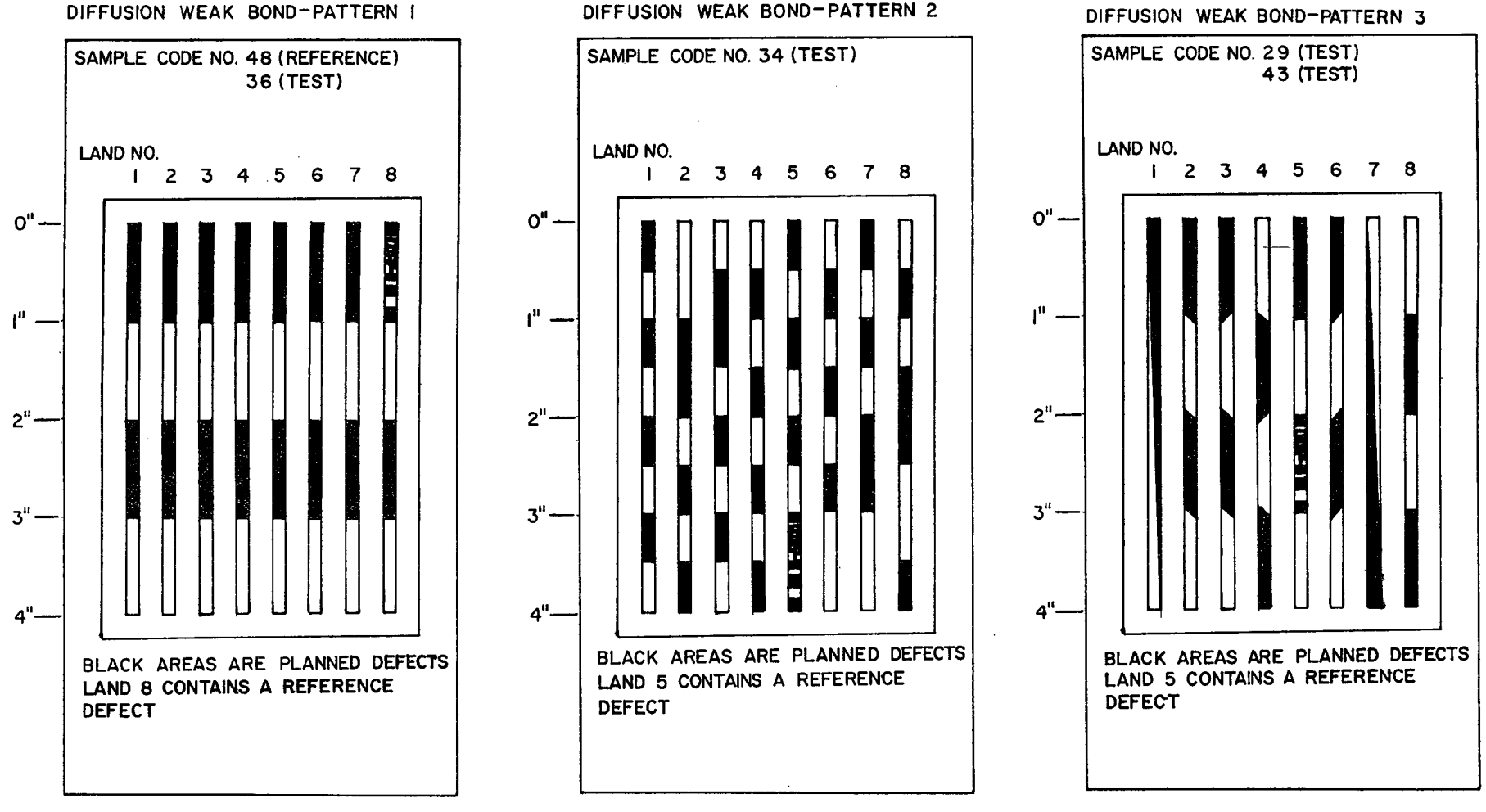

Figure 10. Diffusion Weak Bond Patterns

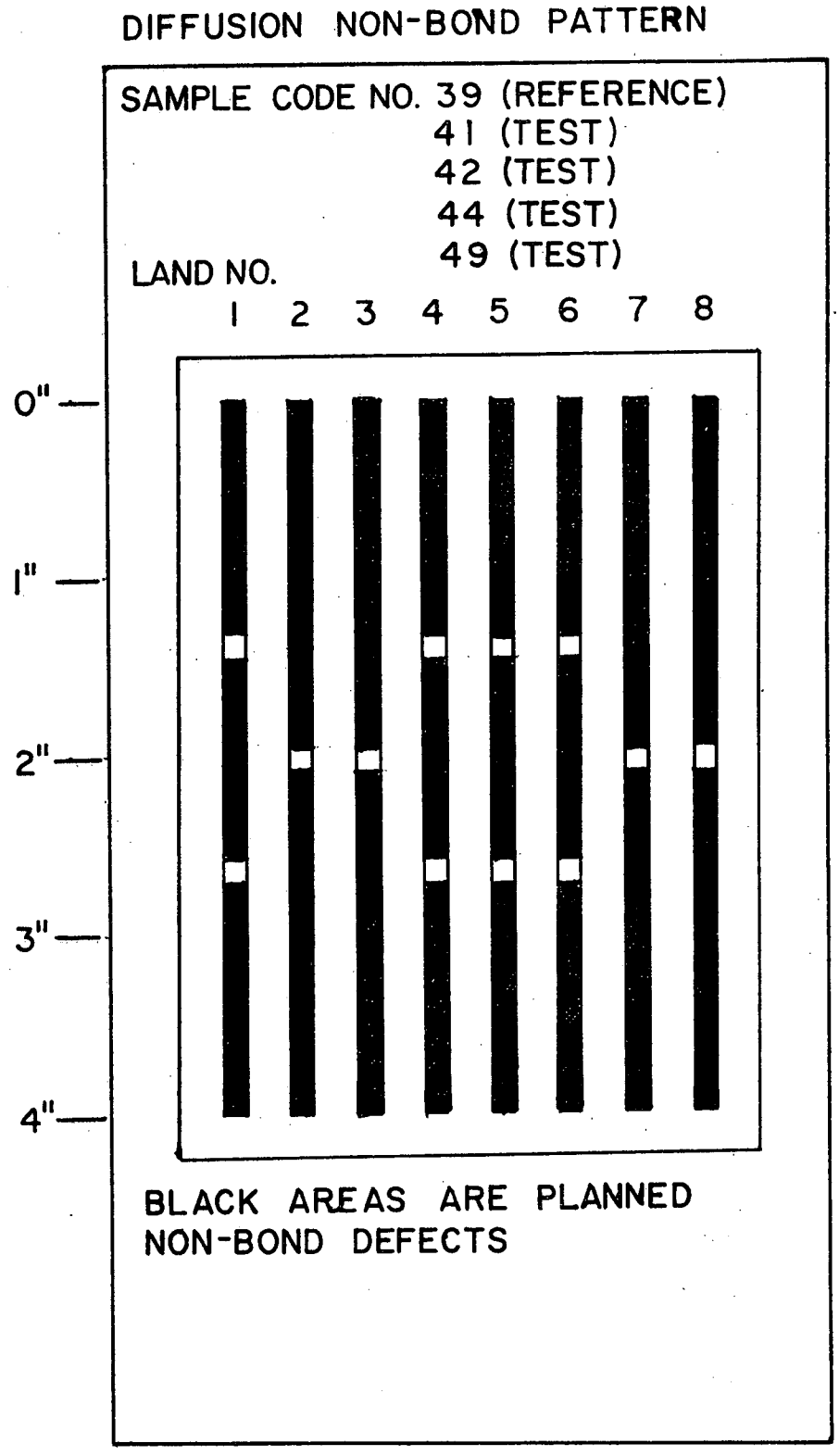

Figure 11. Diffusion Non-Bond Patterns

TABLE II
MATERIAL MECHANICAL PROPERTIES AND CHEMICAL ANALYSES

Material:	Nickel 200 Sheet		Inconel 600 Sheet	
Condition:	Cold Rolled Annealed		Cold Rolled Annealed and Pickled	
Specification:	ASTM B-162		MIL-N-6840A	
Size:	1/8 in. x 48 in. x 48 in.		1/8 in. x 36 in. x 48 in.	
Heat No.:	533A		NX 2907	
Chemistry %	**Actual**	**Required**	**Actual**	**Required**
C	0.05	0.15 Max.	0.03	0.15 Max.
Mn	0.28	0.35 Max.	0.23	1.00 Max.
Fe	0.05	0.40 Max.	9.58	6.0-10.0
S	0.005	0.01 Max.	0.007	0.015 Max.
Si	0.05	0.35 Max.	0.25	0.50 Max.
Cu	0.02	0.25 Max.	0.22	0.50 Max.
Cr			15.81	14.0-17.0
Ni	99.52	99.0 Min.	73.85	72.0 Min.
Mechanical Properties				
Tensile Str. (psi)	63,000		92,000	
Yield Str. (psi)	25,000		45,500	
Elongation, % in 2 in.	47		43	

TABLE III
CHEMICAL AND MECHANICAL PROPERTIES OF 0.250 INCH THICK NICKEL 200 ALLOY

Chemical Analysis (%)

C	Mn	Fe	S	Si	Cu	Ni
0.03	0.26	0.03	0.005	0.03	0.01	99.61

Mechanical Properties

Yield Strength (psi)	31,000
Ultimate Strength (psi)	61,000
Elongation, %	48
Hardness, R_B	63

Condition: Cold Rolled, Annealed Sheet

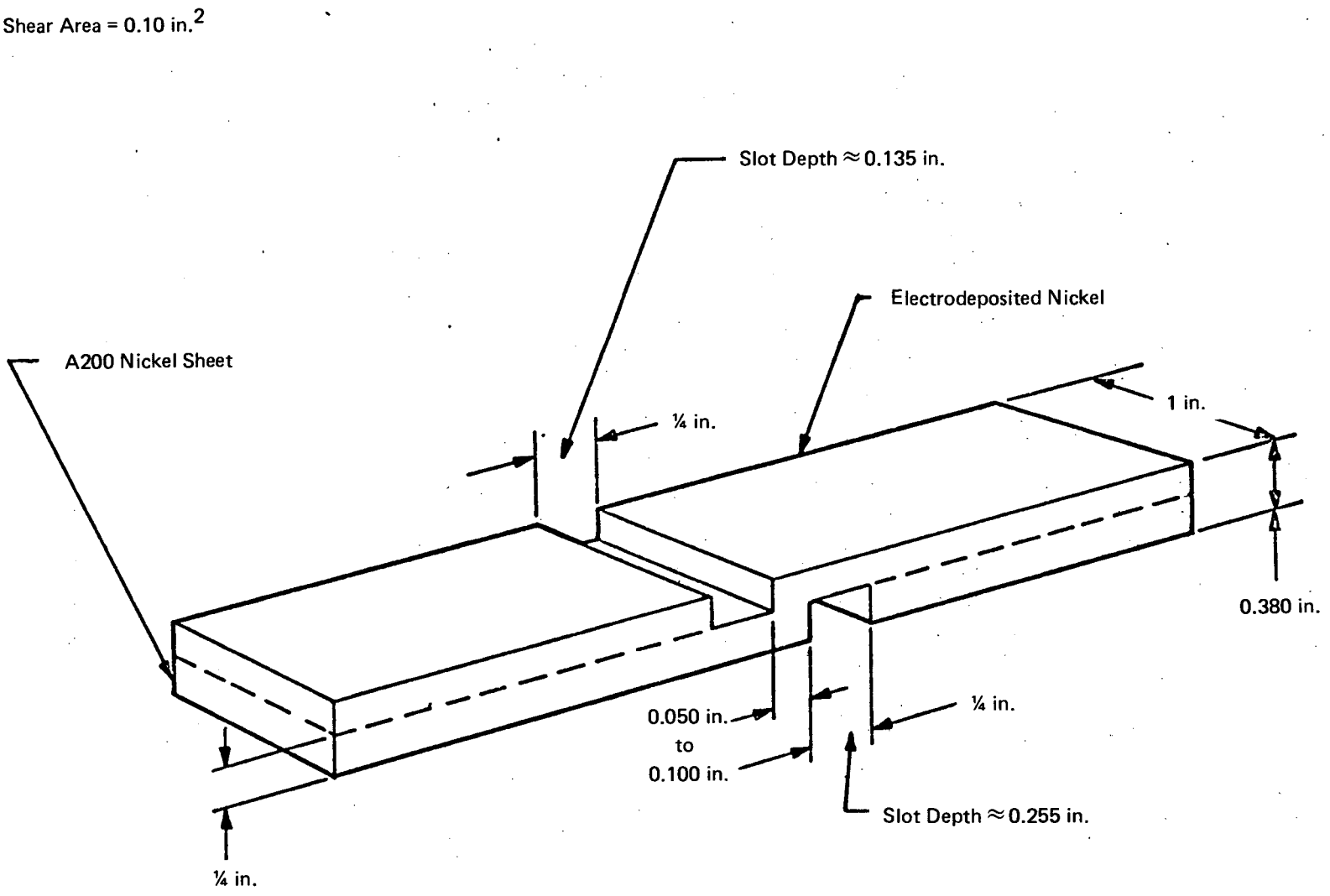

Figure 12. Typical Configuration of Lap-Shear Specimens

(To Convert to Meters, Multiply Values by 0.0254)

Nickel 200 baseplates were cut to a size of 1.0 by 8.0 inches (0.0254 x 0.203 m.) and the edges surface ground for uniformity. All surfaces were chemically etched to remove oxides and other imperfections which might affect bonding. A minimum of three specimens for each bond type (i.e., -full, weak, and non-bond) were prepared for electroforming. The actual procedures used to produce each bond type are discussed in Subsection E, Electroforming.

Electrodeposition was performed in a 200 gallon (0.757 $m.^3$) nickel sulfamate electroforming bath at a current density of 60 amperes per square foot (5.574 amperes/$meter^2$) and an electrolyte temperature of 110° to 120°F (317.2° to 322.1°K). This current density was higher than that used to produce the full size test panels. The current density only affects the rate of electroforming and mechanical properties of the deposit. Bond strength is related to proper activation of the nickel substrate and cathodic protection of this surface until the instant electrodeposition begins. It is essential that all traces of oxides and organic contaminants be removed from the surface before bonding.

After electroforming, the specimens were surface ground to remove external roughness normal for thick electrodeposits. Overgrowth (nodules) on the edges were removed by mechanical milling. Notches shown in Figure 12 were milled into the coverplate and baseplate on selected specimens. The remaining test bars were retained for use as test samples in practical application studies on some of the nondestructive evaluation methods under consideration early in the project. Notches for lap-shear testing were then electric discharge machined in these specimens and the shear strength determined. Bond strength results for those specimens produced by the processes evaluated for test panel fabrication are shown in Table IV. It was noted that producing notches for lap shear testing by electric discharge machining resulted in higher bond strength results than were encountered on specimens with mechanically milled notches. Figure 13 illustrates typical lap-shear specimens after test.

TABLE IV
EVALUATION OF PROCESSES TO PRODUCE ELECTROFORMED BONDS

Sample No.	Bond Type	Width		Length		Area		Breaking Load		Shear Strength	
		Inches	Meters	Inches	Meters	$In.^2$	$Meters^2$	Lb.	Newtons	psi	N/m^2
1	Full	0.996	0.0253	0.110	0.00279	0.1096	7.071×10^{-5}	4,850	21,573	44,250	305.1×10^6
2	Full	0.974	0.0247	0.125	0.00317	0.1218	7.858×10^{-5}	6,250	27,800	52,100	359.2×10^6
3	Full	0.997	0.0253	0.050	0.00127	0.0499	3.219×10^{-5}	2,265	10,075	45,400	313.0×10^6
4	Full	Retained for Sonic Frequency Analysis Evaluation									
5	Full	0.993	0.0252	0.080	0.00203	0.0794	5.122×10^{-5}	3,450	15,346	43,350	298.9×10^6
6	Full	1.003	0.0255	0.117	0.00297	0.1178	7.600×10^{-5}	5,550	24,686	47,100	324.7×10^6
12	Weak	0.975	0.0248	0.095	0.00241	0.0926	5.974×10^{-5}	4,000	17,792	43,200	297.9×10^6
13	Weak	0.993	0.0252	0.095	0.00241	0.0943	6.084×10^{-5}	4,325	19,238	45,850	316.1×10^6
14	Weak	Retained for Sonic Frequency Analysis Evaluation									
15*	Weak	0.947	0.0247	0.100	0.00254	0.0974	6.284×10^{-5}	2,700	12,010	27,800	191.7×10^6
16	Weak	Broke in Milling									
17	Weak	Broke in Milling									
21	Weak	0.981	0.0249	0.097	0.00246	0.0951	6.135×10^{-5}	45	200	470	3.24×10^6
22*	Weak	0.991	0.0252	0.120	0.00305	0.1189	7.671×10^{-5}	2,750	12,232	23,120	159.4×10^6
23	Weak	Retained for Sonic Frequency Analysis Evaluation									
18	Nonbond	Retained for Sonic Frequency Analysis Evaluation									
19	Nonbond	0.995	0.0253	0.086	0.00218	0.0856	5.522×10^{-5}	625	2,780	7,300**	50.3×10^6
20	Nonbond	0.997	0.0253	0.098	0.00249	0.0977	6.303×10^{-5}	1,050	4,670	10,750**	74.1×10^6

* Notched by Electric Discharge Machining

** Values Due to Full Bond on Specimen Edges (1/8 inch or 0.003175 meters, each edge).

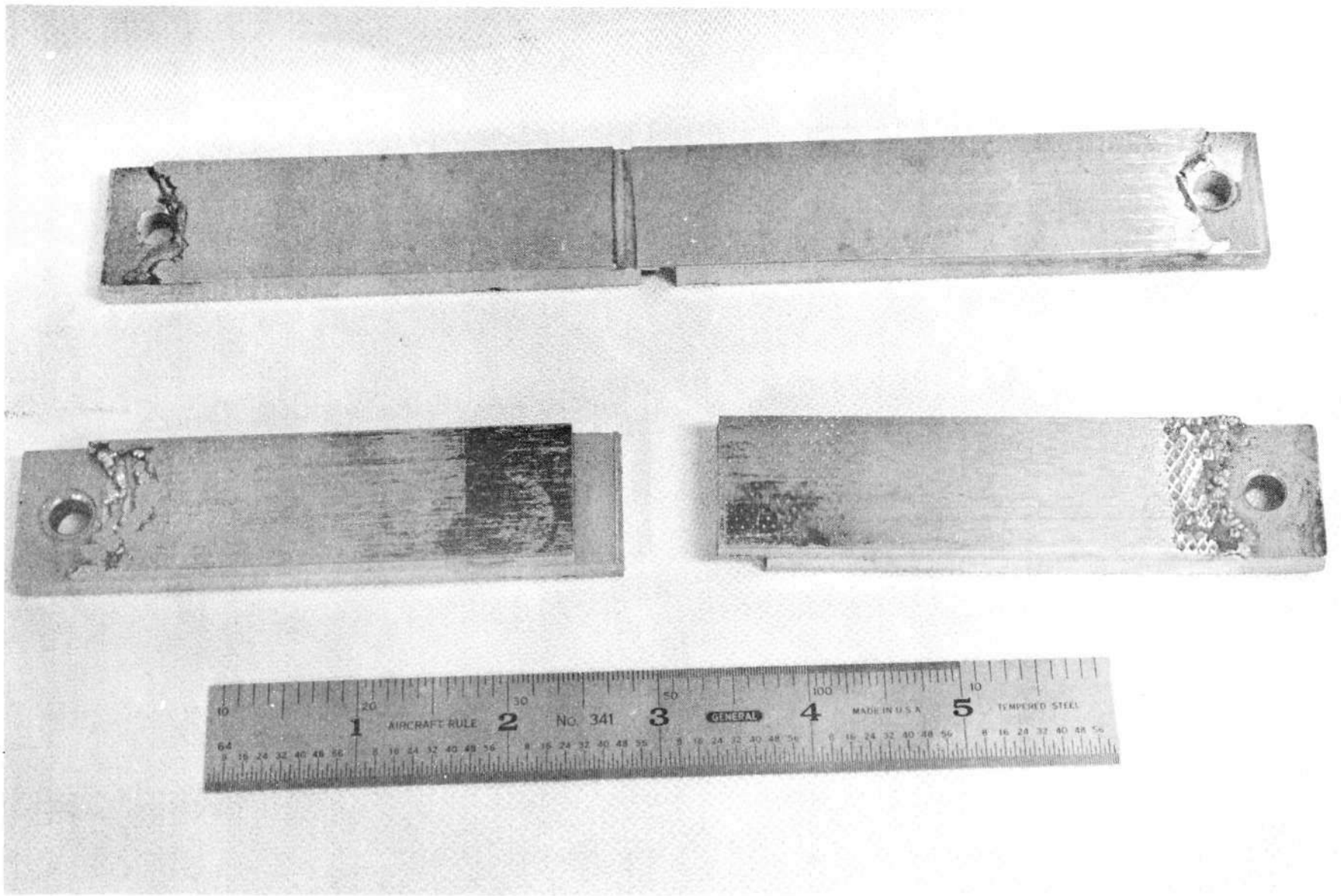

Figure 13. Typical Electroform Bonded Lap-Shear Specimens (Scale in Inches)

2. Brazed Test Specimens

Lap-shear specimens were fabricated and tested to establish the optimum brazing parameters for producing the various bond strength levels required on the full size test panels for nondestructive evaluation. The samples consisted of Inconel 600 coverplates and Nickel 200 baseplates with overall dimensions of 5 inches by 3.1 inches (0.127 x 0.0787 m.). Each component material was 0.125 inch (3.17×10^{-3} m.) thick. The final braze metal selected was OFHC copper, 5 inches by 3.1 inches by 0.003 inch thick (0.1270 x 0.0787 m.; 7.62×10^{-5} m. thick). The photofabrication process (photo-resist masking and chemical etching) was used to produce the defect patterns in the weak and non-bond samples. Table V lists the bond strength results and brazing parameters for each bond type.

TABLE V
BRAZE BOND LAP-SHEAR STRENGTHS AND BRAZING PARAMETERS*

Bond Type	Braze Temp. °F	Braze Temp. °K	Time At Temp. (Sec.)	Lap-Shear Strength: Strip 1 psi	Strip 1 N/m^2	Strip 2 psi	Strip 2 N/m^2	Strip 3 psi	Strip 3 N/m^2
Full	2000	1366	30	43,650	301.0×10^6	47,200	325.4×10^6	44,450	306.5×10^6
Weak	2000	1366	30	25,200	173.7×10^6	47,950	330.6×10^6	36,650	252.7×10^6
Nonbond	2000	1366	30	36,500	251.7×10^6	15,750	108.6×10^6	21,000	144.8×10^6

*Vacuum was maintained at 5×10^{-5} Torr (6.665×10^{-3} N/m^2)

The nickel and Inconel sheet stocks were sheared to size and belt sanded (240 grit) to improve the surface condition. It was noted that the plates contained variations in surface flatness, as well as normal thickness variations to 0.010 inch (2.54×10^{-4} m.). Since plates were, in extreme cases, as much as 0.020 inch (5.08×10^{-4} m.) out-of-flat, brazing would be difficult to control.

To alleviate this condition, the Inconel 600 plates were stress relief annealed at 1600°F (1144°K) for three hours in vacuum using a hot press with an applied pressure of 750 psig (5.171×10^6 N/m^2). As many as twelve plates were cycled at one time. Plates were electrophoretically coated with 0.03 micron aluminum oxide particles to prevent bonding during the anneal. The Nickel 200 baseplates were similarly stress relieved, but the annealing temperature was reduced to 1300°F (978°K) for the same period of time.

Stress relieving did not fully flatten the plates. Surface grinding was evaluated as a possible means of obtaining flatness within 0.001 inch (2.54×10^{-5} m.). This was not satisfactory; bowing was still pronounced.

The process by which best flatness was obtained was as follows:

(a) Stress relief anneal plates with hot press flattening load, and

(b) Surface lap plates on both sides.

The resulting flatness variations in Nickel 200 and Inconel 600 ranged from 0.0005 inch to 0.0060 inch (1.27×10^{-5} to 1.52×10^{-4} m.) in the free-standing condition.

Initially it was planned to electrodeposit the copper braze metal on the Nickel 200 plates. An acid copper electrolyte was used to deposit 0.002 inch to 0.003 inch (5.08×10^{-5} to 7.62×10^{-5} m.) of copper for brazing. Because of edge buildup in the deposition process, it was necessary to polish the excess copper

away to obtain a flat matching surface for the Inconel 600 coverplate. A bright acid leveling bath was evaluated and found to solve the edge buildup problem. However, upon brazing a test coupon with this copper, porous area developed. This may have been due to trace quantities of leveling agent incorporated in the copper deposit.

Copper foil of 0.003 inch (7.62×10^{-5} m.) thickness was cut to the Nickel 200 plate size and brazed successfully. To produce the defect patterns, the copper foil was coated with a commercial photoresist compound and cured. Photomasters of the defect patterns for weak bond and non-bond were applied over the photoresist and and exposed. Chemical etching was used to remove the unprotected copper and the pattern was produced. The remaining photoresist compound was removed with solvent.

The photofabricated copper foil patterns were applied over the Nickel 200 plates. Inconel coverplates were placed over the braze foils and brazing was conducted in a vacuum furnace. A baseplate and dead weight of alloy D6AC were used to sandwich the plates being brazed. Aluminum oxide coated separator sheets were inserted between braze specimens to prevent undesired bonding. The alloy D6AC was drilled through the sides to accommodate thermocouples, Figure 14. This assured that the entire braze pack could be brought to a temperature of 1900°F (1311°K) and quickly elevated to 2000°F (1365°K) to accomplish brazing (copper melting point is 1980°F or 1355°K).

After brazing, the composite panels were cut into three 1.0 inch (0.0254 m.) wide strips, each 5 inches (0.127 m.) long and 0.250 inch (6.35×10^{-3} m.) thick. Lap-shear notches were electric discharge machined on each side to provide a bond with dimensions of one inch by 0.060 inch (0.0254×0.00152 m.) to be tested.

3. Diffusion Bonded Test Specimens

Specimens for evaluating bond strengths from the diffusion bonding process were identical in size to those used in the brazing work. The photofabrication process was used to produce accurate defect patterns in the Nickel 200 baseplates of the weak bond and non-bond specimens. Table VI lists diffusion bonding parameters and the corresponding bond strengths obtained.

TABLE VI
DIFFUSION BOND LAP-SHEAR STRENGTHS AND BONDING PARAMETERS*

Bond Type	Bonding Time (Minutes)	Temperature		Bond Surface Load		Shear Strength					
						Strip 1		Strip 2		Strip 3	
		°F	°K	psi	N/m²	psi	N/m²	psi	N/m²	psi	N/m²
Full	180	2100	1422	750	5.171×10^6	37,000	255.1×10^6	61,200	422.0×10^6	28,750	198.2×10^6
Weak	180	2100	1422	750	5.171×10^6	8,250	56.9×10^6	16,850	116.2×10^6	24,850	171.3×10^6
Nonbond	180	2100	1422	750	5.171×10^6	1,550	10.7×10^6	3,250	22.4×10^6	15,850	109.3×10^6

*Vacuum ranged from 4×10^{-5} to 5×10^{-4} Torr (5.332×10^{-3} to 6.665×10^{-2} N/m²)

Surface flatness was more critical on plates used for diffusion bonding than for the other fabricating techniques. For this reason, all plates subjected to surface lapping were selected for flatness suitable to diffusion bond. Surface preparation of the nickel was the same as used for brazing. However, to produce the weak and non-bond patters, etching was used to relieve the Nickel 200 surface profile at predetermined areas.

For chemical etching, the photoresist method used to fabricate braze foil patterns was applied. The same defect photomaster patterns were used. To bond the photoresist compound (due to application of a more severe and longer etch), nickel surfaces were phosphatized by immersion in a phosphoric acid

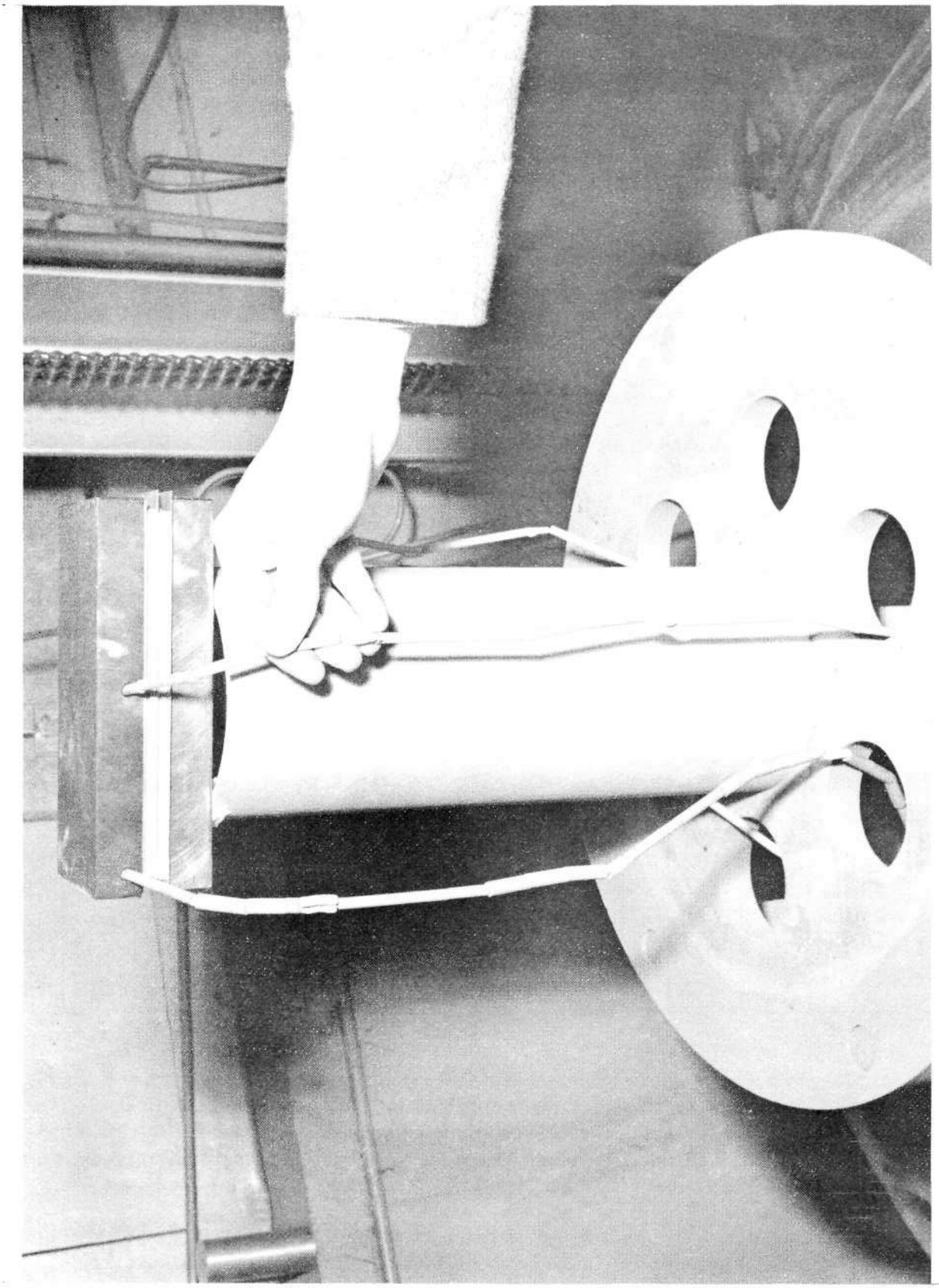

Figure 14. Braze Pack and Thermocouple Positioning in Vacuum Furnace

solution at 180°F (355°K). Photoresist was applied and exposed to the bond pattern photomaster (transparency). After developing the photosensitive coating, chemical etching removed 0.003 to 0.004 inch (7.62×10^{-5} to 10.16×10^{-5} m.) of nickel to create the planned flaw pattern. The etchant was nitric acid containing ferric chloride. The photoresist was removed by solvent and the phosphatized layer was stripped by a brief immersion in nitric acid.

The Inconel 600 plates were deoxidized and surface cleaned by dipping in nitric acid-ferric chloride etch at room temperature. The etch rate was sufficiently slow that no thickness changes were observed. After rinsing, a nickel plating strike was applied to the plates from a Wood's nickel solution. This was primarily used to afford a bonded layer of "pure" nickel as a diffusion aid on the Inconel.

Diffusion bonding was accomplished in a vacuum hot press. The furnace, Figure 15, has resistance heated tungsten elements and molybdenum platens. The bottom platen was covered with an aluminum oxide coated steel plate as a diffusion barrier. Over this was placed a Nickel 200 plate, etched side exposed. The Inconel 600 coverplate was placed on top of the nickel plate. An aluminum oxide coated separator was positioned on the Inconel, and the entire assembly was centered on the bottom platen. The top platen was lowered to make contact with the assembly, but no pressure was applied to the ram.

The furnace was closed and evacuated to a vacuum of 5×10^{-4} torr (6.665×10^{-3} N/m^2.). At a temperature of 1000° F (811°K), a load of 750 psig (5.171×10^6 N/m^2.) was applied on the parts being bonded. The diffusion bonding was performed at 2100°F (1422°K) for a three hour holding period at temperature. After bonding, each plate was cut into three strips and notched for lap-shear testing in the same manner as the brazed specimens.

D. ELECTRIC DISCHARGE MACHINING BASEPLATES

Fifty-one Nickel 200 base plates were sheared from 0.125 inch (3.175×10^{-3} m.) thickness stock to dimensions of 7.75 inches (0.1968 m.) long by 4 inches (0.1016 m.) wide. These plates were assigned code numbers by stamping in the upper left corner on the side opposite that to be machined for channels. All plates were electric discharge machined using a graphite composite electrode as shown in Figure 16. Dimensional checks showed that all critical channel and manifold tolerances were met. Mounting holes for fixturing of the plates for electroforming were drilled into each end of every plate. These holes also served as indexing positions for a template to be used later to machine the bolt hole pattern and pressurization ports necessary in nondestructive evaluation with holography and acoustic emission. A typical base plate with the channel pattern is shown in Figure 17.

The individual base plates were cleaned by vapor degreasing and alkaline cleaning to remove dielectric fluid from the electric discharge machining operation.

E. ELECTROFORMING TEST PANELS

Mechanical properties of nickel deposits produced by the electrolyte operating parameters planned for panel production were first obtained, Table VII

Twenty-one electric discharge machined baseplates were randomly selected for bonding by electroforming. This included the six plates for panels to be later subjected to thermal diffusion treatment to determine if bond flaws could be repaired by this technique and verified by nondestructive evaluation.

Five base plates were randomly selected from this group to receive a full bond. A pentagonal shaped fixture was fabricated from stainless steel sheet to support the plates during cleaning, masking, and electro-

TABLE VII
ELECTRODEPOSIT MECHANICAL PROPERTIES* (NICKEL SULFAMATE ELECTROLYTE)

Electrolyte Composition				Temp.		Current Density		Mechanical Properties			
Units	Ni Metal	Ni Cl_2	PH	°F	°K	Amp/Ft^2	Amp/M^2	Units	Ultimate Strength	Yield Strength	% Elong. In.^{2}
oz/gal kg/m^3	9.4 70.4	1.2 9.0	4.0	120	322	30	2.79	psi N/m^2	97,100 669 x 10^6	65,100 449 x 10^6	9
oz/gal kg/m^3	9.0 67.4	1.4 10.5	4.1	110	316	30	2.79	psi N/m^2	100,000 689 x 10^6	67,200 463 x 10^6	8
oz/gal kg/m^3	9.2 68.9	1.1 8.2	3.9	105	314	30	2.79	psi N/m^2	90,900 627 x 10^6	60,700 418 x 10^6	8

*Data represents an average for six tests under each electroforming condition.

forming operations. Figure 18 illustrates this fixture with plates attached. The fixture was designed to provide close proximity between panels so as to minimize edge built-up along the sides. However, build-up on the plate ends was not restricted due to the subsequent necessity to surface grind for proper sealing surface for the pressure fittings used in non-destructive tests.

The plates were individually immersed in a nitric acid-ferric chloride solution to remove recast metal from the electric discharge machining. Each baseplate was dipped in molten plater's wax (melting range of 180° to 185°F or 355° to 358°K) to fill the channels. By repeated dipping, wax layers were built up to completely fill the channels and manifolds. The excess wax was then trimmed flat to the panel surface using a plexiglass scraping tool. Any residual wax films on the channel lands were removed by scrubbing the plates with a bristle brush and a cleaning compound composed of Alconox (a commercial detergent cleaner) and Shipley's No. 11 Scrub Cleaner (a fine pumice-type compound). The panels were then rinsed and examined for a water break free surface to confirm complete wax removal from surfaces to receive a full electroform bond.

The panels were mounted on the electroforming fixture and the Nickel 200 activated for full bonding by anodic-cathodic treatment in a 30% by weight solution of sulfuric acid. The panels were made anodes at a current density of 50 amperes/ft^2 (4.64 amperes/m^2) for two minutes and cathodes at a current density of 100 amperes/ft^2 (9.29 amperes/m^2.) for two minutes. While still wet with sulfuric acid, the fixture and panels were transferred into a 200 gallon (0.757 m^3.) nickel sulfamate electrolyte with current applied. The fixture was mechanically rotated to assure each plate receiving equal exposure to the nickel anodes and to agitate the cathode film of electrolyte sufficiently to dislodge hydrogen gas which tends to codeposit with nickel during electroforming.

Agitation of the electrolyte was aided by compressed air (oil-less pump) bubbled through the bath and by a high volume pump with an outlet directed at the parts being electroformed. The bath temperature was maintained between 90° and 100°F (305° and 311°K) and the current density held at 30 amperes per square foot (2.79 amperes/m^2.) of cathode surface. A one mil (0.001 inch or 2.54 x 10^{-5} m.) build-up of fully bonded nickel was made. The fixture and panels were withdrawn from the electrolyte in order to make the wax conductive so bridging of nickel over the channels could occur.

The wax was made conductive by the silver spray reduction method. A two nozzle spray gun was used to apply simultaneously a stream of silver nitrate solution and an organic reducing agent such as formaldehyde. On impingement of these two chemicals the silver nitrate is reduced to metallic silver. Since metallic silver on the Nickel 200 surfaces would be a contaminant leading to poor bonds, a way of removing this material without disturbing the conductive layer on the wax was needed. The silver was efficiently removed

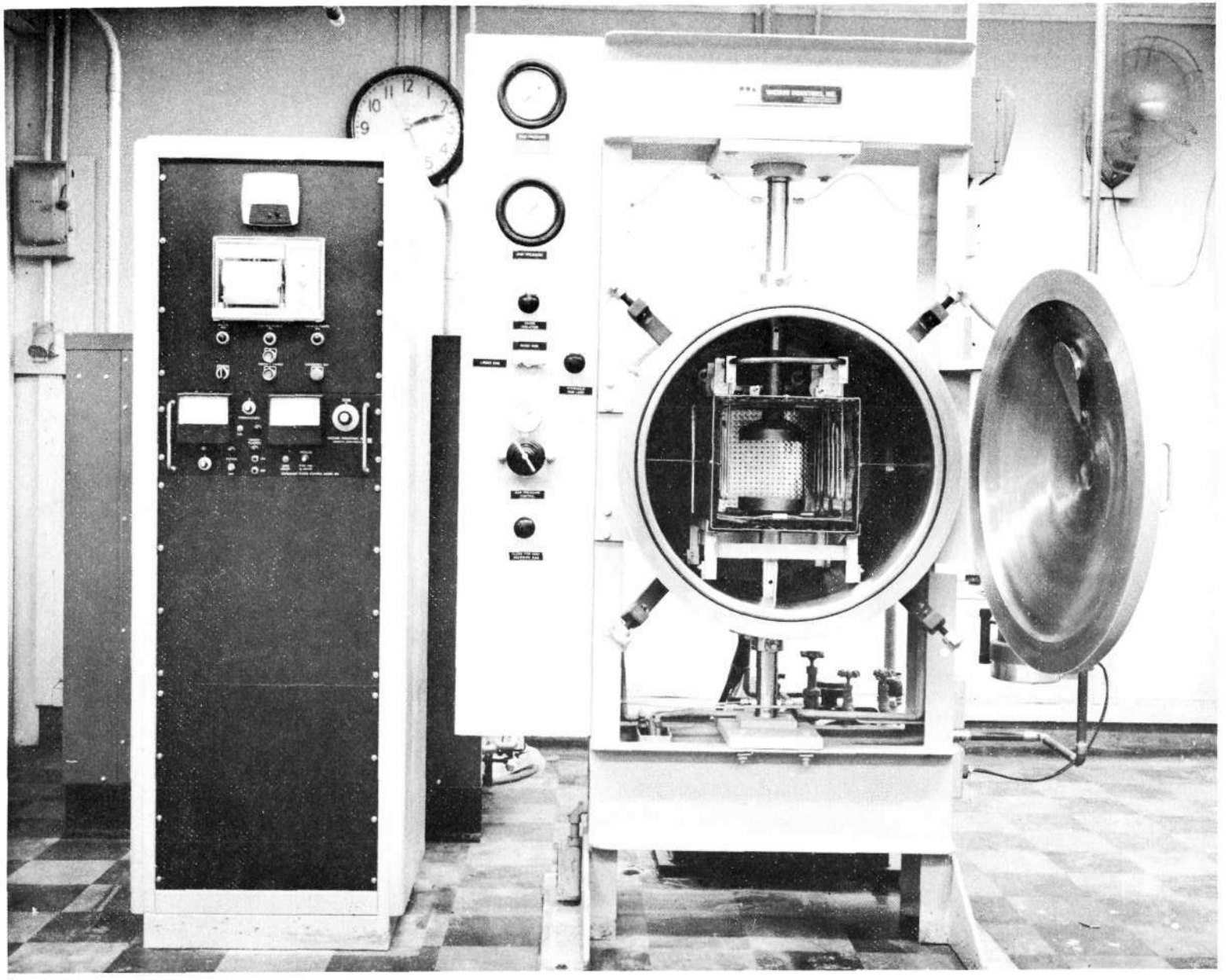

Figure 15. Vacuum Hot Press – Door Open

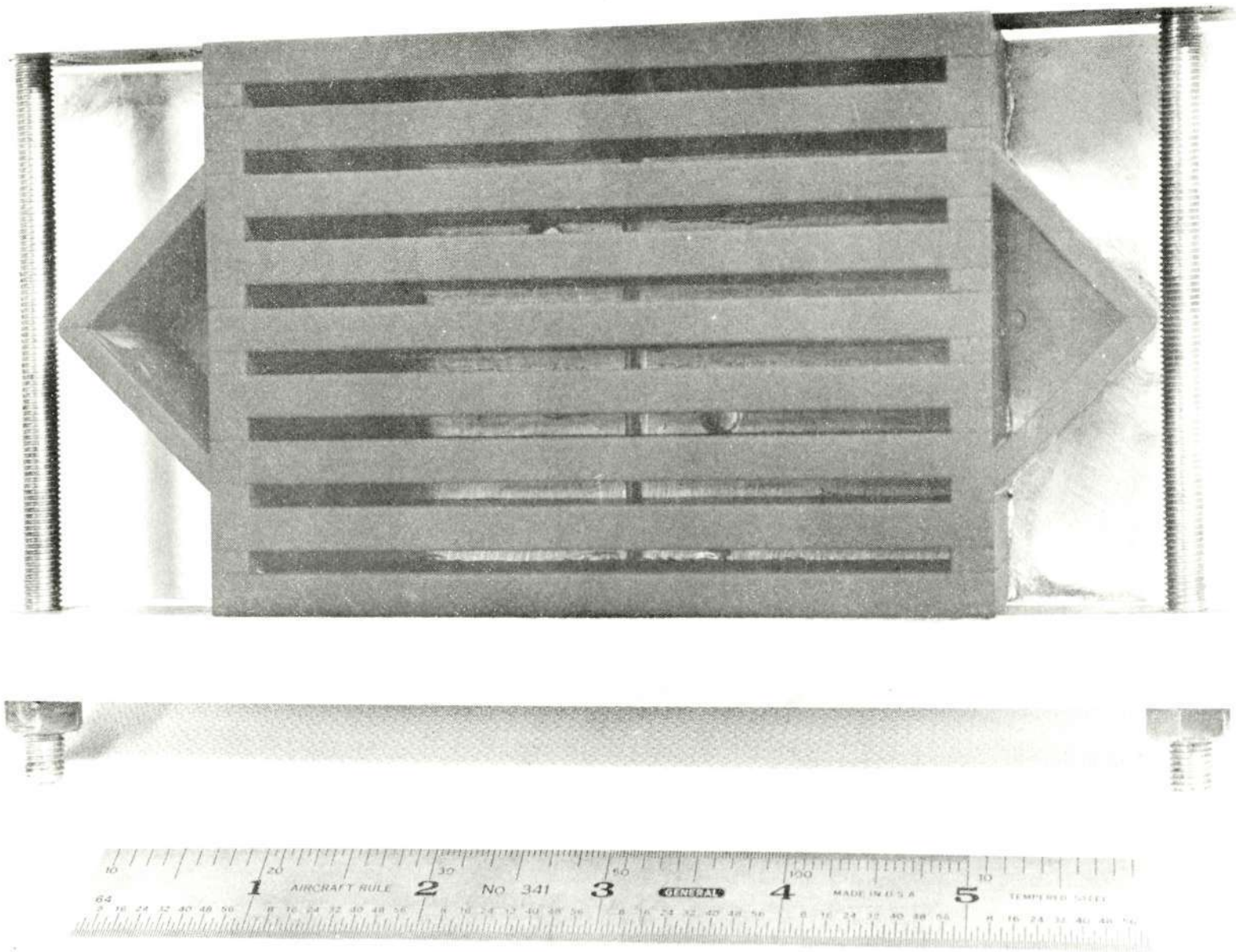

Figure 16. Electrode for Electric Discharge Machining Channel Pattern in Nickel Baseplates
(Scale in Inches)

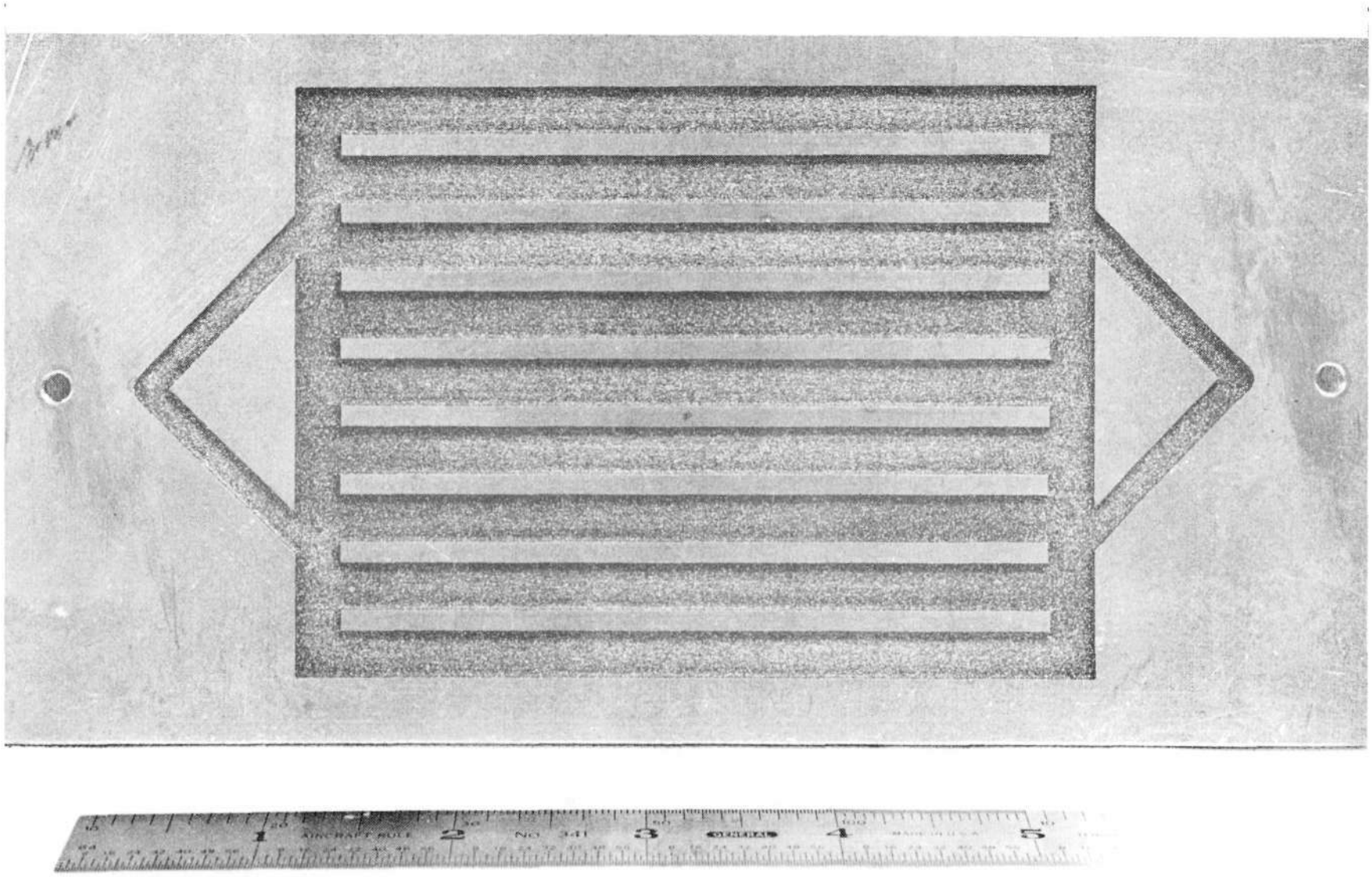

Figure 17. Typical Electric Discharge Machined Nickel 200 Baseplate (Scale in Inches)

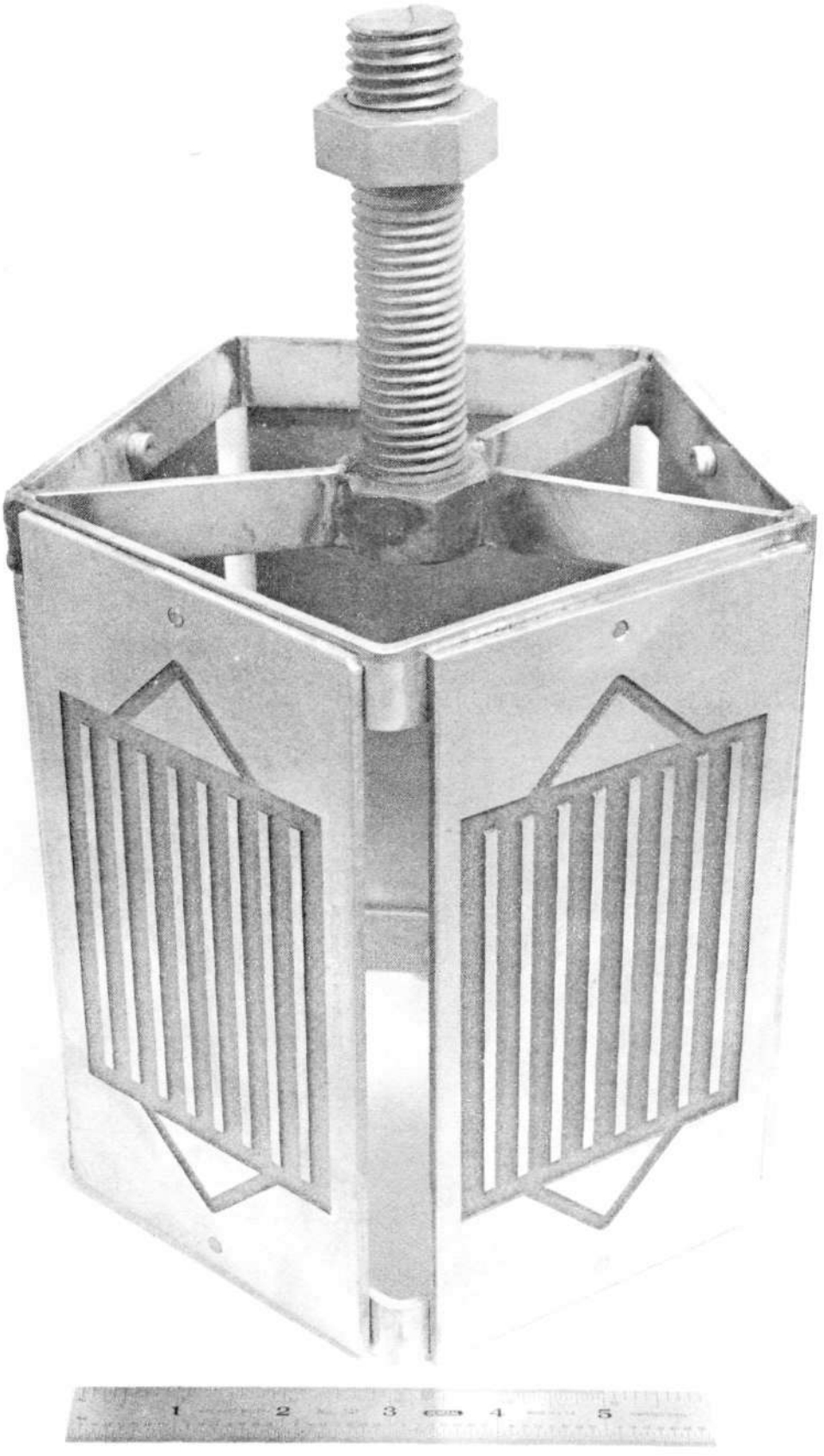

Figure 18. Electroforming Fixture for Deposition on Nickel Coverplates
(Scale in Inches)

from the nickel by reverse plating in a separate tank of nickel sulfamate solution. After rinsing, the parts could then be activated in sulfuric acid and electroformed as previously described.

After electroforming a build-up of 0.025 inch (6.35×10^{-4} m.) and grinding, the panels had the general appearance shown in Figure 19. Thickness of deposit at the bottom was slightly thicker due to length of the anodes employed. The channel pattern is faithfully reproduced throughout the electroforming due to initial conductivity differences in the nickel lands and the conductivized wax. Surface grinding and polishing removed all visible pattern.

The expected condition of porosity in thin deposits over the silver conductivized layer on wax in the channels was found. This was corrected by surface grinding the porous regions, filling the pores with a silver-butyl acetate preparation, dressing excess preparation from the surface, and resuming the electroform operation. After wax removal, the residual preparation was flushed out with solvent. The effectiveness of this procedure was evident when the panels were later exposed to pressures exceeding 1500 psig (10.34×10^6 $N/m.^2$) with no leakage.

The nonbond pattern panels were produced in the same manner as the full bond with the exception of the initial 0.001 inch (2.54×10^{-5} m.) deposit. The Nickel 200 surface was activated and a deposit of 0.001 inch nickel applied. Plater's tape was applied over the lands and wax filled channels. Using a sharp blade and metal straight edge, the pre-determined pattern was scribed into the tape.

After removal of the tape from the non-bond areas, the panels appeared as shown in Figure 20. These plates were etched in nitric acid-ferric chloride solution until 0.0015 inch (3.81×10^{-5} m.) of metal was removed. This exposed the original Nickel 200 surface in a pattern exactly as desired for disbonds. For the ensuing electroform operation, the exposed areas were passivated to prevent bonding by dipping in a sodium dichromate solution. The edges of the passivated areas were scratched with a sharp blade to provide places for "tack" bonding so the disbonds would not inadvertently separate. The etched disbond areas were rebuilt by depositing 0.0015 inch (3.81×10^{-5} m.) of nickel. Masking was removed and the entire panel surface built-up by another 0.001 inch (2.54×10^{-5} m.) to lock the disbonds in place.

After conductivizing (described earlier), the entire nickel surface was electroformed to a thickness of 0.025 inch. (6.35×10^{-4} m.) Appearance of the panel at this point is shown in Figure 21. The bond pattern is readily visible. Roughness exists over the channels due to the silver film and plating conditions maintained in early deposition – low agitation and low current density were employed so as not to disturb the silver bridge over the wax. The pattern and roughness were removed by surface grinding; copious amounts of cooling fluid were applied so as not to disturb the wax. It was desired to leave the wax in the channels until the pattern was removed by grinding, and the surface examined for defects or porosity. This made subsequent repairs or build-up easier.

The weak bond panels were made exactly as the non-bond panels with the exception that the weak bond regions were not passivated. Instead, the etched weak bond pattern in the 0.001 inch (2.54×10^{-5} m.) build-up was subjected only to a dip in 30% by weight sulphuric acid (no current application), and the plates were transferred to the electroforming bath with no current applied. After a delay of two minutes, direct current was applied to start electroforming. The length of delay in starting the plating is proportional to the strength of the bond obtained.

The electroformed-thermally diffused panels were produced by the same processes as the electroformed test panels. After electroforming, the panels were examined by ultrasonics for reference data before thermal treatment. The thermal cycle consisted of heating in vacuum to 1800°F (1255°K) for one-half hour.

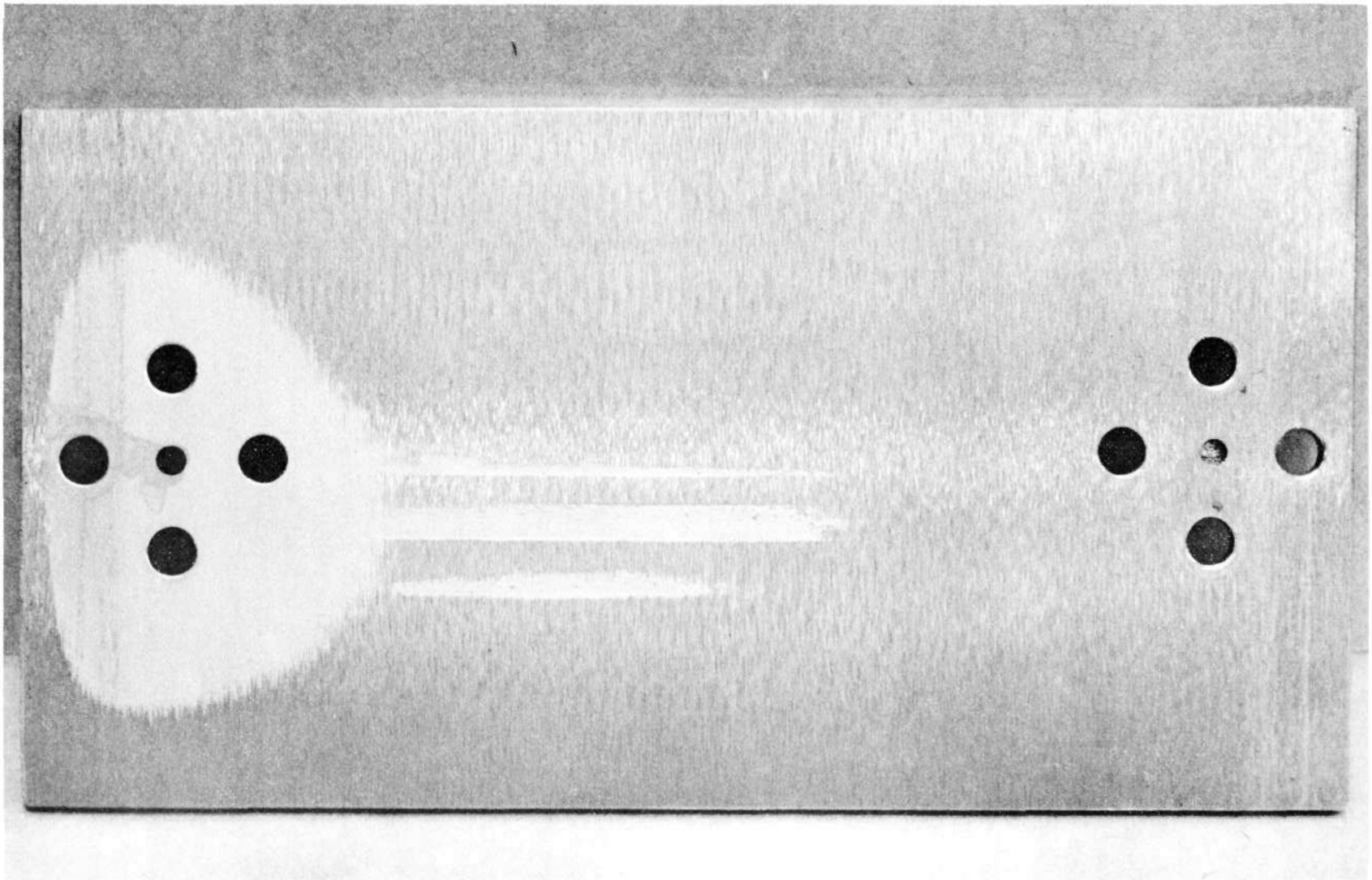

Figure 19. Typical Electroformed Plate After Initial Surface Grinding to Remove Edge Build-up

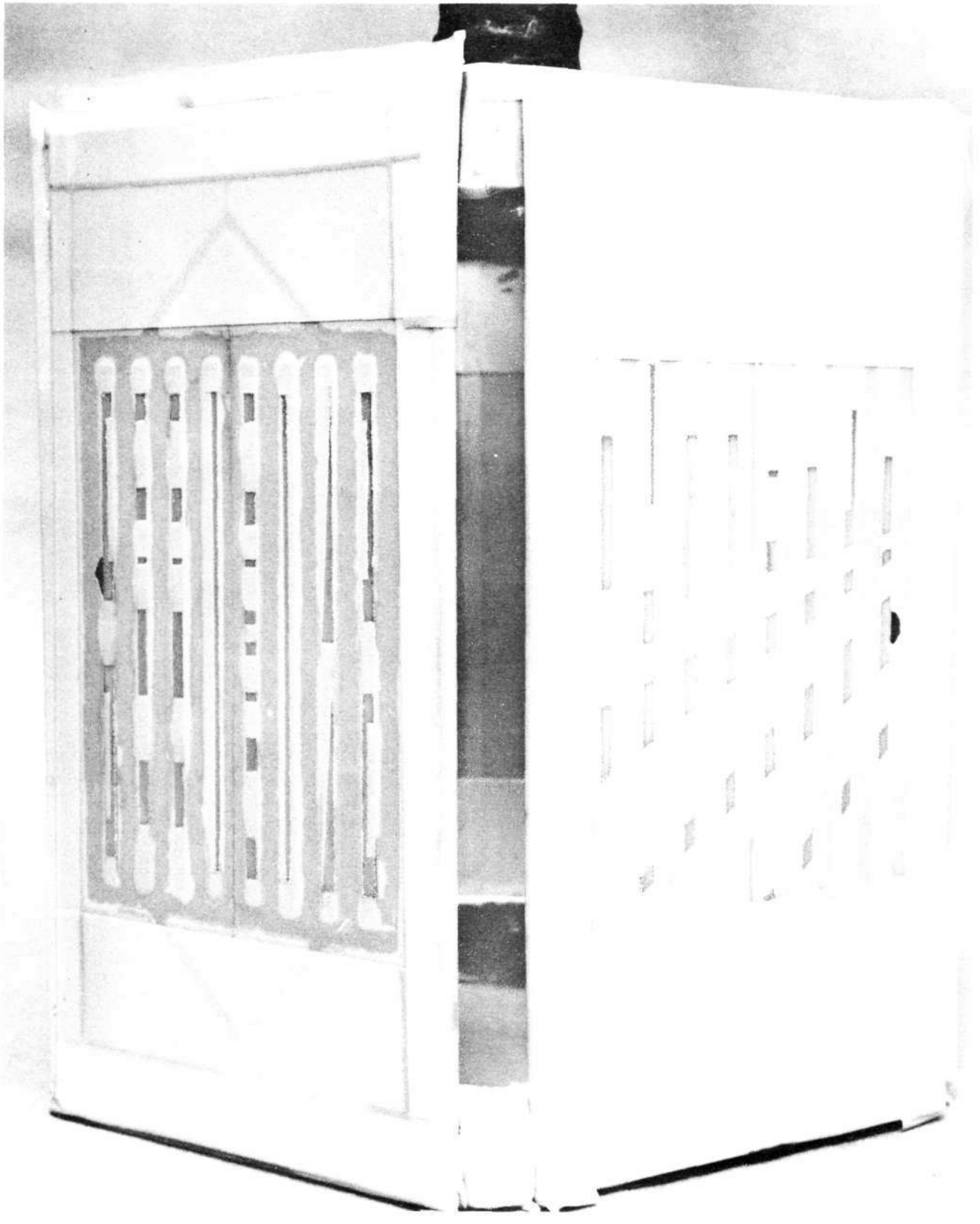

Figure 20. Masking Patterns for Electroforming Weak and Disbond Area on Channel Lands

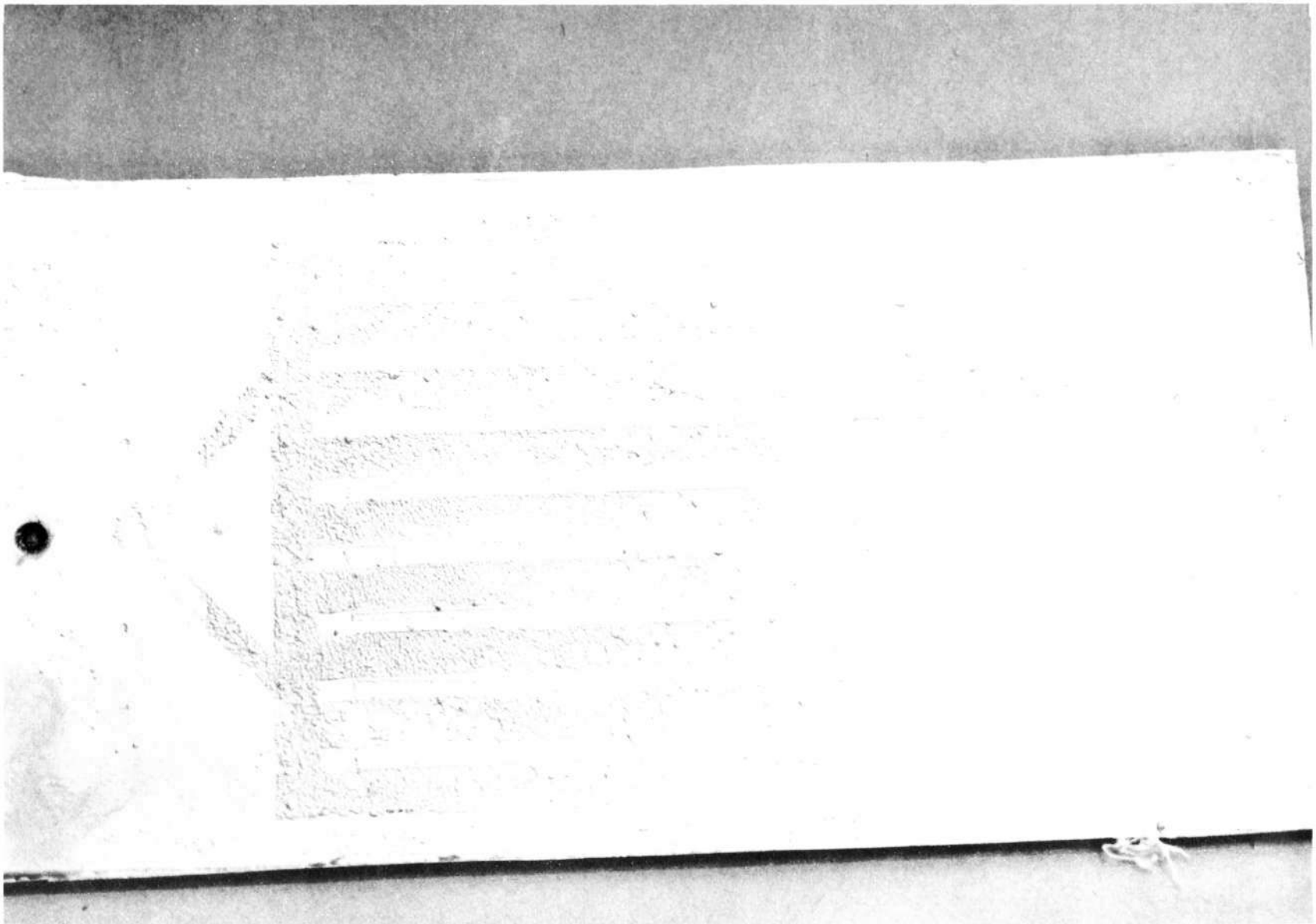

Figure 21. Appearance of Bond Patterns After 0.0025 Inch (6.35×10^{-4} m.) Deposit

F. FABRICATION OF BRAZE BONDED TEST SPECIMENS

Fifteen Nickel 200 baseplates and a similar number of Inconel 600 coverplates were sheared from 0.125 inch (3.17×10^{-3} m.) thick sheet stock. All material was in the annealed and pickled condition. 0.125 inch (3.17×10^{-3} m.) diameter holes were drilled in the top right corners of each Inconel cover plate to provide a means of suspending plates in chemical cleaning and plating solutions later in the specimen fabrication.

It was observed that all baseplates and coverplates contained variations in surface flatness after shearing. This same condition was noted in the preliminary work to determine strength values for various bond integrities. The additional operation of electric discharge machining the channels and manifolds introduced increased flatness deviation. This required modification of the previously developed procedure for obtaining satisfactory flatness as follows:

(1) Stress relief anneal sheared plates.

(2) Electric discharge machine (Nickel 200 plates only).

(3) Chemically etch plates in nitric acid - ferric chloride solution to remove all recast metal and surface contaminants.

(4) Repeat the stress relief anneal.

(5) Surface lap the plates on both sides.

(6) Re-etch chemically to remove any surface contamination.

Resulting flatness variation in Nickel 200 and Inconel 600 ranged from about 0.001 inch to 0.006 inch (2.54×10^{-5} m. to 1.52×10^{-4} m.).

Copper foil of 0.003 inch (7.62×10^{-5} m.) thickness was cut to the Nickel 200 plate size and brazed successfully. To produce the channel patterns, the copper foil was coated with a photoresist, Figure 22. After curing, a photomaster of the channel and manifold pattern was applied over the photoresist and exposed, Figure 23. Figure 24 illustrates several foil sections of various bond patterns after developing of the exposed photoresist. The etching operation is illustrated in Figure 25.

Tabs were incorporated in the pattern design to maintain position of individual copper sections of the pattern after etching of the foil. Figure 26 shows patterns for the full bond (being held), weak bond, and non-bond (adjacent to the measuring scale). It will be noted that an inch long detail pattern of bond discontinuities exists on the weak and non-bond patterns. This is for the purpose of evaluating NDT method sensitivity to flaw size.

The photofabricated copper foil pattern was applied over the Nickel 200 baseplate so as to line up copper braze with the channel lands. For this purpose, reference holes were drilled in the nickel and etched in the copper, Figure 27. An Inconel cover plate was placed over the braze foil, Figure 28. Typical braze patterns for various bond integrities are shown in Figures 29 through 32.

The brazing was conducted in a vacuum furnace. A baseplate and dead weight of Alloy D6AC were used to sandwich the plates to be brazed. Aluminum oxide coated stainless separator sheets were used between braze specimens to prevent undesired bonding. The Alloy D6AC was drilled through the sides to accommodate thermocouples. This assured that the entire braze pack could be brought to a temperature of

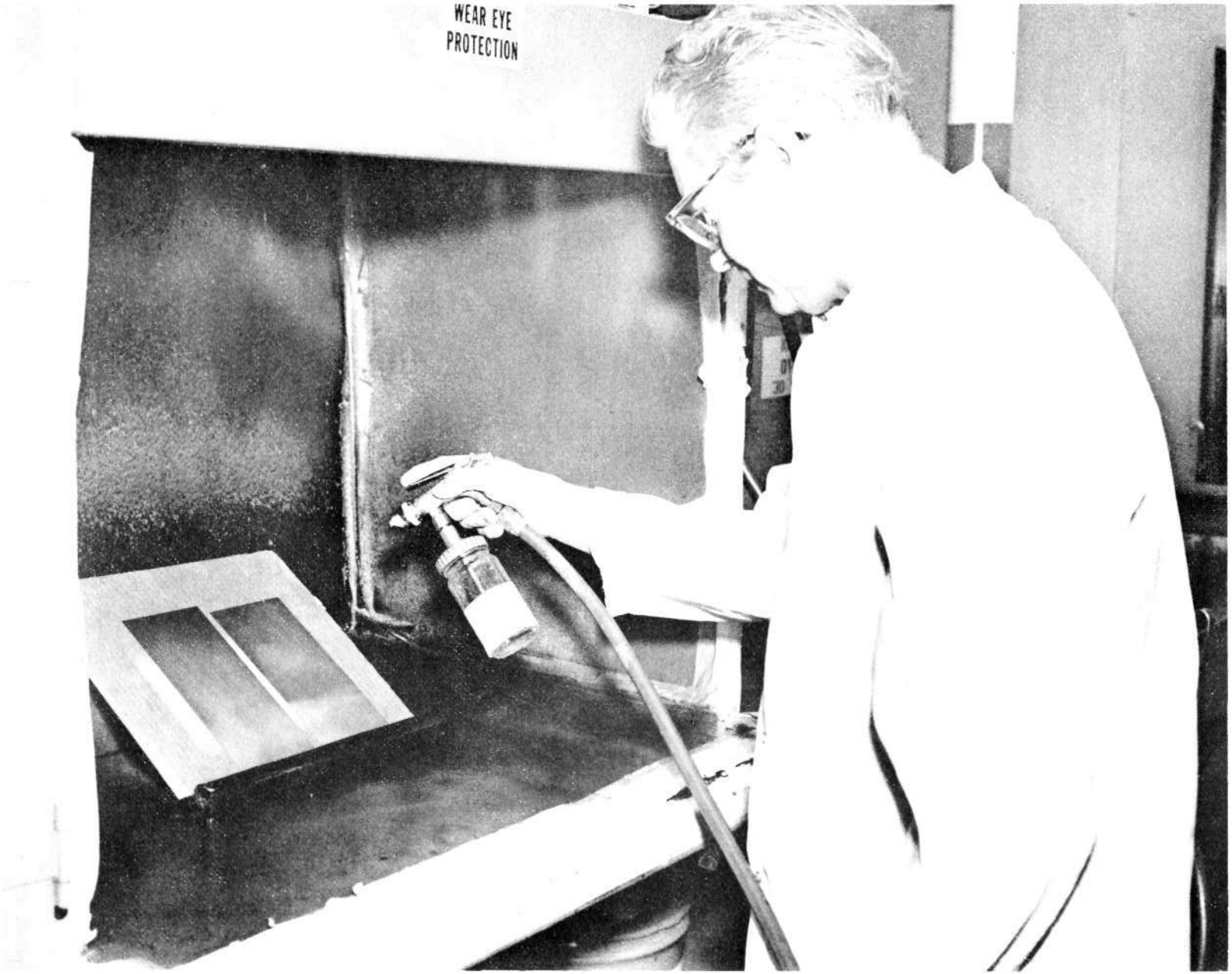

Figure 22. Coating Braze Foil with Photoresist for Photofabrication of Bond Patterns

Figure 23. Application of Bond Pattern Photomaster for Exposure of Photoresist on Braze Foil

Figure 24. Development of Photoresist Bond Patterns for Brazing

Figure 25. Chemical Etching of Braze Foil Bond Flow Patterns

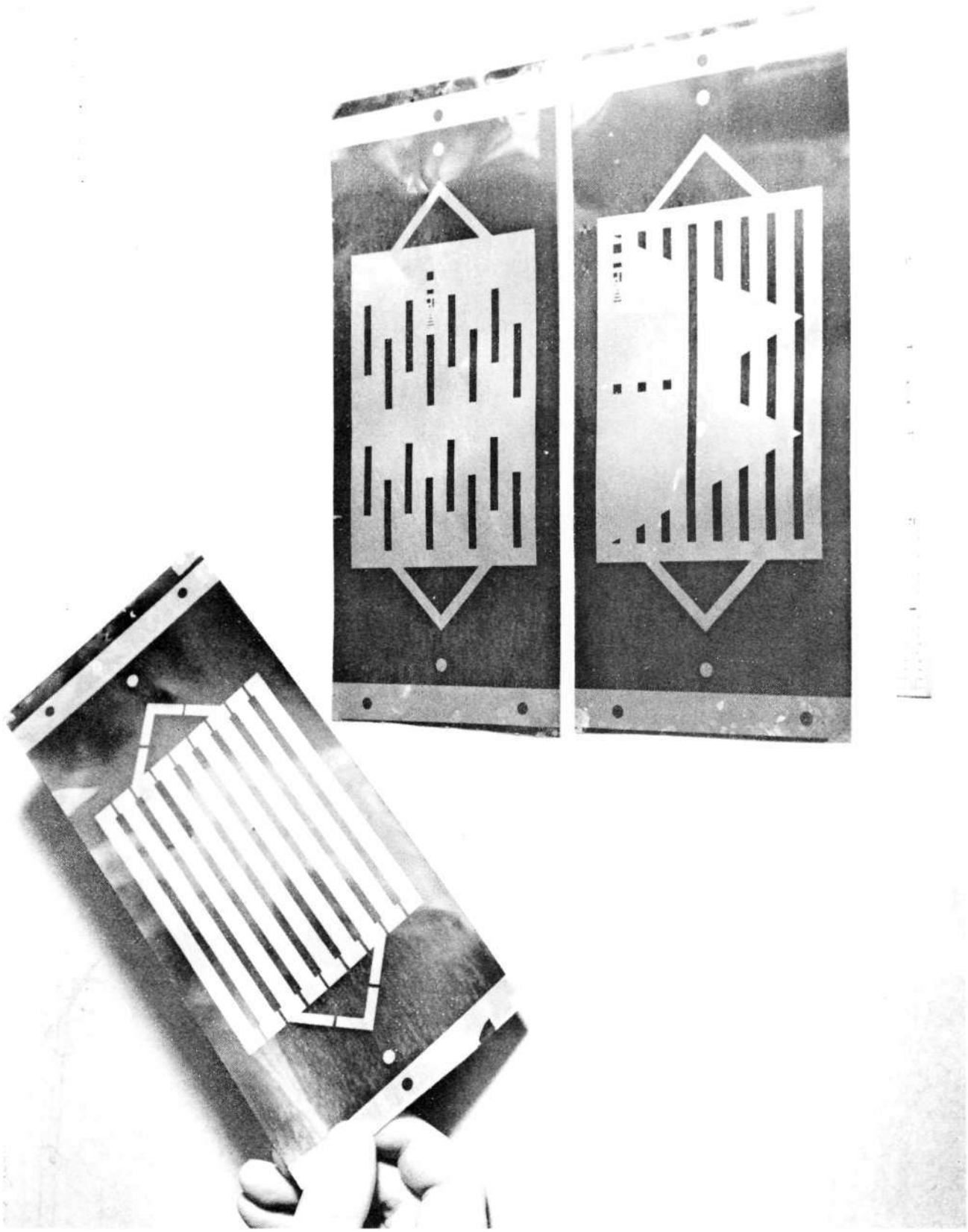

Figure 26. Full, Weak, and Non-bond Braze Foil Patterns Before Chemical Etching

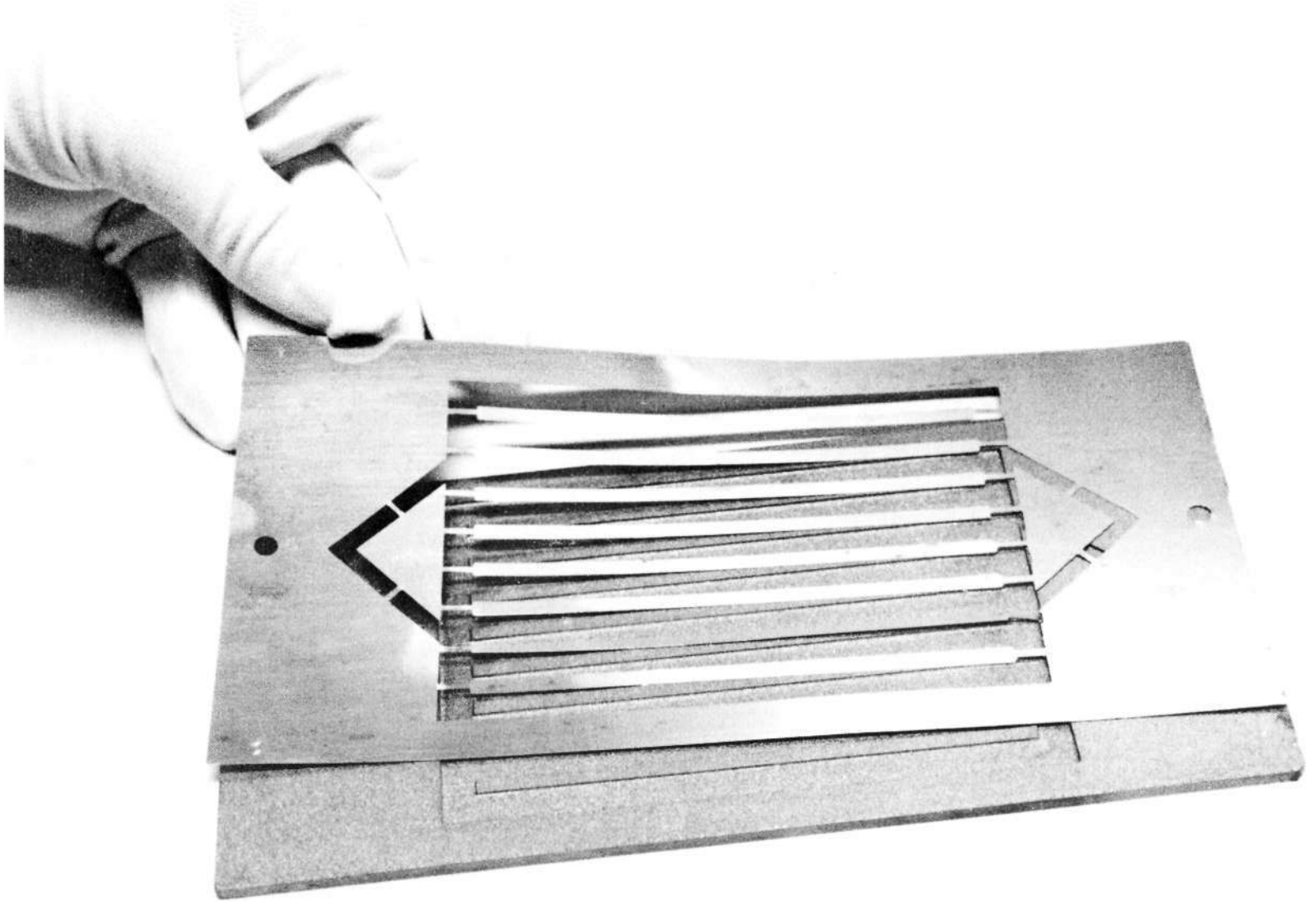

Figure 27. Photofabricated Copper Braze Pattern Located on Nickel Baseplate Using Reference Holes

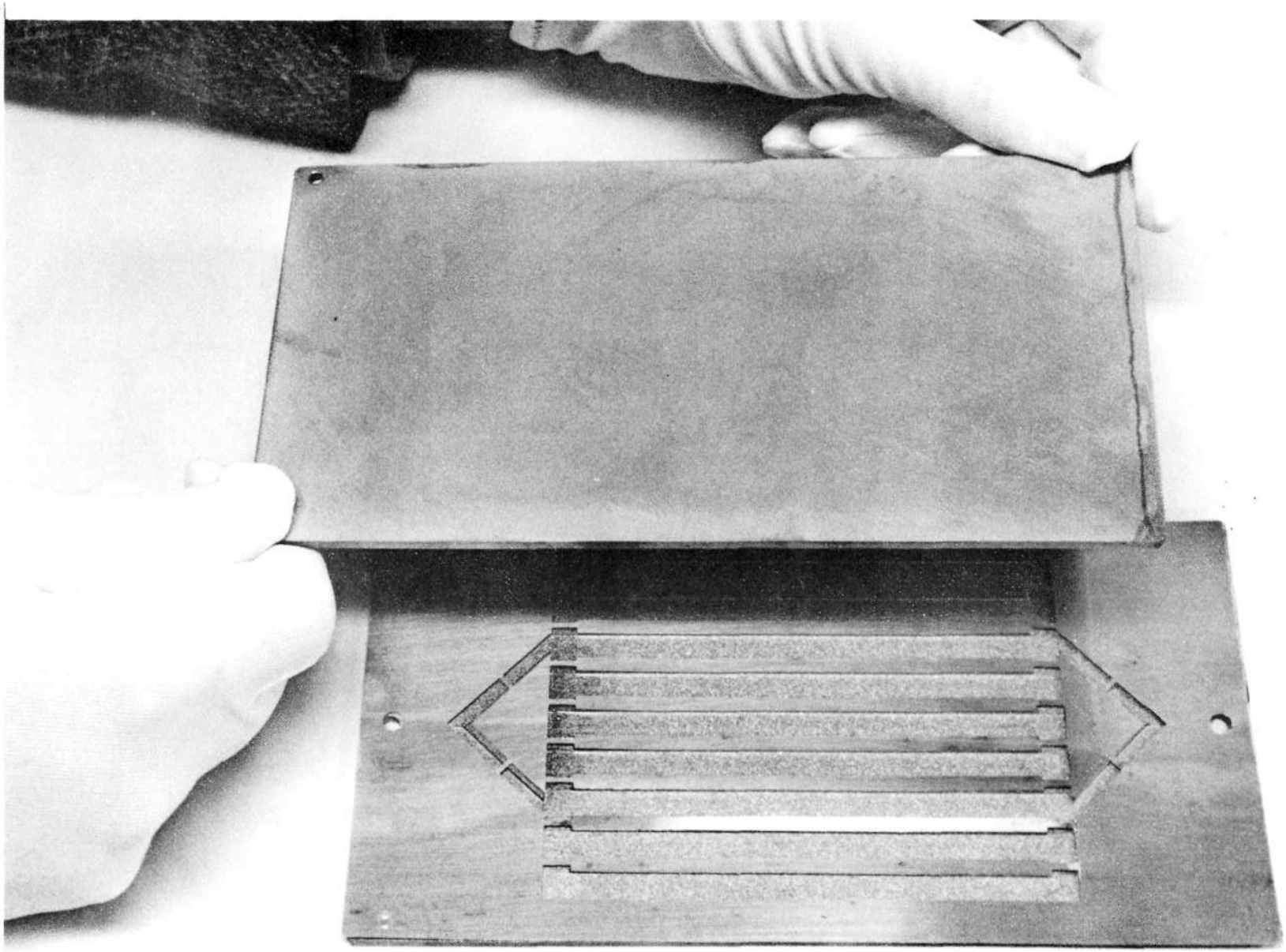

Figure 28. Assembly of a Full Bond Braze Test Panel

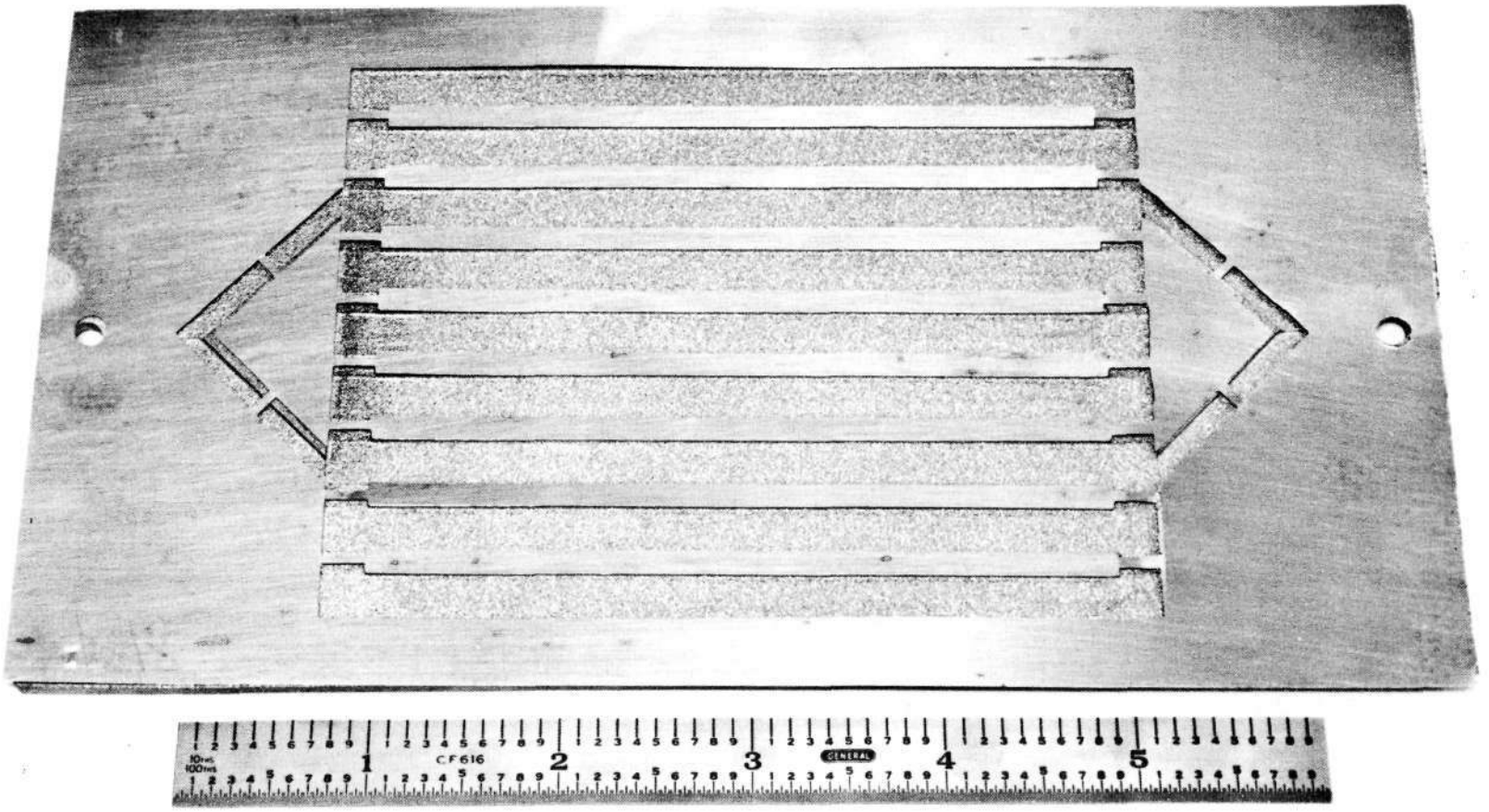

Figure 29. Etched Full Bond Braze Foil Pattern on Nickel 200 Baseplate
(Scale in Inches)

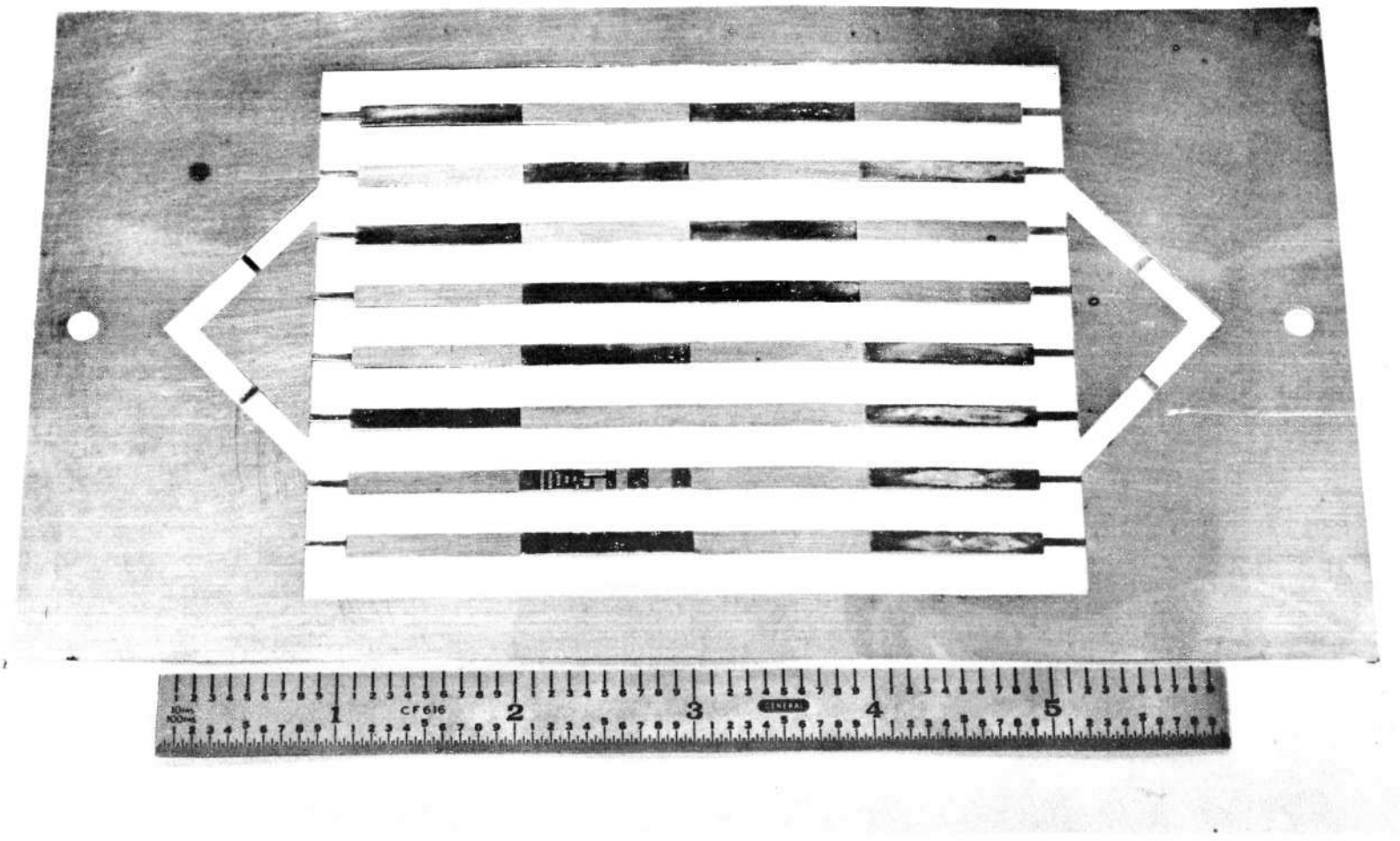

Figure 30. Etched Weak Bond Braze Foil Pattern No. 1 on Nickel 200 Baseplate
(Scale in Inches)

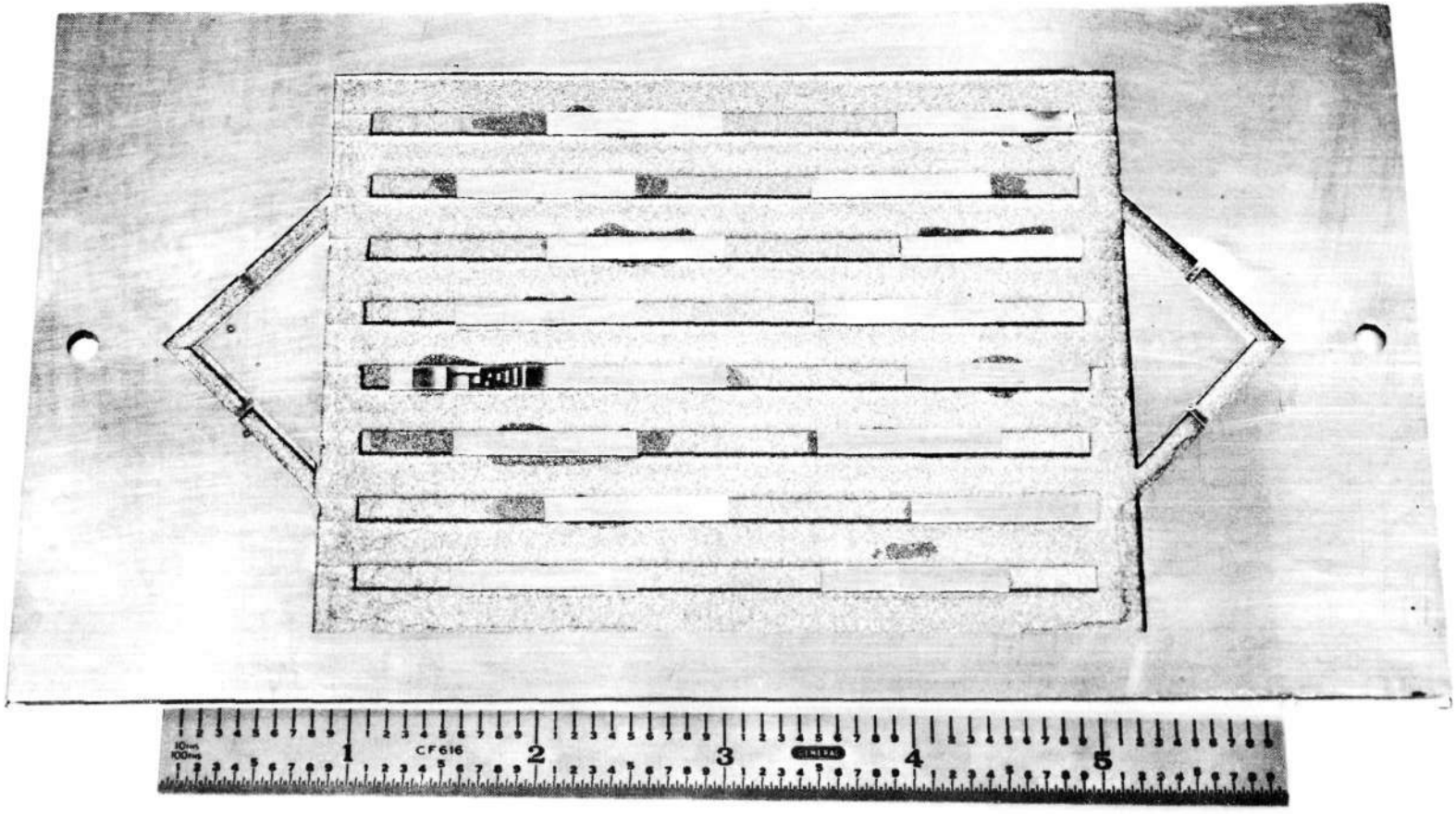

Figure 31. Etched Weak Bond Braze Foil Pattern No. 2 on Nickel 200 Baseplate
(Scale in Inches)

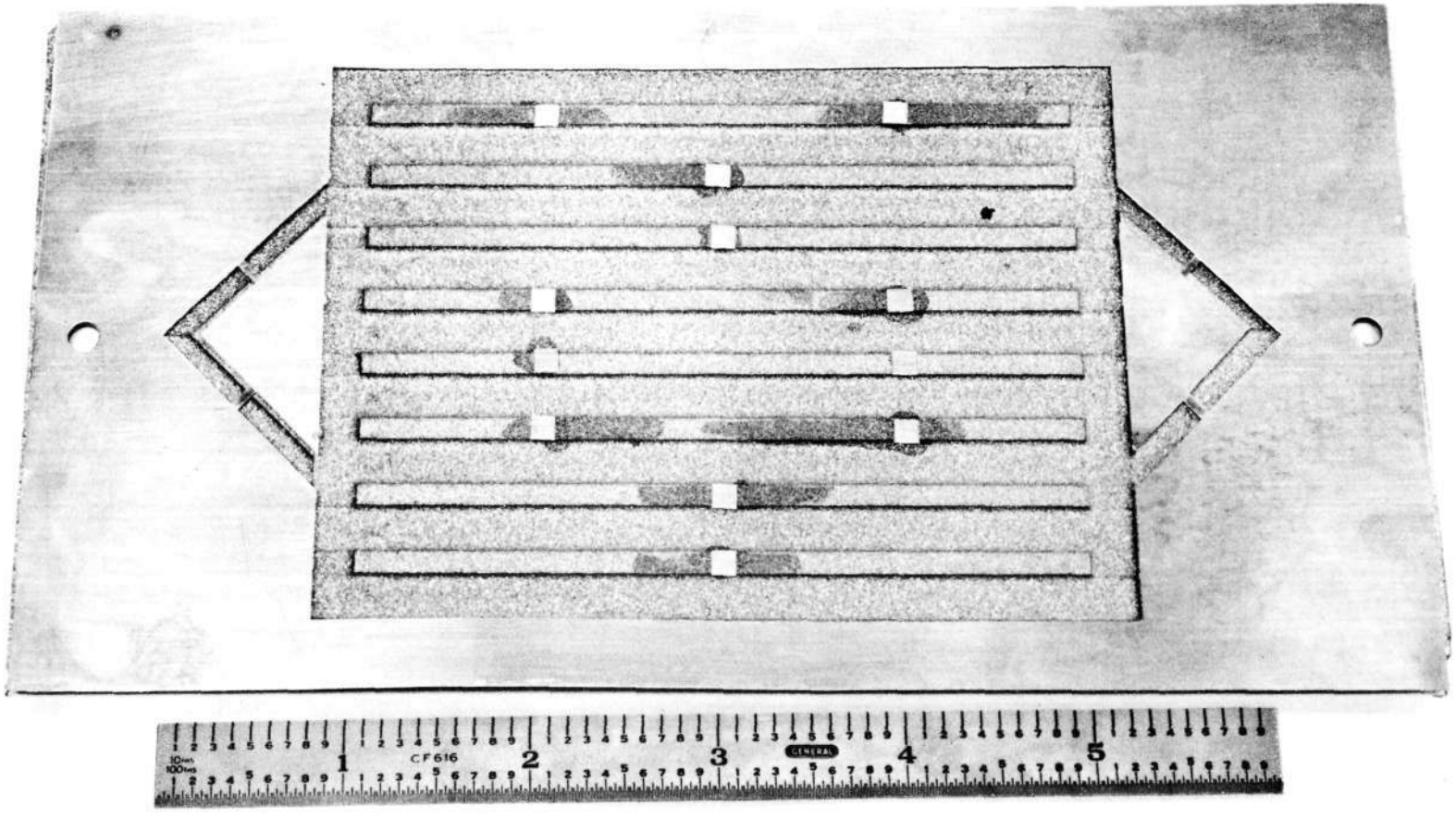

Figure 32. Etched Non-Bond Braze Foil Pattern on Nickel 200 Baseplate
(Scale in Inches)

1900°F (1311°K) and quickly elevated to 2000°F (1366°K) to convert the copper to an alloy with the nickel and Inconel. The braze furnace is shown in Figure 33.

Blockage of channel passages by braze run-out was checked by pressurizing one of the two fitting ports after filling the other with water. No blockage was expected due to the resistance of the copper nickel alloy to flow. However, some run-out in the vicinity of the pressurization port (at one end usually) was encountered. This proved no serious problem because the exact extent of blockage could be determined by ultrasonic "C" scan. The plugged end was placed down in a tank of hot water and the air in the channels was displaced with liquid for subsequent hydrostatic tests during non-destructive evaluation.

G. FABRICATION OF DIFFUSION BONDED TEST SPECIMENS

Surface preparation of the Nickel 200 and Inconel 600 plates was the same as used for brazing. However, the weak and nonbond patterns were produced on the Nickel 200 baseplates by chemical etching to relieve the channel lands at predetermined regions. The photofabrication process was again employed to produce the flaw patterns which would permit selective acid attack on the surface to be removed to a specific depth of 0.003 inch to 0.004 inch. (7.62×10^{-5} m. to 10.16×10^{-5} m.) The etching operation is shown in Figure 34.

The weak bond patterns are illustrated in Figures 35, 36, and 37. The baseplates in these pictures have the photo resist applied, exposed, and developed to allow etching to occur in selected areas. Figure 38 shows the nonbond pattern.

The bottom platen of the diffusion bonding hot press was covered with an aluminum oxide coated steel plate as a diffusion barrier. Over this was placed a Nickel 200 channeled baseplate with exposed channels facing up. The Inconel coverplate was placed on the Nickel 200 and aligned by means of referencing holes drilled at end locations where subsequent pressure fixture bolts would be inserted.

Another aluminum oxide coated separator was placed over the Inconel and the entire assembly was centered on the bottom furnace platen. The top platen was lowered to make contact with the assembly, but no pressure was applied to the ram.

The furnace was closed and evacuated to a vacuum of 5×10^{-4} Torr (6.665×10^{-2} N/m.^{2}). At a temperature of 1000°F, a load of 750 psig (5.171×10^6 N/m.^{2}) was applied on the parts being bonded. The bonding was performed at 2100°F (1422°K) for a three hour holding period at this temperature

H. POST BOND PROCESSING AND DISCUSSION

During fabrication of the electroformed panels, it was necessary to stop the deposition process at intervals to remove edge build-up. This was performed by grinding to obtain a flat surface considered desirable in ultrasonic and holographic inspection. The bondline was expected to be out-of-flat due the the variation in surface flatness of the nickel 200 baseplates. Flatness variation diagonally across the electroformed panels was as high as 0.020 inch (5.08×10^{-4} m.) in some cases. This contributed to difficulty in obtaining a desirable gate setting to determine flaws ultrasonically on the electroformed panels with only 0.020 inch (5.08×10^{-4} m.) of deposit build-up. As the deposit thickness was increased, this effect was of less significance.

All electroformed panels were ultrasonic examined after a build-up of 0.020 inch to 0.030 inch (5.08×10^{-4} m. to 7.62×10^{-4} m.) of nickel as a coverplate. Reference panel No. 3 (full bond) and 8 (weak bond) were subjected to a pressure of approximately 1270 psig (8.76×10^6 N/m.^{2}) for determination of

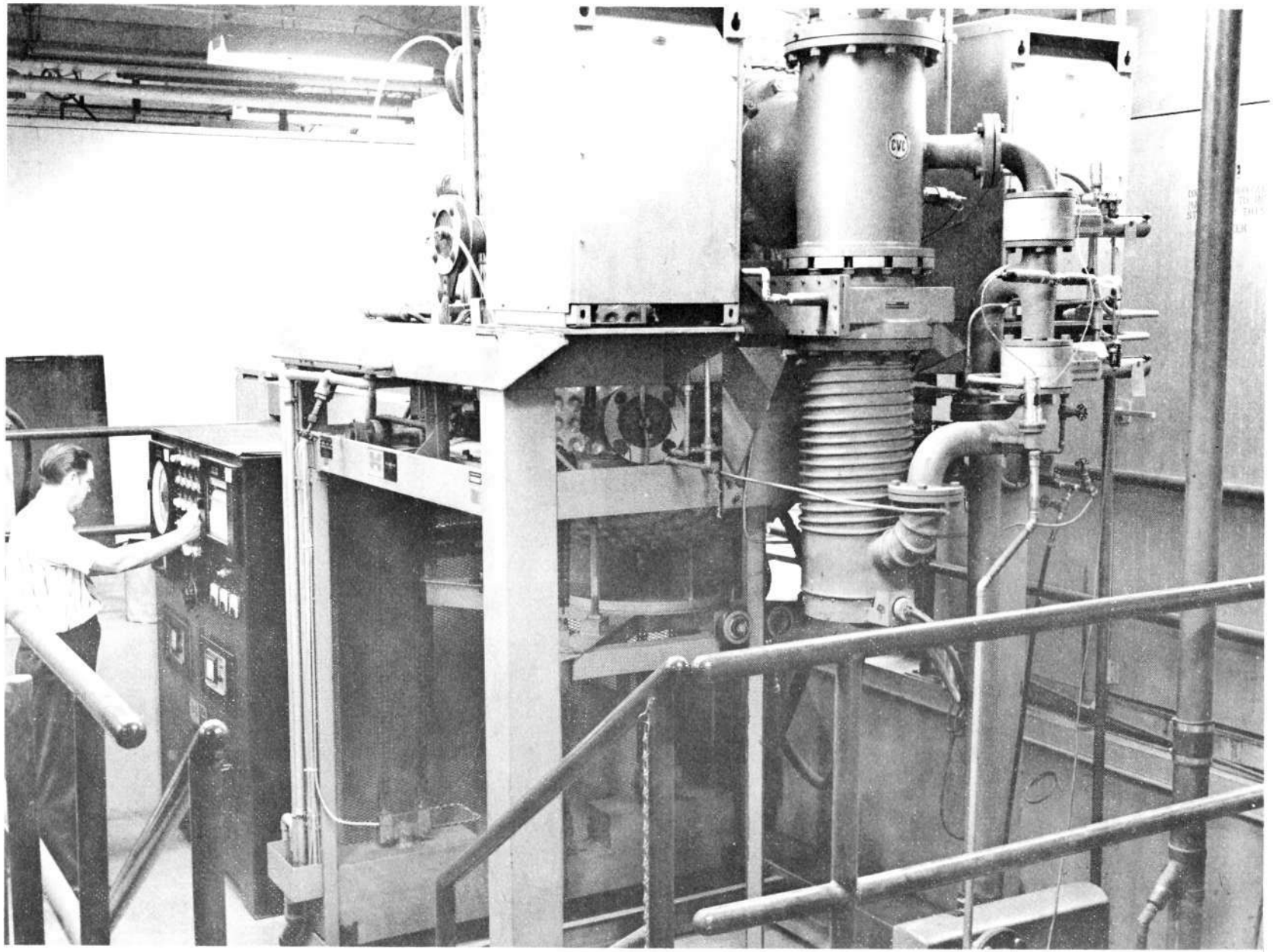

Figure 33. Vacuum Brazing Furnace

Figure 34. Chemical Etching to Produce Diffusion Bond Pattern in Nickel 200 Baseplate

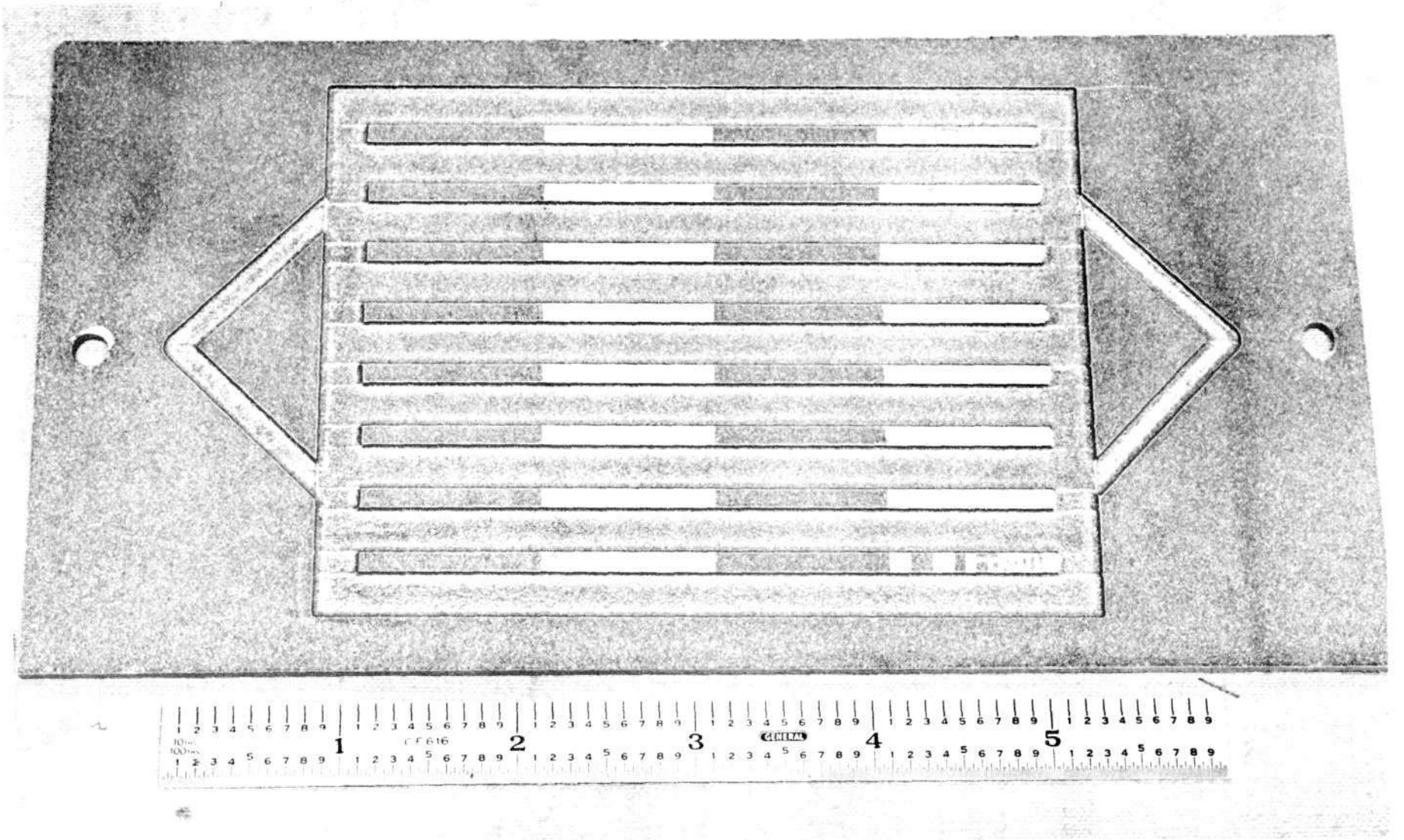

Figure 35. Weak Diffusion Bond Pattern No. 1 on Baseplate Before Etching
(Scale in Inches)

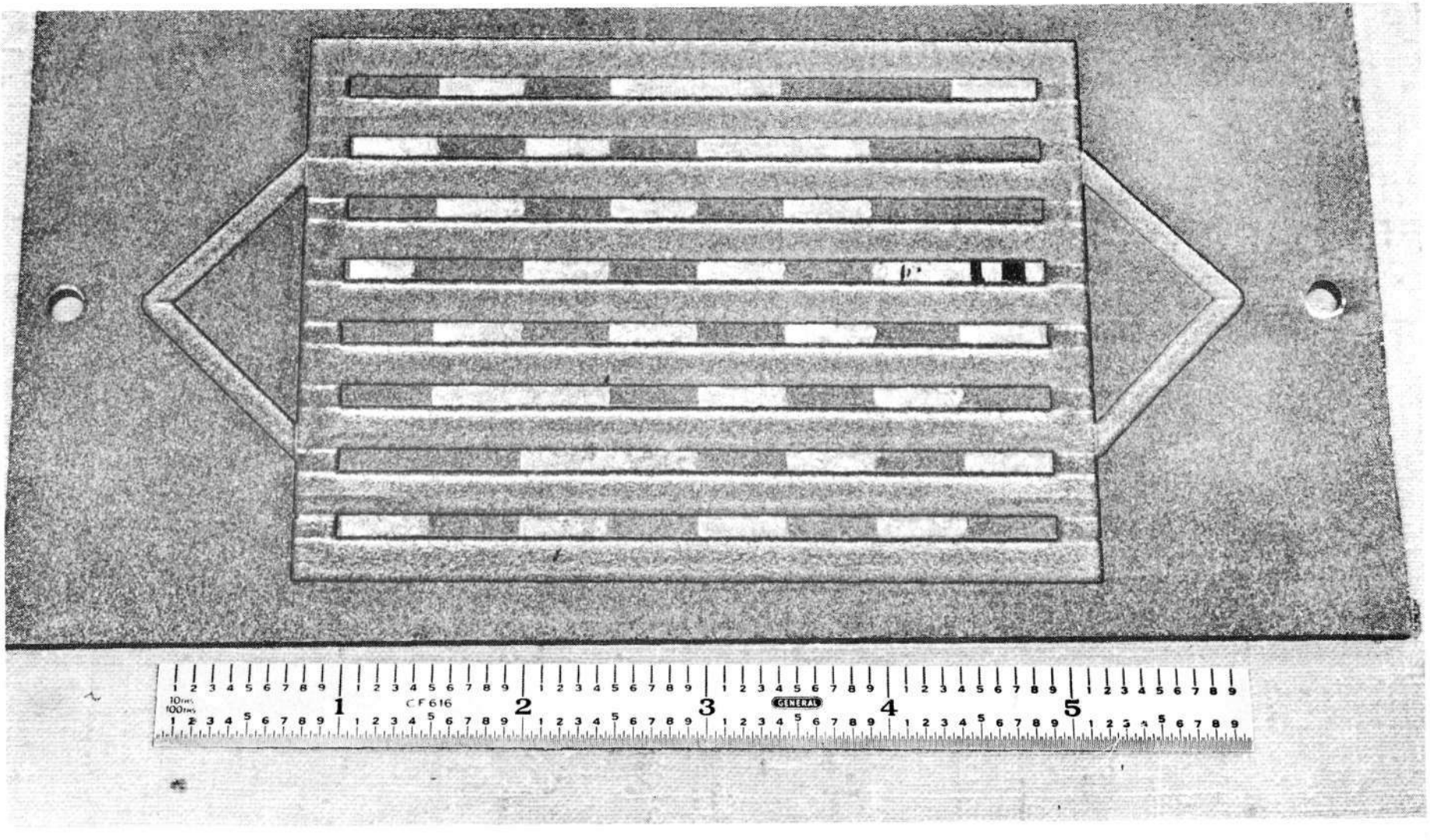

Figure 36. Weak Diffusion Bond Pattern No. 2 on Baseplate Before Etching
(Scale in Inches)

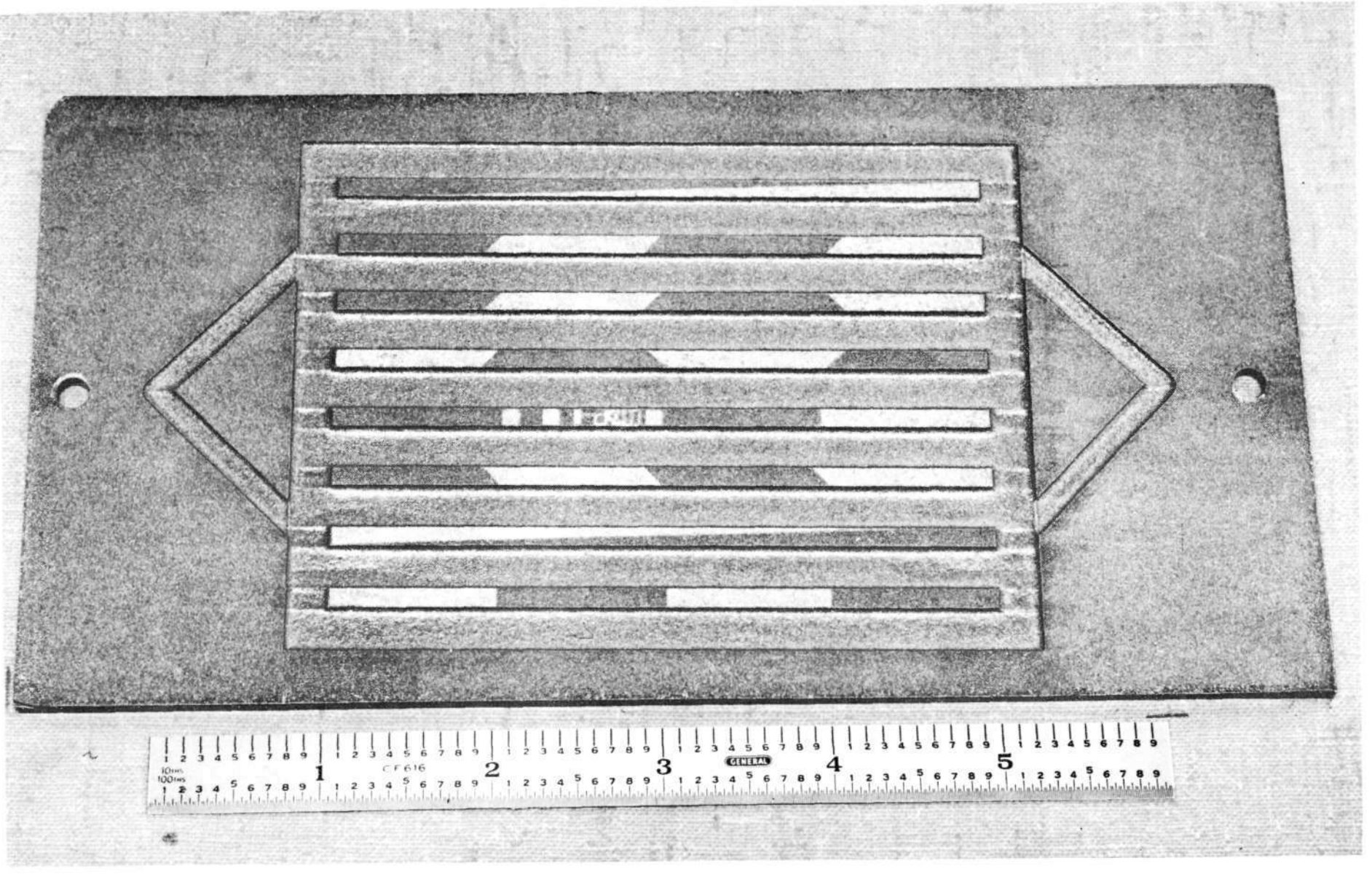

Figure 37. Weak Diffusion Bond Pattern No. 3 on Baseplate Before Etching
(Scale in Inches)

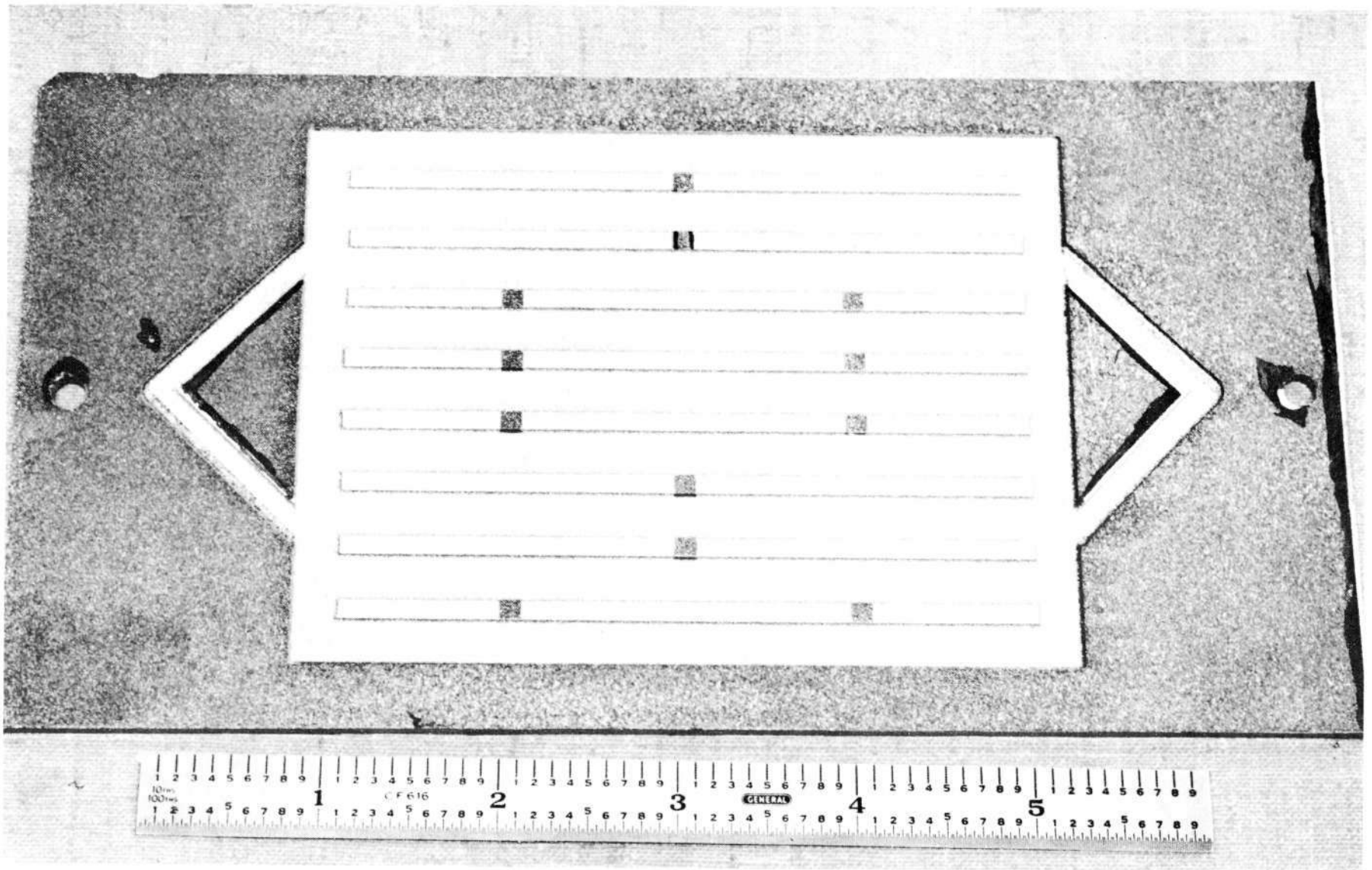

Figure 38. Diffusion Nonbond Pattern on Baseplate Before Etching
(Scale in Inches)

acoustic emission response. Panel No. 3 developed a bulge next to Land No. 8. Panel No. 8 emitted noise and developed pin-hole leakage in the channel next to Land No. 8. The bulge was pressed flat on Panel No. 3 and an electroform repair corrected the leakage on Panel No. 8. Re-examination of both panels by ultrasonics gave no indication of detectable defect propagation. Since Panel No. 8 was a weak bond reference panel which may have been influenced by the pressure testing, it was decided to change the reference designation to a companion specimen, Panel No. 2.

During the surface grinding operations, Panel No. 9 was inadvertently ground out-of-parallel due to a fixturing problem. This panel was successfully repaired by electroforming and tested after full build-up to about 0.060 inch (1.52×10^{-3} m.) of nickel as coverplate.

Residual stress from the electrodeposited nickel also contributed to out-of-flatness and subsequent thickness variations after flat surface grinding. This stress is tensile in nature and normal for nickel electrodeposits from electrolytes not containing stress reducers. Thickness and flatness variability could have been corrected by stress relieving, but this was undesireable due to possible thermal changes to planned bond integrities. The resulting thickness profile (diagonally across the panel face) for each electroformed panel is furnished in Table VIII.

After testing at a build-up of 0.060 inch (1.52×10^{-3} m.) of nickel, Panel No. 11 was electroformed to a final thickness of 0.110 inch (2.79×10^{-3} m.) for comparison with brazed and diffusion bonded panels having coverplates of similar thickness.

The electroformed-thermally diffused panels underwent blistering during the thermal treatment at 1800°F (1255°K). This effect was similar to laminations occurring at plating restarts and possible reasons for this condition are discussed in Section V.

Braze bond patterns were successfully achieved as planned. Several panels exhibited minor variations or defects not planned. However, these panels provided useful information in the investigation. Panel Nos. 23 and 33 leaked in the pressure fitting regions due to inadequate braze flow. Silver soldering, at a temperature below that at which brazing occurred, was successful in correcting this condition.

The temperature at which brazing was performed resulted in some grain growth in the Nickel 200. This would account for premature yielding of the channel webs during pressurization for nondestructive evaluation. In order to minimize the effect of this condition on performance of holographic evaluation and to enable destructive evaluation to be conducted, the Nickel 200 baseplates were strengthened by electroforming a full bond layer of higher strength nickel on the backside of each brazed panel. There were no indications that this operation adversely affected ultrasonics, holography, or acoustic emission results.

In some instances, braze flow was greater than anticipated and planned non-bond or weak bond regions had greater bond strength than desired. This did not appear to be a serious problem because the metallographic analysis and nondestructive evaluation results generally confirmed the true bond condition in existence.

The coverplate and baseplates for brazing contained previously discussed flatness variations corrected to a serviceable condition by grinding and lapping. The resulting plate parallelism was varied and total panel thicknesses after brazing and electroforming structural backing are shown in Table IX.

Planned bond patterns were achieved on the diffusion bonded panels, but to a lesser degree than on the other methods. This is due to the difficulty of maintaining nonbond without the use of diffusion stop-off compounds. Such compounds were purposefully avoided to prevent undesireable detection by the nondestructive methods under evaluation.

TABLE VIII
FINAL THICKNESS PROFILE OF ELECTROFORMED TEST PANELS*

Test Panel No.	Nickel 200 Base Plate Thickness						Electroformed Cover Thickness					
	Position						Position					
	A		B		C		A		B		C	
	Inches	Meters	Inches	Meters	Inches	Meters	Inches	Meters	Inches	Meters	Inches	Meters
1	0.129	0.00328	0.129	0.00328	0.129	0.00328	0.059	0.00150	0.063	0.00160	0.062	0.00157
2	0.128	0.00325	0.128	0.00325	0.127	0.00323	0.066	0.00168	0.068	0.00173	0.063	0.00160
3	0.128	0.00325	0.129	0.00328	0.130	0.00330	0.065	0.00165	0.058	0.00147	0.064	0.00163
4	0.130	0.00330	0.130	0.00330	0.130	0.00330	0.058	0.00147	0.061	0.00155	0.063	0.00160
5	0.129	0.00328	0.129	0.00328	0.128	0.00325	0.060	0.00152	0.065	0.00165	0.061	0.00155
6	0.131	0.00333	0.129	0.00328	0.130	0.00330	0.063	0.00160	0.067	0.00170	0.063	0.00160
7	0.127	0.00323	0.125	0.00317	0.126	0.00320	0.062	0.00157	0.069	0.00175	0.062	0.00157
8	0.130	0.00330	0.130	0.00330	0.130	0.00330	0.066	0.00168	0.062	0.00157	0.064	0.00163
9	0.128	0.00325	0.128	0.00325	0.128	0.00325	0.062	0.00157	0.069	0.00175	0.061	0.00155
10	0.128	0.00325	0.129	0.00328	0.129	0.00328	0.055	0.00140	0.056	0.00142	0.056	0.00142
11	0.128	0.00325	0.127	0.00323	0.127	0.00323	0.060	0.00152	0.065	0.00165	0.067	0.00170
12	0.128	0.00325	0.128	0.00325	0.128	0.00325	0.058	0.00147	0.059	0.00150	0.057	0.00145
13	0.126	0.00320	0.127	0.00323	0.128	0.00325	0.063	0.00160	0.064	0.00163	0.066	0.00168
14	0.126	0.00320	0.126	0.00320	0.126	0.00320	0.061	0.00155	0.061	0.00155	0.063	0.00160
15	0.129	0.00328	0.128	0.00325	0.131	0.00333	0.062	0.00157	0.062	0.00157	0.057	0.00145

*Position A is the top left channel corner as viewed in the planned pattern drawings of Figures 2, 3 and 4. Position B is the center, and Position C is the bottom right channel corner.

TABLE IX
FINAL THICKNESS PROFILE OF BRAZED TEST PANELS*

Test Panel No.	Nickel 200 Base Plate Thickness						Brazed Panel Thickness					
	Position						Position					
	A		B		C		A		B		C	
	Inches	Meters	Inches	Meters	Inches	Meters	Inches	Meters	Inches	Meters	Inches	Meters
17	0.119	0.00302	0.119	0.00302	0.118	0.00300	0.233	0.00592	0.232	0.00589	0.237	0.00602
18	0.096	0.00244	0.098	0.00249	0.103	0.00262	0.250	0.00635	0.245	0.00622	0.244	0.00620
21	0.108	0.00274	0.106	0.00269	0.107	0.00272	0.257	0.00653	0.253	0.00643	0.256	0.00650
22	0.105	0.00267	0.109	0.00277	0.113	0.00287	0.220	0.00559	0.224	0.00569	0.229	0.00582
23	0.094	0.00239	0.095	0.00241	0.095	0.00241	0.250	0.00635	0.248	0.00630	0.241	0.00612
24	0.089	0.00226	0.086	0.00218	0.088	0.00224	0.248	0.00630	0.239	0.00607	0.245	0.00622
26	0.101	0.00257	0.098	0.00249	0.094	0.00239	0.241	0.00612	0.239	0.00607	0.239	0.00607
28	0.086	0.00218	0.087	0.00221	0.092	0.00234	0.238	0.00605	0.236	0.00599	0.241	0.00612
30	0.087	0.00221	0.087	0.00221	0.087	0.00221	0.230	0.00584	0.206	0.00523	0.227	0.00577
31	0.099	0.00251	0.095	0.00241	0.094	0.00239	0.230	0.00584	0.231	0.00587	0.230	0.00584
33	0.096	0.00244	0.093	0.00236	0.094	0.00239	0.227	0.00577	0.229	0.00582	0.224	0.00569
35	0.104	0.00264	0.106	0.00269	0.100	0.00254	0.241	0.00612	0.239	0.00607	0.240	0.00610
38	0.104	0.00264	0.103	0.00262	0.100	0.00254	0.248	0.00630	0.243	0.00617	0.248	0.00630
45	0.082	0.00208	0.083	0.00211	0.087	0.00221	0.210	0.00533	0.216	0.00549	0.214	0.00544

*Positions correspond to those described in Table VIII. (Nickel 200 thicknesses vary by the number and severity of necessary flatness grinding and lapping operations.)

Table X presents measured thickness variations resulting from flatness grinding operations required to achieve planned bond patterns. Electroformed full bond backing was applied to the backside of the panels to minimize channel web yielding during tests.

It was originally planned that a section from an experimental chamber be subjected to nondestructive evaluation. This segment was sectioned for evaluation but was not tested. The section contained channels of various depths and a porous region existed in the liner which had a thickness varying from 0.030 inch to 0.019 inch (7.62×10^{-4} m. to 4.83×10^{-4} m.). Repair of this section to provide useful test data did not appear feasible at this time. Test results on flat specimens indicated liner deformation was likely to occur at pressures anticipated for acoustic emission evaluation of the liner-to-shell bond.

TABLE X
FINAL THICKNESS PROFILE OF DIFFUSION BONDED TEST PANELS*

Test Panel No.	Nickel 200 Base Plate Thickness						Diffusion Bonded Panel Thickness					
	Position						Position					
	A		B		C		A		B		C	
	Inches	Meters	Inches	Meters	Inches	Meters	Inches	Meters	Inches	Meters	Inches	Meters
19	0.096	0.00244	0.100	0.00254	0.104	0.00264	0.194	0.00493	0.195	0.00495	0.193	0.00490
27	0.110	0.00279	0.107	0.00272	0.109	0.00277	0.250	0.00635	0.250	0.00635	0.253	0.00643
29	0.093	0.00236	0.090	0.00229	0.092	0.00234	0.234	0.00594	0.233	0.00592	0.235	0.00597
32	0.091	0.00231	0.093	0.00236	0.097	0.00246	0.225	0.00571	0.223	0.00566	0.221	0.00561
34	0.105	0.00267	0.102	0.00259	0.105	0.00267	0.219	0.00556	0.217	0.00551	0.221	0.00561
37	0.105	0.00267	0.105	0.00267	0.110	0.00279	0.205	0.00521	0.202	0.00513	0.205	0.00521
39	0.106	0.00269	0.104	0.00264	0.109	0.00277	0.269	0.00683	0.260	0.00660	0.266	0.00676
40	0.082	0.00208	0.085	0.00216	0.086	0.00218	0.223	0.00566	0.226	0.00574	0.227	0.00577
41	0.100	0.00254	0.095	0.00241	0.096	0.00244	0.232	0.00589	0.235	0.00597	0.239	0.00607
42	0.116	0.00295	0.115	0.00292	0.115	0.00292	0.233	0.00592	0.231	0.00587	0.234	0.00594
44	0.103	0.00262	0.098	0.00249	0.104	0.00264	0.269	0.00683	0.264	0.00671	0.272	0.00691
48	0.092	0.00234	0.088	0.00224	0.093	0.00236	0.250	0.00635	0.225	0.00571	0.228	0.00579
49	0.088	0.00224	0.086	0.00218	0.089	0.00226	0.218	0.00554	0.217	0.00551	0.219	0.00556

*Positions correspond to those described in Table III. (Nickel 200 thicknesses vary by the number and severity on necessary flatness grinding and lapping operations.)

IV. NONDESTRUCTIVE EVALUATION

A. TEST SELECTION

The initial phase of the contract required selecting a maximum of four nondestructive techniques with which to conduct a feasibility test program on fabricated panels. In order to achieve a completely objective program, a comprehensive literature search was performed to evaluate all of the candidate nondestructive test techniques for their application to the testing of regenerative chambers. The primary objective was to find a test, or test combination, with the ability to detect good, bad, and weak bond conditions in the narrow joint lines produced by electroforming, diffusion bonding, and brazing. Many technical articles were reviewed; however, it was generally concluded that very little information was available which was applicable to the component geometry and fabrication methods under consideration. References 1-27 in Section VII list the relevant literature reviewed. It was thus considered pertinent to conduct practical feasibility evaluations using those techniques which appeared to have the most probability of success based on literature supplemented by fundamental test theory.

For schedule reasons, it was decided to utilize test coupons which had been prepared to demonstrate the ability to produce good, non, and intermediate bond integrity. The coupons used were in every case fabricated by the electroforming technique. These were chosen since the weak bond condition could be created easily, with bond occurring over the entire surface rather than by isolated areas of total nonbond. Totally bonded weak bond is the most critical condition to determine by nondestructive testing. Representative specimens were evaluated by the techniques and organizations shown below:

Test	Test Conducted By
Ultrasonic	Bell Aerospace Company
Holographic	Bell Aerospace Company
Sonic Spectrum Analysis	Aerotech Laboratories
Acoustic Emission	Dunegan Research Corp.
Infrared	Automation Industries

Based on this work, Table XI was compiled to provide a rating of all tests considered for this program. It is important to note that the comments, limitations and recommendations made in this and subsequent tables of this report are related only to the materials and bond characteristics investigated under this contract and should not be considered in any other context.

The first four test methods in Table XI were subsequently proposed to NASA and after discussion these were approved. A provisional test sequence was also established. The selection, reasons and anticipated capabilities are summarized in Table XII.

It was considered that part of the limitations associated with the infrared evaluation might be attributed to the thickness of the test specimen. In order to assure that no method was unjustly eliminated it was agreed to subject three of the electroformed test panels, when only 0.020 in. (5.08×10^{-4} m.) thickness of electroform was present, to infrared testing in addition to the other tests.

B. TEST TECHNIQUES

Following the selection of the four test methods, preliminary development was performed to optimize and standardize the actual test techniques.

TABLE XI
NONDESTRUCTIVE TEST RATING CHART*

Rating Subject			Test Method: 1.1 Ultrasonics	1.2 Spectrum Analysis	1.3 Acoustic Emission	1.4 Holography	1.5 Infrared	1.6 Radiography	1.7 Eddy-Sonic	1.8 Acoustic Imaging	1.9 Radiation Gaging	1.10 Liquid Crystals	1.11 Neutron Radiography	1.12 Eddy Current	1.13 Microwave	1.14 Fluoroscopy	1.15 Magnetic Particle
Availability																	
	A	off shelf	A	A	A	A	A	A	A					A		A	A
	B	requires modification								B	B				B		
	C	not readily available										C	C				
Cost																	
	A	below $15,000	A	A	A				A		A[12]	A		A	A		A
	B	$15,000 - $25,000				B	B	B		C[11]			B			B	
	C	above $25,000															
Ease of Use																	
	A	good	A		A												
	B	fair		B		B[5]	B	A	A		B			B	C	A	C
	C	difficult								C		C	C				
Reliability																	
	A	good	A		A												
	B	fair		B[2]			B			B							
	C	poor				C[6]		C	C		C	C	C	C	C	C	C
Ease of Results Interpretation																	
	A	easy	A[14]						A								
	B	requires expertise		B	B[4]		B	B		B							
	C	difficult				C					C	C	C	C	C	C	C
Applicability to Bonding Techniques on Nickel																	
	A	all three	A	A	A	A				A							
	B	two					C[8]	C[9]	C[10]		C	C[13]	C	C	C	C	C
	C	one or zero															
Application on Thrust Chamber																	
	A	fully					A										
	B	partially	B[1]	B[3]	A	B[7]											
	C	not at all						C	C	C	C	C	C	C	C	C	C
Potential to Detect Incipient Flaws After Firing																	
	A	good															
	B	fair	B	B	A	B											
	C	poor					C	C	C	C	C	C	C	C	C	C	C
Points Rating																	
	A	2 points	14	11	15	8	8	7	8	5	3	2	1	5	3	5	4
	B	1 point															
	C	0 points															
Recommended for Further Evaluation			Yes	Yes	Yes	Yes	No	No	No	No	No	No	No	No	No	No	No

Index of Notes

*NOTE: The grading system used here is intended to judge the test methods applicability to this program only and should not be considered to present the general merits or limitations of the test discussed.

1. Requires expensive tooling and recording devices.
2. To be determined.
3. Spot check only.
4. Requirements not established.
5. Laboratory use only.
6. To be determined.
7. To be proven. Tooling requirements unknown.
8. Applicable to thin nickel 0.020 in. approximately.
9. Applicable to brazes only.
10. Insufficient sensitivity.
11. Cost high size is currently too small for this application.
12. Investigation costs high compared to chances of success.
13. Poor sensitivity and repeatability.
14. Fully bonded weak bond strength not determinable.

TABLE XII
SELECTED METHODS CHART

A Method	B Proposed Sequence	C Reasons For Selection	D Anticipated Major Use	E Limitating Factors
Ultrasonics "C" Scan	First test (independent probably using low pressure).	Provides Planar map of part indicating good bond versus no-bond as black/white condition.	As described in Column C. Plus it provides an internal map to overlay the Holography stress map.	1. Unable to detect unbonds in intimate contact or weak bonds.
Acoustic Emission	Second test use proof pressure (below yield)	1. Separates weak-bond from good bond by monitoring pulsed count versus time/pressure. 2. Can be used to monitor defect propagation at constant pressure.	To separate bond conditions (Column C). 1. Determine at what pressures more noise is emitted by monitoring pressure in increments versus pulsed emission count. 2 Using noise summation against time.	1. Not expected to detect full unbonds. 2. Cannot locate emission source readily. 3. Effect is not reversible (Kaiser). Part cannot be stressed significantly prior to test.
Holography	Third test (in conjunction with test two)	Provides location of high stress areas as a result of pressure, not determinable with acoustic emission.	Simultaneous with acoustic emission test to provide a time-lapse or real time stress map of the surface.	1. Insensitive to small unbonds. 2. Difficult to adequately stress part(s). 3. Repeatibility unproven.
Spectrum Analysis	Fourth test (probably alongside two and three. All panels will be tested).	Provide bond information in areas not affected by pressure such as center of bonding lands.	Spot check where tests 2 and 3 indicate additional information is required.	1. Extensive tooling and recording apparatus required to perform full scan. 2. Must have gated signal.
Acoustic Emission	Fifth (in unison with destruct pressure test).	To provide information not obtainable with normal stress stain curves plus provide definitive information with the initial acoustic emission test.	During final pressure test to destruction - not a nondestructive evaluation - monitor summation versus load (pressure) on log graph.	1. Test at any pressure irreversible.

1. Ultrasonics

Ultrasonic inspection is based on emitted and received short wave length and relatively low energy vibrations which are transmitted through the material under evaluation. In many ways the behavior of the sound within the material and at joint lines or flaw locations can be considered analogous to that of light passing thru different media interfaces. As such this sound may be closely monitored by choice of the angle of sound incidence, focusing, and the selection of frequency dependent on sensitivity/resolution and penetration desired. In general higher frequencies are used for increased sensitivity while the lower frequencies yield greater penetration.

There are several means of employing the sound which are dependent on joint configuration and the inherent nature of the flaw associated with the fabrication process.

The more commonly used of these are:

a. Pulse-echo longitudinal wave which introduces the sound normal to the entry surface and detects delaminations and bond defects parallel to the entry surface.

b. Pulse-echo shear wave which introduces the sound at any specified angle and detects defects oriented off-normal to the surface such as lack of fusion in weldments and longitudinal seams in raw materials.

c. Thru-transmission which uses two transducers (one transmitter and one receiver) located on opposite sides of the part, and also detects delaminations and bond defects especially where several interlaminar bonded layers are involved.

d. Reflector method which is similar to the thru-transmission method with the exception that a smooth surface replaces the receiving transducer and acts as a reflector, returning the sound back to the transmitting transducer. This method is useful on thin materials in which the front and back surface signals cannot be electronically separated on the scope (resolved). It detects delaminations and bond defects.

All of the aforementioned techniques can employ focused transducers which concentrate the sound similar to a light lens and thus increase sensitivity. A "gate", which permits monitoring and recording of the results at any selected interface, can also be used in conjunction with these techniques. A "C" scan recorder provides a planar X-Y axis facsimile of the gated interface.

The perferred technique for inspecting bonds of this nature is the pulse-echo longitudinal wave method, using a high frequency (15 - 25 MHz) focused transducer. Using this approach, it was possible to gate the bond interface and achieve a high sensitivity level. The technique shown in Figure 39 was established for evaluation of all full thickness electroform (0.060 in. or 1.52×10^{-3} m. thickness) diffusion (0.120 in. or 3.04×10^{-3} m. thickness) and braze (0.120 in. or 3.04×10^{-3} m. thickness) bonds.

With the aim of determining bond quality at the earliest possible fabrication stage, it was decided to attempt ultrasonic inspection of the electroform panels at the 0.025 in. (6.35×10^{-4} m.) buildup stage. However, it was determined that the pulse-echo method previously established could not be used due to resolution limitations. These were principally associated with gating and differentiating entry and bond interface signals. Instead, a technique based on the reflector method previously described was employed. This

DATE N/A
REV. N/A
QUALITY ENGINEERING APPROVAL N/A

Bell Aerospace Company

ULTRASONIC TECHNIQUE NO. N/A

NOTE: † Optional
* Equivalent items may be substituted subject to Quality Engineering approval

PART NAME - NASA NAS3-14376 Panels Electroformed, Brazed and Diffusion Bonded Processes
~~PART NUMBER~~ -
Part Number - 8654-470001
~~JOINT NO.~~ -
MATERIAL - Nickel, Nickel 200, Inconel 600
METHOD - Pulse-echo Longitudinal Wave Immersion

★ EQUIPMENT	★ TOOLING
Sperry	Automation
721 Reflectoscope	Inds immersion
HRL Pulser Receiver	Research Tank with 11"
Fast Transigate	Alden "C" Scan Recording
Special Function	Option
Cabinet containing	
Alden Drive Inter-	
connect and Amplifier	

SCAN PLAN

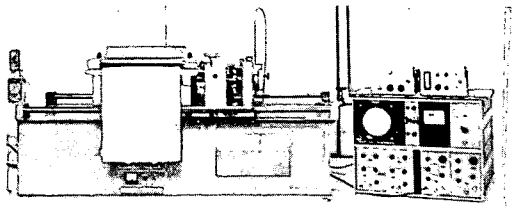

Scanning Direction 5.0 Setting ←→

Indexing Direction 3.5 Setting ↓

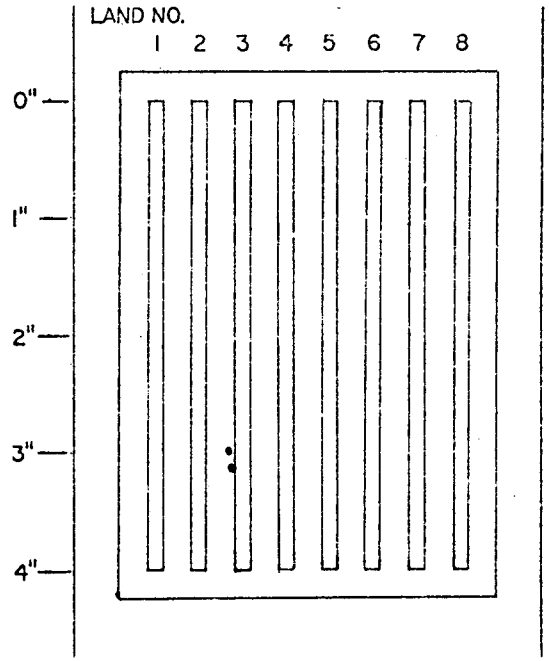

Instrument Settings:
+ Gate, bond interface, 3-6 line Threshold Level, Lo Gain, Peaked 10-15 Line Operating Level.

★ RECOMMENDED TRANSDUCER TYPE — 3/4" Dia., Lithium Sulfate, 1.5" Focal Point, 15-25 MHz Freq.

REFERENCE STANDARD CRITERIA

STANDARD NO.	MATERIAL	HOLE SIZE	DEPTH	SHAPE	REMARKS
N/A	Nickel	N/A	.1195" Thick	Flat	Used for normalization and focus control.

Figure 39

technique consists of introducing 10 MHz focused sound (longitudinal wave) which is transmitted through the panel to a smooth glass reflector where the sound is reflected back through the panel to the transducer. Any changes affecting attenuation in the sound due to thickness, surface irregularies, or bond variance can be seen at the reflector as negative amplitude changes. Gating the reflector for these negative changes provides a "C" scan similar to the pulse-echo method with the exception that factors other than bond variance are also recorded. Figure 40 graphically displays the technique used for this study. The 25 to 45 percent trigger setting (recording threshold level) is indicated, since this was varied between panels and greatly influenced the resulting sensitivity. The need to change this recorder threshold setting occurred due to variations in surface finish, thickness, and parallelism. The test was only sensitive at the 45 percent setting where more ideal panel conditions existed. A further technique innovation used in testing the 0.025 in. (6.35×10^{-4} m.) thick panels by the reflector method was the introduction of 500 psi (3.45×10^6 N/m.^{2}) internal pressure. The theory behind this approach was that the capability of detecting intimate contact nonbonds open to pressurization would be enhanced due to the increase in the nonbond separation width. The choice of 500 psi (3.45×10^6 N/m.^{2}) maximum was made for two reasons:

a. To minimize the risk of panel distortion, and

b. To avoid destroying low level acoustic emission data.

The study was conducted using the reflector method by first obtaining a "C" scan, pressurizing the panel, repositioning it exactly as before, and obtaining a second dynamic scan without changing any instrument settings. The scans were than visually compared for any nonbond growth resulting from the pressure.

2. Acoustic Emission

Unlike ultrasonics, acoustic emission does not introduce sound in any manner, but instead only listens. This listening may be performed within selected frequency ranges and be permanently recorded. Sound emissions from material deformation travel to a broadband transducer via surface, longitudinal and shear waves, where they are converted to an amplifiable electrical signal. Since the test is dependent on noise emitted during material movement, the application of acoustic emission requires some form of stressing to create these inaudible emissions of sound energy. These emissions may be monitored and recorded as:

a. Summation - graphically

b. Rate - graphically

c. Real-time-oscilliscope

d. Direct - tape recorder

Since all acoustic emission feasibility work was performed on lapshear specimens, several unknowns existed with respect to instrumentation settings and test pressurization methods. These consisted of:

a. Gain settings (decibel selection)

b. Filter requirements (frequency range)

c. Pressure (stress)

d. Recording method

C

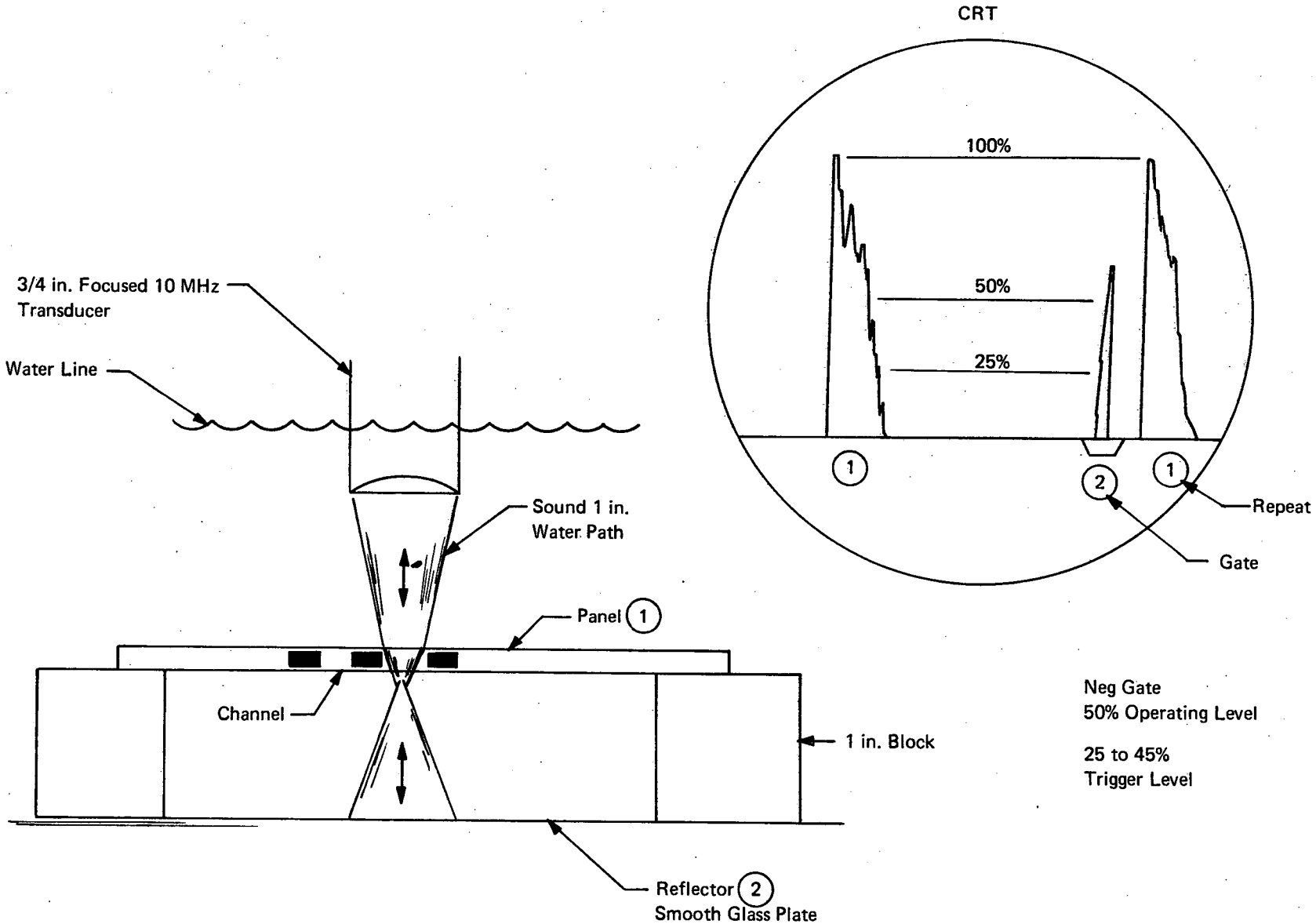

Figure 40. Ultrasonic Reflector Method

Based on limited information available from a test run by Dunegan Research Inc., and a trial panel tested at BAC, it was decided to attempt testing on panel 3 using an 80 db gain setting, 1-3 KHz filter setting and bottled nitrogen gas as a means of pressurization to 1,500 psi (10.34×10^6 N/m.^{2}) maximum. Panel 3 was chosen for safety reasons as it represented an almost full strength bond. The digital counter was set in an intermediate range (x 100) for a summation count in the memory mode. The memory/summation recording method was chosen since manual pressurization could not be applied consistently enough for acceptable rate recordings. Furthermore, the count obtained periodically (from the memory recorder) would enable simple rate graphs to be constructed. The result of this test on Panel 3, at 0.025 in.(6.35×10^{-4} m.) buildup, was that no noise emission was detected either on the X-Y recorder or the audio monitor. Some evidence of leakage was noted. As a result, it was decided to conduct the next test on Panel 8, also at 0.025 in.(6.35×10^{-4} m.) buildup and containing weak bonds (i.e., one which was expected to emit sound), using hydrostatic pressure so that pressures up to 3,500 psi (24.13×10^6 N/m.^{2}) could be achieved. In addition, it was decided to remove all filters. During the test some noise was emitted in reaching 2,500 psi (17.24×10^6 N/m.^{2}). This was so low that it was decided to decrease the Multiplier level from x 100 to x 10 in order to obtain full scale Y axis deflection. After reaching 3,500 psi (24.13×10^6 N/m.^{2}), a short evaluation of gain was made by increasing the setting-first to 90DB and then to 95DB. At these settings, pump and background interference was experienced. The panel was found to show some evidence of distortion over the channel region, and thus it was concluded that all further acoustic emission tests would be conducted at full build up.

As a result of this work the test technique shown in Figure 41 was established for testing the remaining panels.

3. Holography

There are three basic techniques for producing holograms. These are:

a. Real-time (dynamic flaw detection)

b. Time-lapse (static, captured image, flaw detection)

c. Time-average (inherent and load induced stress patterns)

The principles of approach with these techniques are briefly outlined below:

a. To produce a real-time image, a hologram is taken of the test object and developed before the object is deformed by stress. If the hologram is then viewed so that the reconstructed virtual image is superimposed on the object, any stress-induced deformation will appear as a dynamic display of fringe patterns. Data concerning the object is not restricted to static object displacements, and fringes can be formed or modified by any localized motion or deformation of the surface. Changes in the topology or shape of the surface cause instantaneous variations in the fringe geometry.

b. To produce a time-lapse hologram an initial exposure is made but not developed. The object is then slightly deformed statically, and a second hologram is recorded on the same film. When developed and reconstructed, this double exposure displays fringes superimposed over the object image. These fringes are the result of interference between the first and second object beams which represent the two positions of the object. These fringes present a highly accurate recording of the deformation undergone by the test specimen. Surface regions above sub-surface discontinuities are deformed differently

ACOUSTIC EMISSION TECHNIQUE

*EQUIPMENT

Dunegan Research Corp.
702 Audio Monitor
301 Totalizer
502 Ramp Generator
402 Reset Clock
801P Preamplifier
D140A Differential Transducer
Hewlett Packard
7035B XY Recorder
Enerpac 10K Max
Hydrostatic Pump

TEST CRITERIA

Mode: Sum [X] Log [ ]
Set: Rate [ ] Mem [X] Rate [ ]
Trans. Dual End
Sum X 10 Gain 80 DB
Filter None Reset 1 Sec.
Ramp Gen. 5 Min.
Stress Hydrostatic

Total Count Recorded in 500 psi Increments from 0 to 3500 psi

TEST LAY-OUT

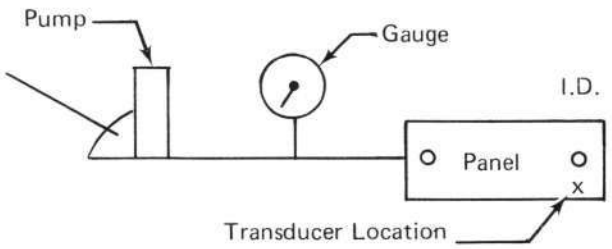

INSTRUMENT

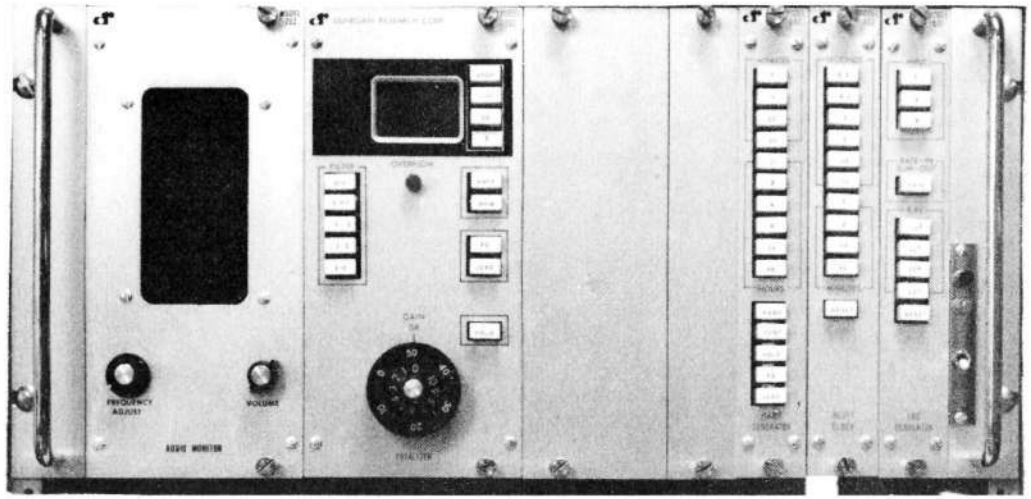

RECORDER

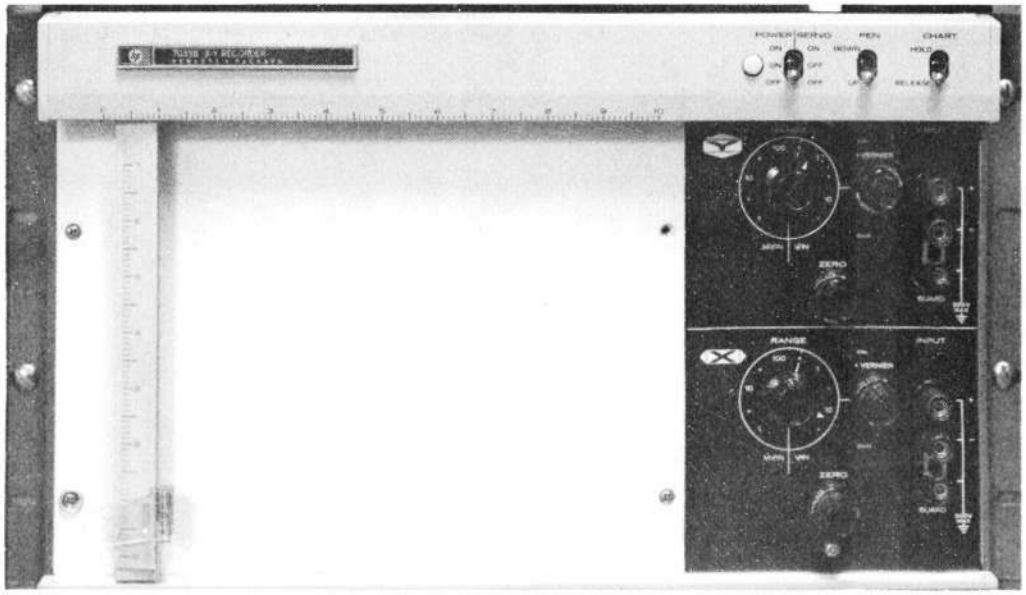

Figure 41

from the rest of the surface as a result of the applied stress, and hence, produce anomalies in the fringe patterns which are readily discernible.

c. Similarly, a time-average hologram may be produced by exposing the object while it is undergoing dynamic vibrational movements. The reconstructed image displays fringes that accurately reveal the dynamic deformation of the test specimen.

During the test method selection it was postulated that real-time holography would be conducted. The optimum test response pressure was to be established on each panel by viewing the fringe response as the pressure was increased. It was also intended to record the real-time fringe patterns on a polariod photograph. Although this approach was made on the initial 0.060 in.(1.524×10^{-3} m.) thick electroformed panels after acoustic emission testing, the results were disappointing in that image quality/repeatability was poor and the fringe patterns were almost impossible to consistently capture on a photograph.

In view of these difficulties, the other holographic techniques of time-lapse and time-average were than evaluated practically. Time-lapse was found to produce excellent quality holograms which were both repeatable and reproducible. Time-average was found unsuccessful, and it was therefore decided to standardize on the time-lapse technique. Figure 42 shows typical examples of the results obtained. The choice of time-lapse, however, meant that a standard test pressure must also be established. Electroform Panel 3 was tested at several pressures, Figure 43, and review of these led to the selection of 500 psi (3.45×10^{6} N/m.^{2}) gas pressure for the test, since it was the lowest pressure showing good definition.

Subsequent testing revealed that although this pressure worked well on all electroformed panels, the thicker (0.120 in. or 3.048×10^{-3} m.) diffusion and braze bonded panels required higher pressured (up to 1,450 psi or 10.00×10^{6} N/m.^{2}) to attain similar results. Figure 44 details the finalized holographic technique.

4. Spectrum Analysis

This test differs from the previous three methods in that it is not currently used for nondestructive evaluation. The equipment is designed to analyze transducers, not materials. However, it was considered that by using the equipment in conjunction with a transducer (having a known spectrum) and varying the material (i.e., bond), the resulting spectrum "shifts" might characterize the bond and provide a feasible test application. Since the method is basically that of a specialized ultrasonic technique, many approaches are feasible. Three such approaches were selected for study under this contract. These were:

a. Pulse-echo longitudinal wave using focused immersion transducers at 10, 15 and 25 MHz.

b. Thru-transmission longitudinal wave using a focused immersion 10 MHz transducer.

c. Contact pitch and catch using a fixed angle dual 5 MHz thickness measuring type transducer.

Figure 45 portrays the three approaches and illustrates the typical reflectoscope cathode ray tube (CRT) response from each method.

The instrumentation used to conduct the study consisted of a Sperry 721 Reflectoscope using the HRL or 10N pulser-receiver to set up the test, a Hewlett Packard oscilloscope to display the RF sound trace (to select which interface to gate), a Branson/Aerotech UTA (for gain control and gate selection), and a Hewlett Packard analyzer (for frequency control and display).

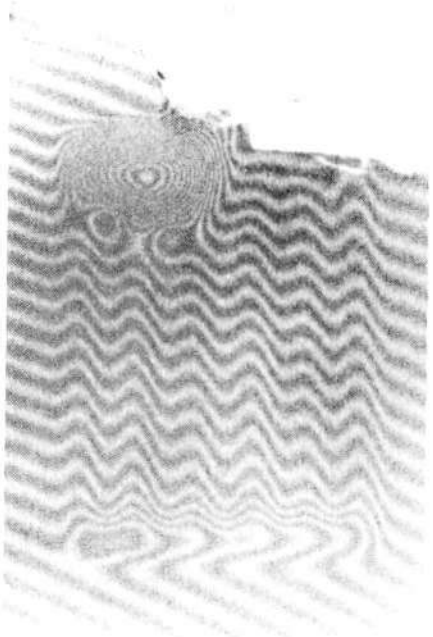

REAL-TIME

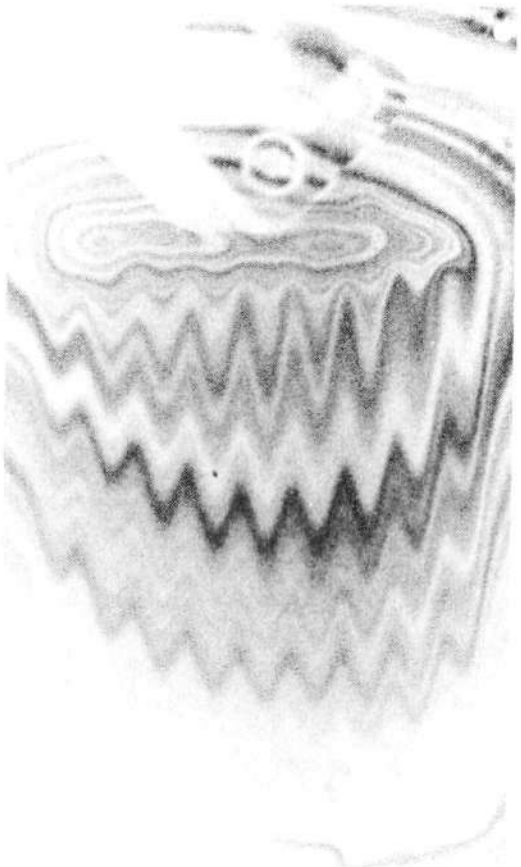

TIME-AVERAGE

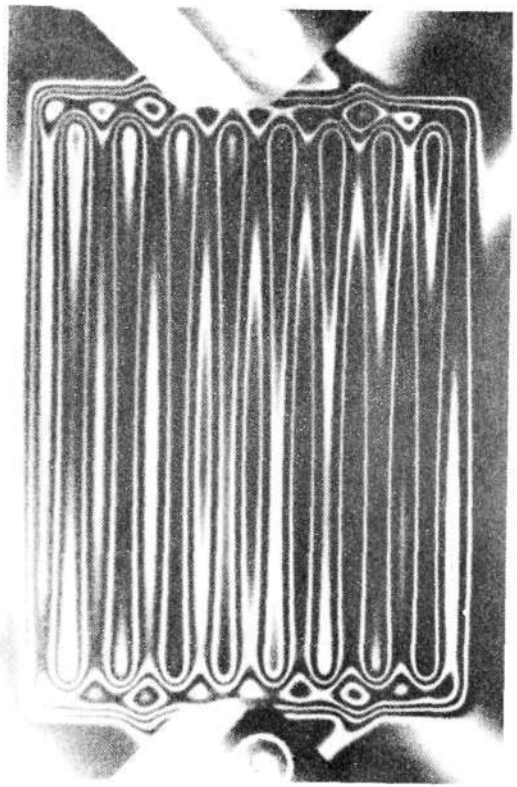

TIME-LAPSE

ILLUSTRATION OF HOLOGRAPHIC METHODS

Figure 42

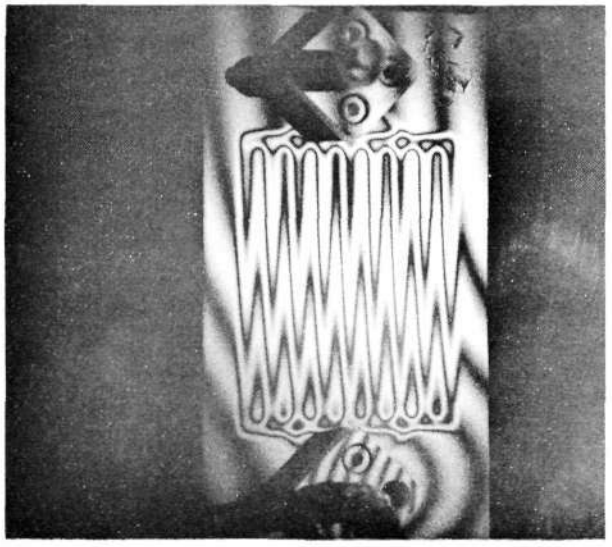

3E 250 psi
(1.72 x 10^6 N/m.^{2})

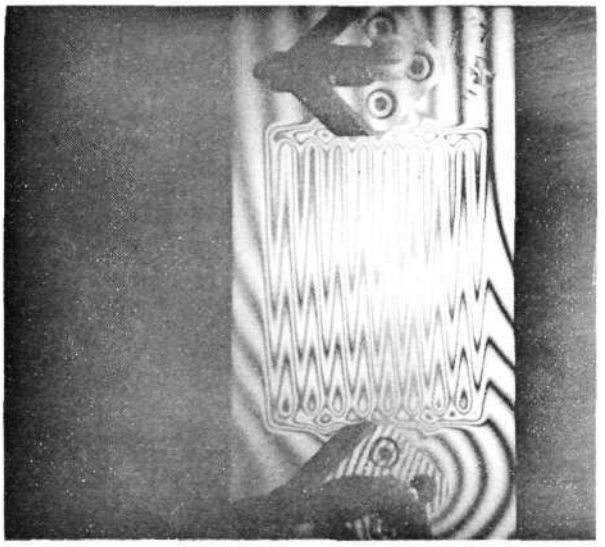

3E 750 psi
(5.17 x 10^6 N/m.^{2})

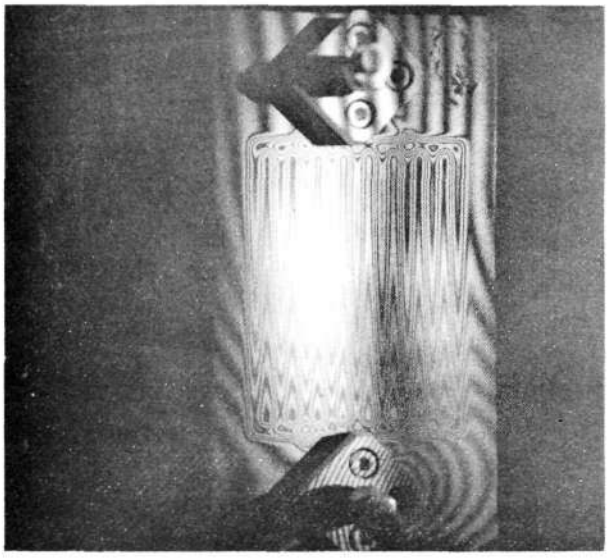

3E 500 psi
(3.45 x 10^6 N/m.^{2})

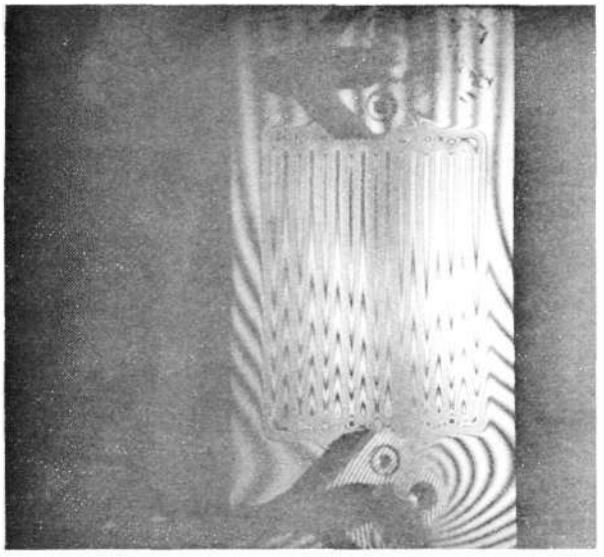

3E 1000 psi
(6.89 x 10^6 N/m.^{2})

EFFECT OF PRESSURE ON HOLOGRAM

Figure 43

HOLOGRAPHIC INTERFERROMETRY TECHNIQUE
JODON HS-1C SYSTEM

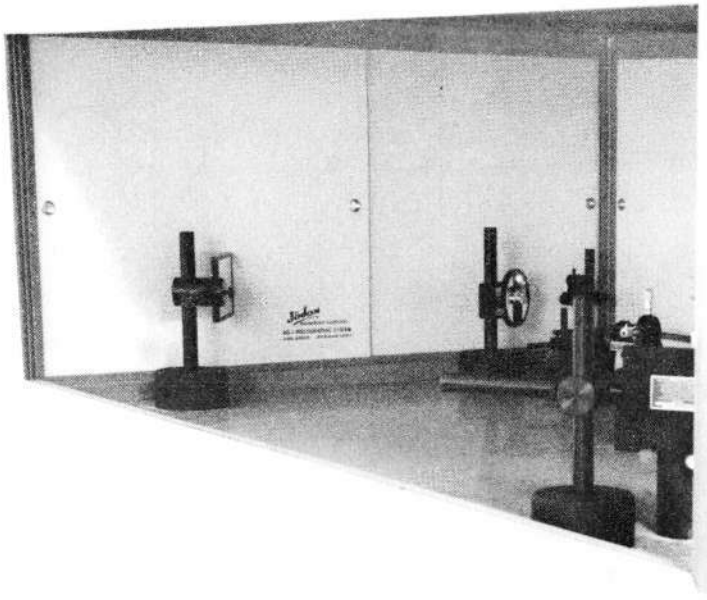

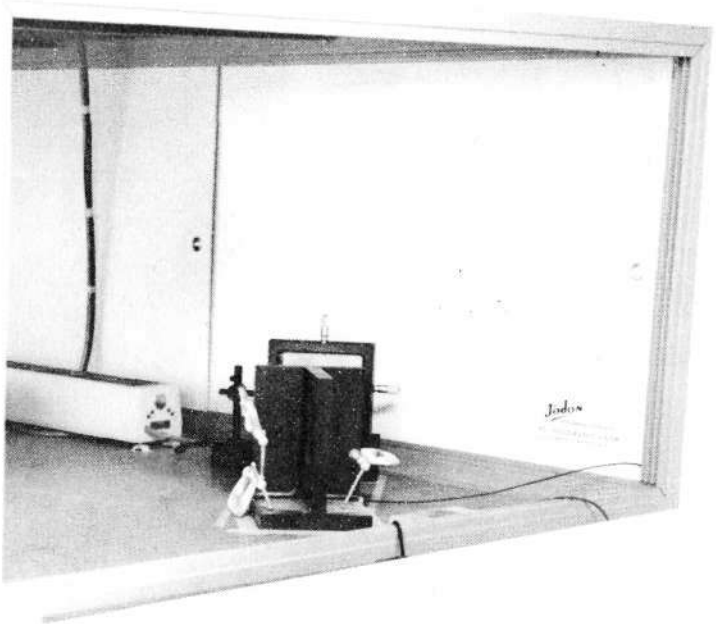

POLAROID CAMERA FACTORS

Type 107 Film.
Close Up Lens.
Inf. Focus.
14 in. Object to Lens Distance
100% Reference
Beam Intensity
F-16 1 Sec Exposure

TEST CRITERIA 1/2 EXP.

Tech: Time-Lapse Time
Mode Integrate Scale Hi
Set 128 Ergs./cm^2 NA Min. Sec.
Vernier 1.8 Beam Coff. 25%
Laser 28 mw Den. 80 mw/cm
Stress Gas-Nitrogen

Regulated to 500 psi
For Electroformed Process;
1380 - 1440 for Braze and Diffusion
Bond Process.

OTHER FACTORS

105 in. Splitter to Film Plate Beam Distance.
20:1 Ratio Divergence Lens.
1.5 to 1 Beam Ratio.
193 Avg. Beam Splitter Position.
12 in. Object to Film Plate Distance
6 Min. Dev. at 68°F
1.6 Avg. Density

ELECTRONIC SHUTTER

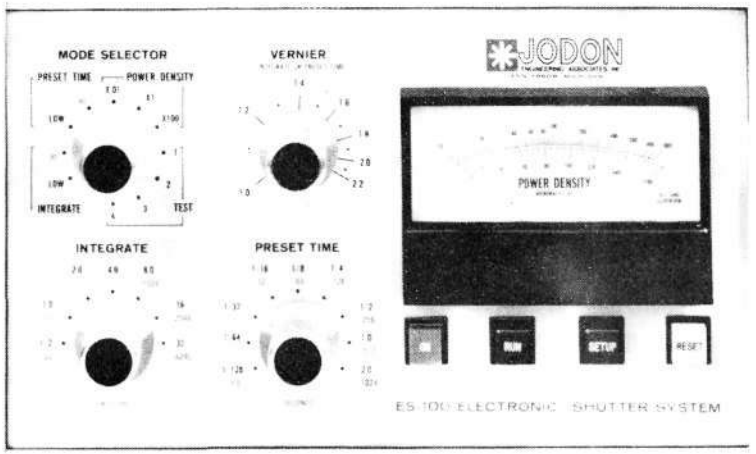

Figure 44

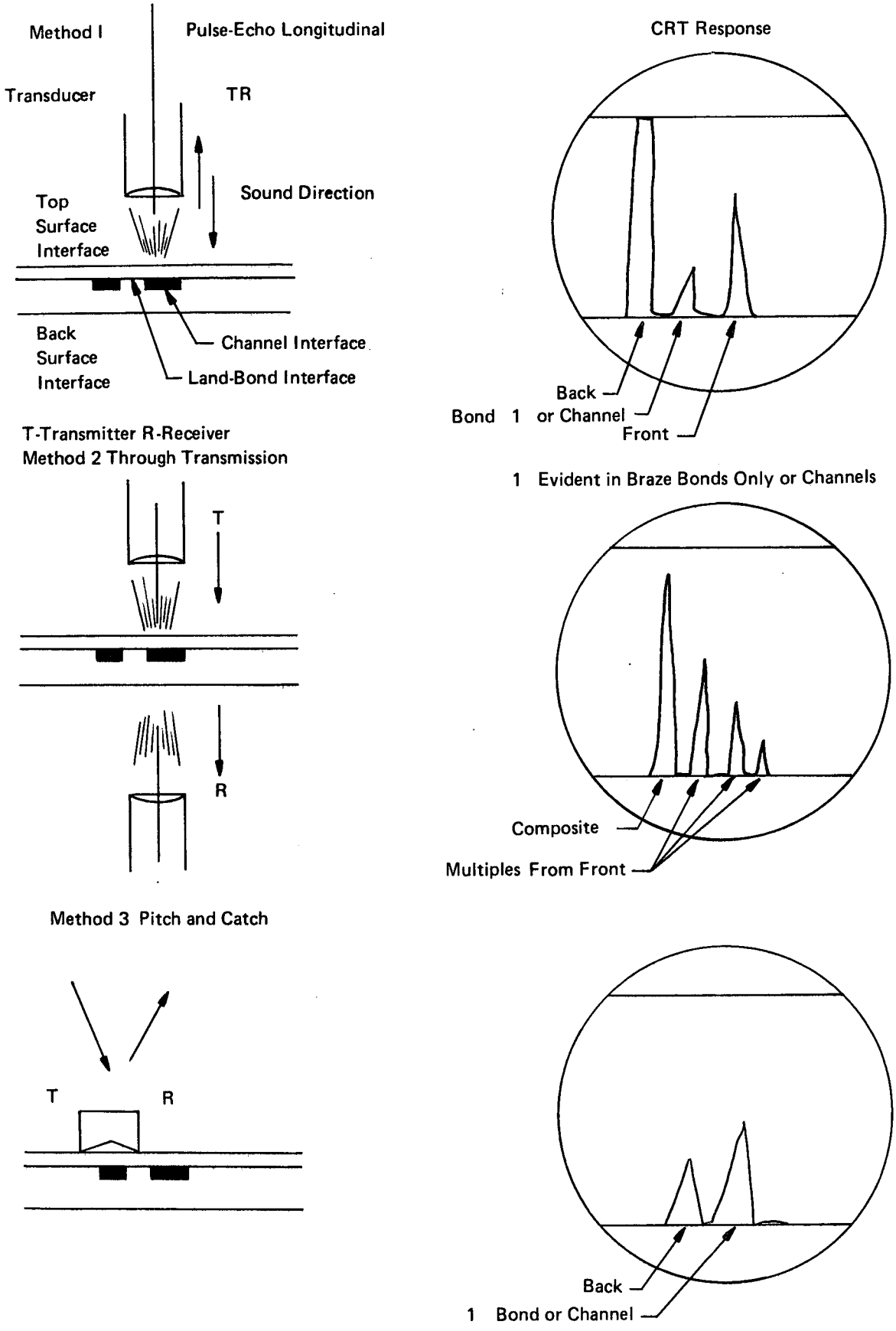

Figure 45. Spectrum Analysis Test Method Approaches

All immersion transducers were 3/4 in. (1.905×10^{-2} m.) dia., lithium sulfate 1.5 in. (3.810×10^{-2} m.) focal point, with the following serial numbers:

Freq.	Supplier	A/N
10	Sperry	13799
15	Branson	CF 27940
25	Branson	KF 8916

The pitch and catch transducer was a Sperry type SRL-Z model 50B1265/ECN 5 MHz. The settings used for these instruments are given in Table XIII.

TABLE XIII
SPECTRUM ANALYSIS INSTRUMENT SETTINGS

Oscilloscope Unit	180A/1801A/1821A	
Magnifier	10X	
Display	Int.	
Ext Input	AC	
Position A	0.1 V/Div	
Display	Alt B	
Position B	0.5 V/Div	
Polarity	- Negative	
Input	AC	
Delay	Delayed 10 μ sec	V
Sweep	Auto Ext	
Scope	+ Positive AC	
UTA Unit	Coupler	
Attenuation	0-20 DB	V
Damping		V
Gain	50 Max	V
Gate Delay		V
Gate Width		V
Rep Rate	Max	
Pulser-Trigger	Int.	
Spectrum Analyzer	141T/8553B/5552A	
Center Freq		V
Bandwidth	300 KHz	
Scan Width per Div		V
Input Attenuation	0	
Clipper	On	Approx 10%
Scan Time	2 MS/per Div.	V
Linear	1 MV/per Div.	
Linear Sensitivity	0	V
Video Filter	Off	
Scan Mode	Int.	
Scan Trigger	Line	

Note: The instrument settings with a "V" indicate those which were variable.

Applying spectrum analysis to selected panels required some standardization, since many factors in theory could be monitored from the spectrum envelope. All of these factors were not necessarily influenced by the bond interface and therefore could lead to misintrepretation of the information. The surface condition, thickness, attentuation factors, grain size, and velocity differentials (impedance mismatch) all influence the resulting spectrum trace. Practical experimentation indicated that the major change occurred to the center frequency as a result of impedance mismatch. For this reason, it was decided to restrict the evaluation to comparison of center frequency shift only. In order to achieve this, it was necessary to vary certain instrument settings (marked V) to provide a constant amplitude envelope for correlation.

5. Test Sequence

Following the establishment of Test Techniques for all methods, it was considered essential to determine test sequence. Based on theoretical data, the following approach was anticipated.

(a) Ultrasonics - To establish basic integrity and provide a 1:1 ratio map of the bondline.

(b) Holography - To view real-time displacement and stress patterns during the acoustic emission test and thus locate emission sources.

(c) Acoustic Emission - To determine bond integrity and flaw propagation by emission level.

(d) Spectrum Analysis - To determine bond characterization potential on selected areas of panels based on the other test results.

Items b and c were initially planned to be conducted simultaneously using the real-time holographic method to 1500 psi (10.34×10^6 N/m.^{2}) maximum gas pressure and acoustic emission to the same pressure.

However, problems were encountered which made this approach impractical. It was discovered that the real-time holographic method was not sufficiently reproducible to permit taking high quality consistent polaroid photographs. This was solved by using the time-lapse technique. It was then found that 1500 psi (10.34×10^6 N/m.^{2}) maximum air pressure was not sufficient to adequately stress the panels for the acoustic emission test. This was resolved by using hydrostatic pressure applied by a hand pump (in stepped pressure increments of 500 psi or 3.45×10^6 N/m.^{2}) to 3,500 psi (24.13×10^6 N/m.^{2}) maximum. 3,500 psi (24.13×10^6 N/m.^{2}) yielded too much surface movement during the time-lapse technique and lost the hologram entirely. Coupling these changes with the irreversibility phenomenon in acoustic emission (Kaiser effect), it was decided to separate the tests in an attempt to minimize data loss and maintain comparability.

The use of the spectrum analyzer was never intended as an overall scanning test, but purely as a "spot" check for bond character (relative strength) in areas highlighted by the other test techniques. In view of the many variables and approaches discussed under the test technique section, and the need for an extensive development program found during the initial tests conducted, it was agreed with the NASA Program Manager to restrict testing to a limited number of panels and evaluate more than one approach.

As a result the original planned test sequence was not followed. The actual sequence used was:

(a) Ultrasonics - Initial map of bond line.

(b) Acoustic Emission - 0 to 3500 psi or 0 to 24.13 x 10^6 N/m.^{2} (in 500 psi or 3.45 x 10^6 N/m.^{2} increments) for bond integrity.

(c) Holography - 500 psi (3.45 x 10^6 N/m.^{2}) on electroformed panels, and 1500 psi (10.34 x 10^6 N/m.^{2}) maximum on brazed and diffusion bonded panels to establish relationship with the preceding tests.

(d) Spectrum Analysis - Separate study on selected panels only.

Note: This finalized sequence should not be misconstrued as the ideal order. Instead, it reflects the practical approach taken to prove test feasibility. Further consideration is given to test sequences under the discussion section.

C. RESULTS AND DISCUSSION

The results of three tests, ultrasonic, acoustic emission and holography on all panels are presented grouped in accordance with the fabrication process in Appendix A. Where a result is indicated by Panel number alone in the following text, the illustration is contained under that "A" designation in the appendix. The fourth method, spectrum analysis, is presented as a separate entity, as is the limited infrared evaluation.

1. General

In considering the merits and correlation of the selected test methods it is essential to take into account both the panel design limitations and fabrication anomalies encountered during the program. These have in all cases been resolved or explained with respect to their source. Certain individual test panel variation, such as flatness and thickness parallelism, have made complete comparison of fabrication processes by test method difficult, since a measure of "nonstandardization" was often a resultant feature. In discussing the merits of each test method these factors will be dealt with in more detail. An opinion of their effect on test results is offered.

The overall objective of the contract, which was to establish feasibility of new test methods, is considered to have been achieved. Three of the four selected methods showed high merit. These were ultrasonic, holography and acoustic emission. A more detailed discussion by test method follows. In order to facilitate the evaluation, Tables XIV, XV and XVI have been prepared. These tables give a synopsis of the results illustrated in Appendix A.

2. Ultrasonic

The pulse-echo technique used on all bonds proved to be an excellent screening method for nonbond condition. As was anticipated, it did prove unsuccessful in determining the true weak bond condition in the electroformed panels. The best correlation with planned defects was evident in braze bonded samples. The diffusion bond process presented more difficulty in achieving planned defects as discussed in Section III. Ultrasonic evaluation proved a valuable tool in demonstrating the true nature of the actual bond patterns achieved. This was later verified by metallographic analysis. In general, the reflector technique used on the thin (0.025 in. or 6.35 x 10^{-4} m. thick) electroformed panels produced a less sensitive test for detecting nonbonds, Figures 46(i) and 46(ii). However, in the case of Panel 12, Figures 46(iii) and 46 (iv), it did show nonbond which was not found at the full buildup thickness by pulse-echo. The presence of this planned defect (at the base of Land8) was clearly confirmed by hologram Panel 12. The reason for the pulse-echo not seeing this defect is due to the surface finish.

Surface finish was also a major factor restricting the clarity of the reflector technique. It proved to be a deterrent to ultrasonic evaluation of the electroformed panels at the thicknesses studied. At least

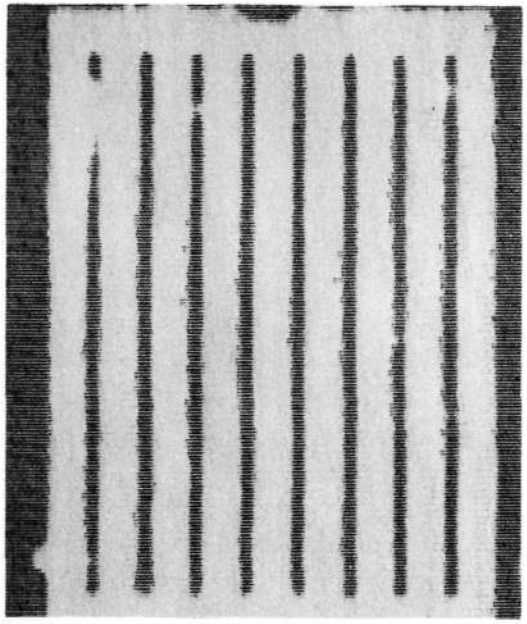

(i) 4 Reflector (No Pressure 0.025 in. Thick)

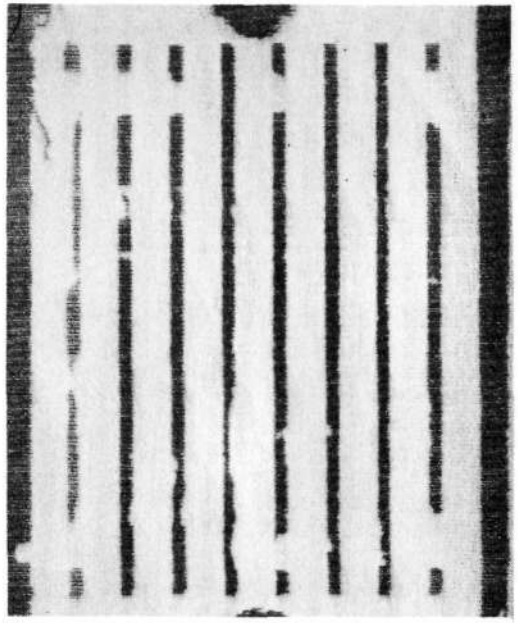

(ii) 4 Pulse Echo (No Pressure 0.060 in. Thick)

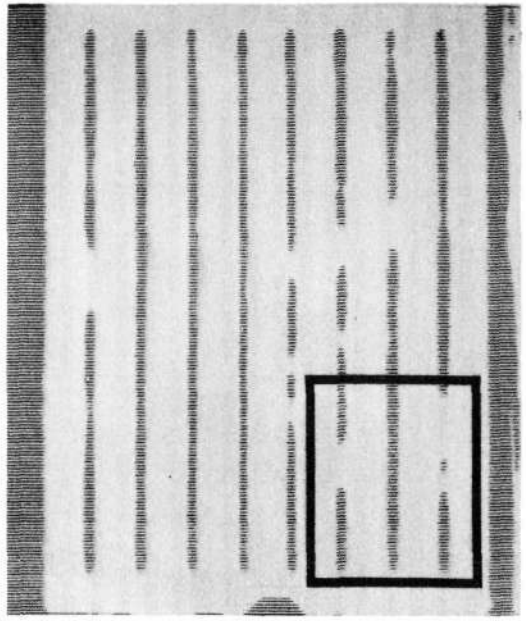

(iii) 12 Reflector (No Pressure 0.025 in. Thick)

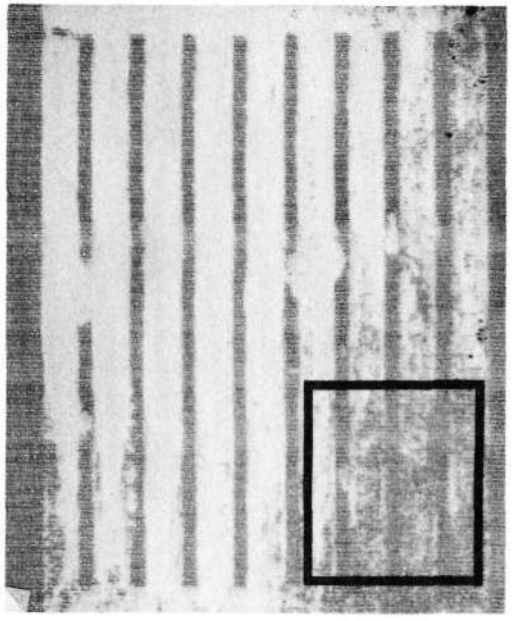

(iv) 12 Pulse Echo (No Pressure 0.060 in. Thick)

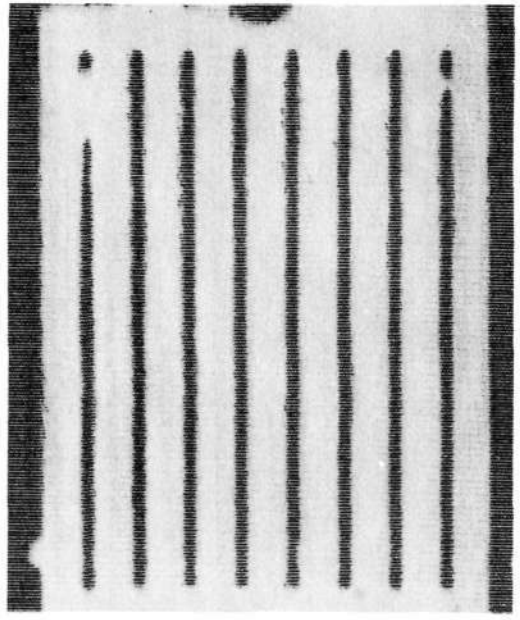

(v) 4 Reflector (500 psi 0.025 in. Thick)

Figure 46

part of the apparent lack of response obtained from the 500 psi (3.45×10^6 N/m.^{2}) pressure tests, e.g., Figures 46 (i) and 46 (v), was due to surface condition coupled with the fact that only thin electroformed samples were evaluated using this less sensitive reflector method. Another factor which may have influenced the pressure study was noted during acoustic emission and destructive testing. The 2:1 ratio of channel to land favored a baseplate and/or coverplate yielding prior to bond line disturbance. It is therefore considered, that the use of pressure to increase sensitivity warrants a more critical evaluation.

3. Acoustic Emission

An intercomparison of the results shown in Tables XIV, XV and XVI does not indicate the high rating and applicability which is predicted for this test. In order to assess the true promise of this test, it is necessary to consider the electroform results separately, because it is the only fabrication technique to give three strength conditions – full, weak and nonbond. The other fabrication methods produced varying degrees of bond/nonbond which resulted in the acoustic emission study being more related to critical defect size. Another experience encountered on the brazed and some diffusion bonded samples, but not the electroformed, was the yielding of the base plate. This probably affected stressing of the bond interfaces, and hence affected the emission data. Consideration of the electroform data shows a distinct trend as related to true weak bonds. A weak bond, regardless of defect pattern, consistently created high emission counts. This is thought to be attributable to the steady yielding of the entire weak bond areas. The full strength bonds, as expected, emitted the least noise, with one exception Panel 1, which appeared to represent a weak bond condition. Examination of the metallurgical results showed that some edge rupturing of the initial electrodeposit layer occurred. This did not propagate or cause disruption of the actual bond line, and probably accounted for the increased emissions. The nonbond panels generally gave intermediate emission counts. The explanation for this is that all nonbonds were terminated purposely by full strength bonds, and thus had a smaller area of strong material being strained – thereby emitting less noise – than the entire weak bond area. The emission count only came from the increased yield local to defect edges and occasionally where higher counts existed from the propagation at these points.

Although not directly comparable to these results, the tests on brazed and diffusion bonded panels support these theories. For example, where braze samples failed at the joint line and crack propagation occurred high emission counts were recorded. When gross plate distortion occurred without significant bond line failure only low counts were recorded. This indicates the test was discriminant to the desired bond line information. In the case of diffusion bonded Panel 40, which was a full bond containing a "reference defect", the emission count was approximately double that of the full bonds without such a defect. This was due to the small areas of unbond within the defect pattern yielding or propagating. The same trend was also shown in Panel 31 which was the brazed full bond with "reference defect".

The results on the weak electroform bonds indicate that, with further development, this test could be capable of classifying bond integrity. Careful study of all results shows several areas which require further evaluation. These include:

(a) Determination of maximum pressure that will still maintain the test truly nondestructive.

(b) Development of capability to differentiate between weak bonds and propagating nonbonds.

Another feature of the acoustic emission results which is worthy of continued study and evaluation is the characteristic shape of curves obtained by graph of total count against pressure. Of the thirteen tests run on electroformed panels, only one (Panel 15) does not categorize. The rate of emitted noise shown in these graphs varies distinctly between full strength bonds and weak or nonbond samples. The weak bonds themselves show an increased rate compared to nonbond.

TABLE XIV

Electroform			Nondestructive Evaluation (Correlation with Attained Pattern)				
Panel	Planned Pattern	Attained Pattern	Ultrasonic ("C" Scan)	Holographic	Acoustic Emission Count	Pressure	
						psi	N/m^2
3	Full bond - two defects	One defect	Good	Defect not detected	-		
6	Full bond - two defects	Microstructure indicates pattern achieved.	Full bond	Full bond	365	3,500	24.13×10^6
1	Full bond - no defects	As planned	Good	Good	729	3,500	24.13×10^6
10	Full bond - no defects	As planned	Good	Good	52	3,500	24.13×10^6
11	Full bond - no defects	As planned	Good	Good	153	3,500	24.13×10^6
2	Weak bond - Pattern 1	Apparently successful	Full bond	Some correlation	635	3,500	24.13×10^6
13	Weak bond - Pattern 1	Generally successful, some unbond on micro-structure.	Some unbond but weak bond pattern not evident	Fair correlation	831	3,500	24.13×10^6
5	Weak bond - Pattern 2	As planned	Full bond	Good correlation	978	3,500	24.13×10^6
8	Weak bond - Pattern 2	Not a total duplicate of Panel 5.	Full bond	Some indications poor correlation	-		
9	Weak bond - Pattern 3	Generally as planned	Full bond	Some indications fair correlation	2,647	3,500	24.13×10^6
7	Nonbond Pattern 1	Generally as planned	Fair	Correlated with U.T. and shows additional defects	188	3,500	24.13×10^6
12	Nonbond Pattern 1	As planned. More defects than panel 7.	Fair	Correlates with U.T. plus some additional defects	529	3,500	24.13×10^6
4	Nonbond Pattern 2	As planned	Good	Good correlation	361	3,500	24.13×10^6
15	Nonbond Pattern 2	Generally as planned fewer defects than panel 4.	Good	Good correlation	281		
14	Nonbond Pattern 3	Not completely successful some weak bonding occurred.	Full bond	Some indications and correlation	1,488	3,500	24.13×10^6

TABLE XV

Panel No.	Braze: Planned Pattern	Braze: Attained Pattern	Nondestructive Evaluation (Correlation with Attained Pattern): Ultrasonic ("C" Scan)	Nondestructive Evaluation (Correlation with Attained Pattern): Holography	Nondestructive Evaluation (Correlation with Attained Pattern): Acoustic Emission Count	Nondestructive Evaluation (Correlation with Attained Pattern): Pressure	
						psi	N/m^2
31	Full bond - ref. defect	Full bond, ref. defect not complete	Full bond including most of ref. defect	Correlates to ultrasonic	126	3,500	24.13×10^6
20	Full bond - no defects	As planned (some braze flaw)	Good (area of braze run)	Good	78	3,500	24.13×10^6
21	Full bond - no defects	As planned	Good (land ends ragged)	Good (some pattern variation)	14	3,500	24.13×10^6
35	Full bond - no defects	As planned	Good	Good	3	3,500	24.13×10^6
45	Full bond - no defects	As planned	Good	No defects (poor hologram)	12	3,500	24.13×10^6
22	Weak bond Pattern 1	Almost fully bonded	Almost full bond (land ends ragged)	Correlates UT (pattern change)	89	3,500	24.13×10^6
24	Weak bond Pattern 1	Generally as planned	Good	Good but exaggerated	23 (back plate failure)	3,500	24.13×10^6
23	Weak bond Pattern 2	As planned	Good	Good but exaggerated	1,198	2,100	14.48×10^6
28	Weak bond Pattern 2	As planned	Good	Exaggerated pattern	181	2,500	17.14×10^6
18	Weak bond Pattern 3	As planned	Good	Good	1,145	2,300	15.86×10^6
17	Nonbond	More bonding than planned	Good - more bond than planned	No fringes failed in test	359	1,900	13.10×10^6
26	Nonbond	As planned	Good	Good	2	1,000	6.89×10^6
30	Nonbond	As planned	Good	Good	1	200	1.38×10^6
33	Nonbond	As planned	Good	No test	439	510	3.52×10^6
38	Nonbond	As planned	Good	Good	10	1,000	6.89×10^6

TABLE XVI

Diffusion Bond			Nondestructive Evaluation (Correlation with Attained Pattern)				
Panel No.	Planned Pattern	Attained Pattern	Ultrasonic ("C" Scan)	Holography	Acoustic Emission Count	Pressure	
						psi	N/m^2
40	Full bond - ref. defect	As planned	Good	Good	222	3,500	24.13×10^6
19	Full bond - no defects	As planned	Good	Good	84	3,500	24.13×10^6
27	Full bond - no defects	As planned	Good	Good	55	3,500	24.13×10^6
32	Full bond - no defects	As planned	Good	Good	115	3,500	24.13×10^6
37	Full bond - no defects	As planned	Good	Good	81	3,500	24.13×10^6
36	Weak bond Pattern 1	Almost fully bonded	Good	Poor	25	3,500	24.13×10^6
48	Weak bond Pattern 1	Some extra bonding but generally as planned	Good	Fair/Poor	85	3,500	24.13×10^6
34	Weak bond Pattern 2	Almost completely bonded	Good	Good	13	3,500	24.13×10^6
29	Weak bond Pattern 3	Generally as planned	Good	Poor	95	3,500	24.13×10^6
43	Weak bond Pattern 3	Generally as planned	Good	Fair	59	3,500	24.13×10^6
39	Nonbond	Full bond	Good	No defects (poor clarity)	55	3,500	24.13×10^6
41	Nonbond	Almost completely bonded	Good	Good	33	3,500	24.13×10^6
42	Nonbond	Almost no bond	Good	No pattern	470	400	2.76×10^6
44	Nonbond	Almost completely bonded	Good	Fair	13	3,500	24.13×10^6
49	Nonbond	Some extra bonding	Good	Good	75	3,500	24.13×10^6

4. Holography

Comparison of holograms with the matching ultrasonic "C" scans shows that excellent correlation was obtained between the two techniques, Figures 47 thru 55. This indicates the ability of the technique to distinguish between bond and nonbond conditions. More important, is that the holograms on weak electroformed bonds also show positive results (e.g., Panels 5 and 9). This establishes two of the four test methods as demonstrating feasibility for determining the weak bond condition. The results of destructive testing showed that holography was also capable of determining the high stress concentration areas which were ultimately the failure regions. This type of information used during initial design research programs for space hardware could provide valuable information to the design engineers.

Study of the results also shows that more understanding of variables affecting holographic image quality and interpretability is required. Some limited work was conducted in the areas of surface flatness requirements, material thickness and pressure variations. Figure 56 is a hologram of the 0.060 in. (1.524×10^{-3} m.) thick electroformed Panel 11 at 500 psi (3.45×10^{6} N/m.^{2}), showing good definition. The same panel after additional buildup to 0.120 in. (3.048×10^{-3} m.) is shown along side. 500 psi (3.45×10^{6} N/m.^{2}) was again applied and the definition is considerably reduced. The fact that pressure can effect and in fact compensate for thickness is indicated by comparing the holograms obtained on diffusion bonded Panel 36 (taken at 500 psi (3.45×10^{6}/m.^{2})) with those on Panels 34 and 43 (taken at 1440 psi or 9.93×10^{6} N/m.^{2}). Changes in thickness uniformity within the same panel also produced differences, with the thicker sections being less interpretable than the thinner ones due to less surface movement for a given pressure. Figure 57 is a hologram indicating the zig-zag pattern attributable to the greater thickness on the right hand side. The adjacent hologram shows the complete absence of this pattern on the same panel after surface grinding flat. The results on test panels also are highly indicative that thickness and pressure variances influence definition, (compare holograms on Panels 11, 22, 31, and 44). A more detailed study is required to fully explain all these variations. The fringe patterns also vary to some extent. The hologram on Panel 22 shows the bands going transverse to the panel width when in all other cases the bands tended to follow the major axis of the lands.

An important factor which requires further investigation is the effect of test sequence on the results. As a consequence of the established sequence, holography was always performed subsequent to acoustic emission. This means that some prestressing to considerably higher pressure (at least 2x) than that used for the holograms had always occurred prior to holography. It is not known whether stress patterns and detection sensitivity were enhanced by this factor. The results definitely indicate that in some cases permanent deformation had already occurred, i.e., Panels 17 and 33 on which fringe patterns could not be obtained, due to gross movement. This means that in at least these cases the test had been destructive. It is essential to ensure that effective results are obtainable without any suspicion of permanent deformation. In view of this, a closer evaluation of the acoustic emission data showed that little or no significant data would be lost by performing holography, to a maximum of approximately 1000 psi (6.89×10^{6} N/m.^{2}), prior to acoustic emission testing. Any future work would be carefully scrutinized in this area with two major objectives of test succession in mind. These are:

(a) Review test approach with the ideal of conducting holography and acoustic emission concurrently.

(b) If this is not possible carefully evaluate configuration design and conduct holography at as low a pressure as possible prior to acoustic emission at proof pressure level.

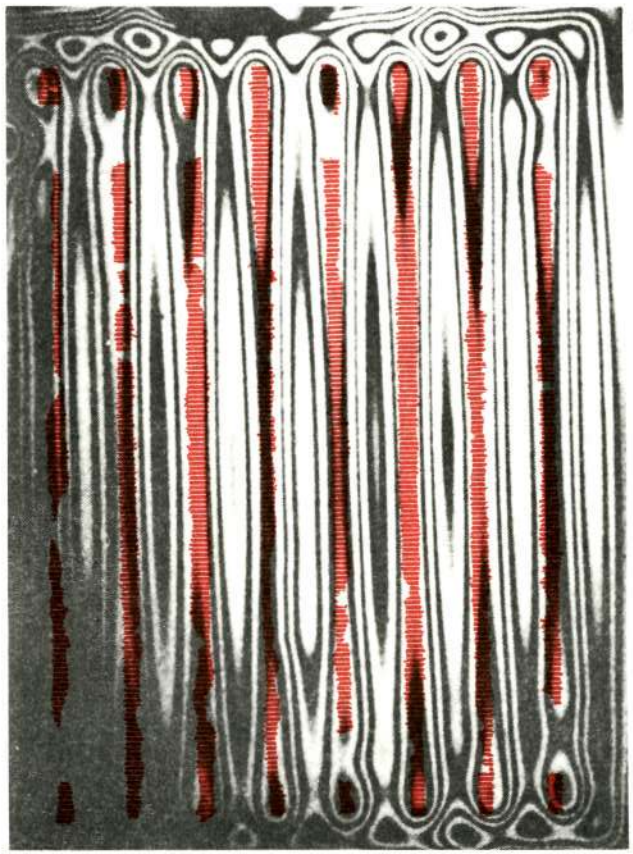

OVERLAY OF ULTRASONIC RESULT ON
THE HOLOGRAM FOR PANEL 4E

Figure 47

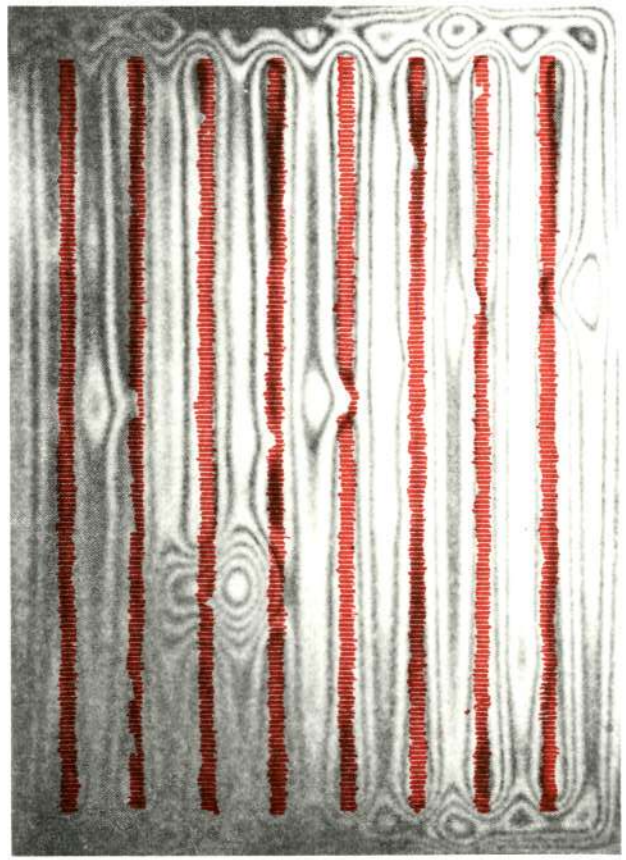

OVERLAY OF ULTRASONIC RESULT ON
THE HOLOGRAM FOR PANEL 7E

Figure 48

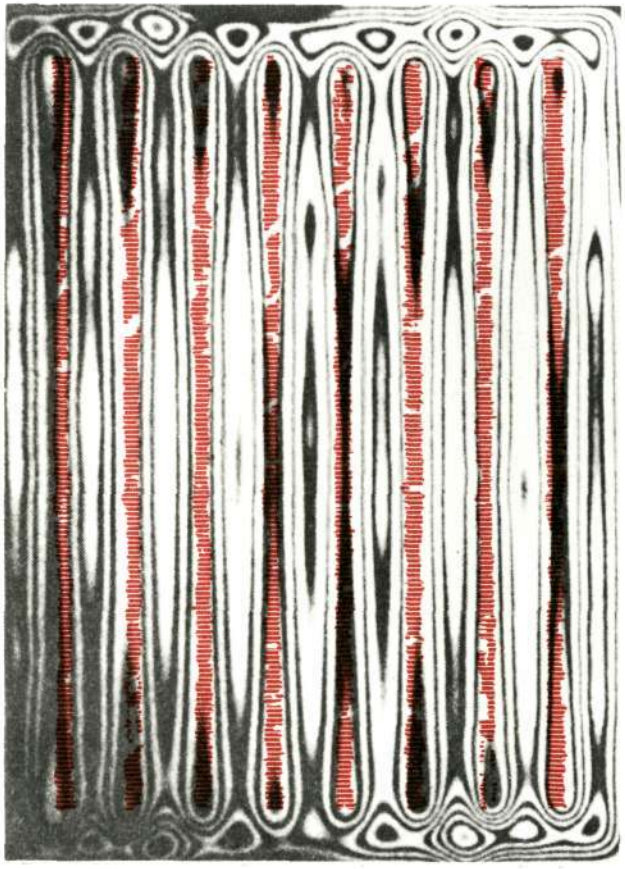

OVERLAY OF ULTRASONIC RESULT ON HOLOGRAM FOR PANEL 13E

Figure 49

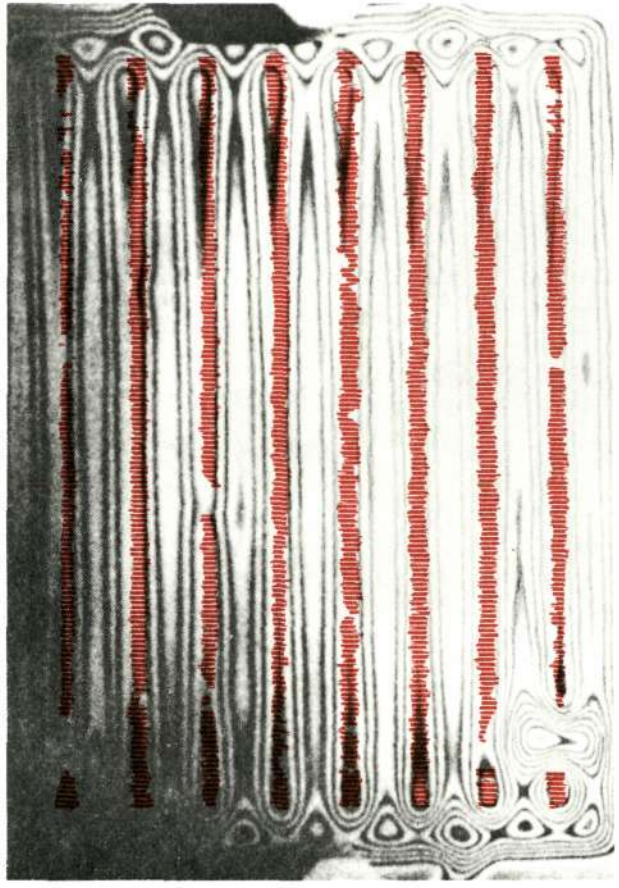

OVERLAY OF ULTRASONIC RESULT ON HOLOGRAM FOR PANEL 15E

Figure 50

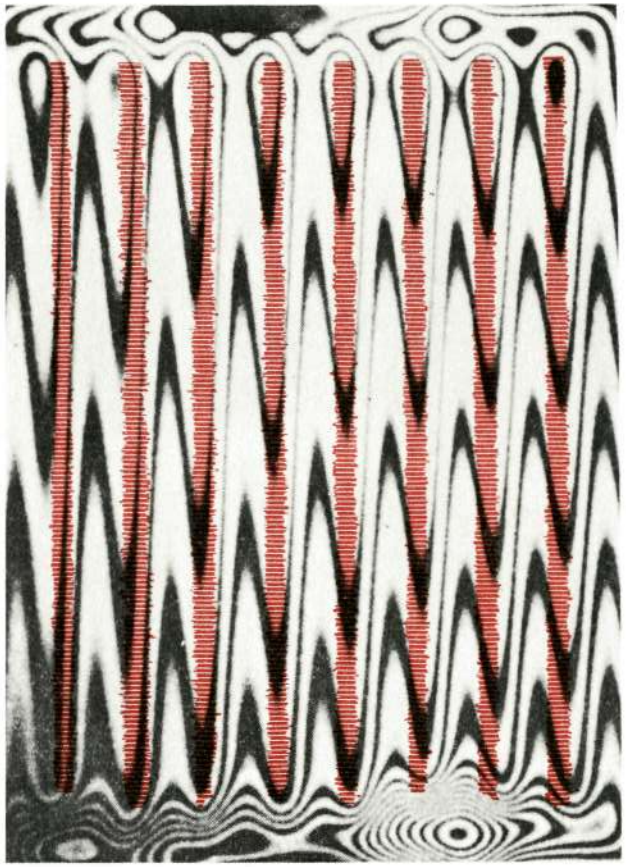

OVERLAY OF ULTRASONIC RESULT ON HOLOGRAM
FOR PANEL 21B

Figure 51

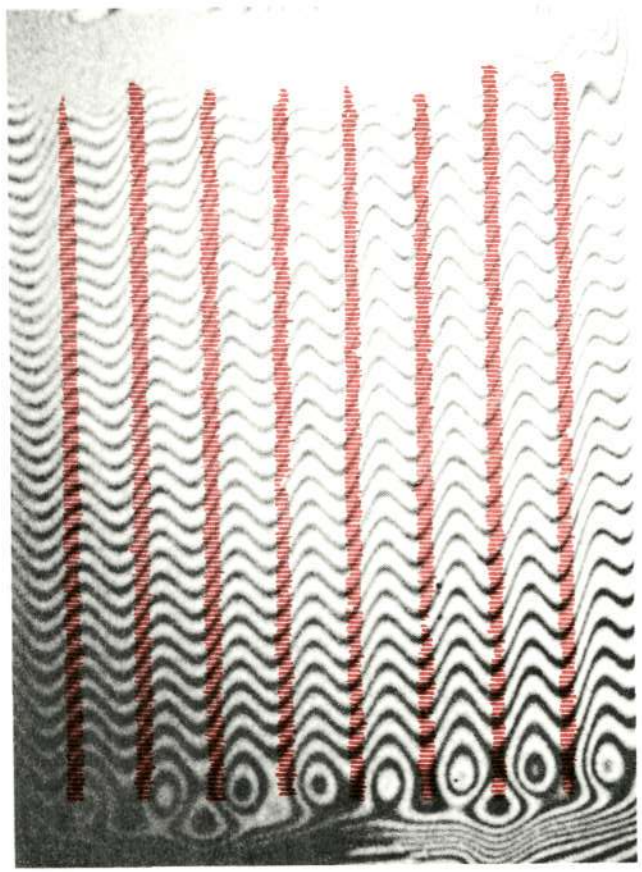

OVERLAY OF ULTRASONIC RESULT ON
HOLOGRAM FOR PANEL 22B

Figure 52

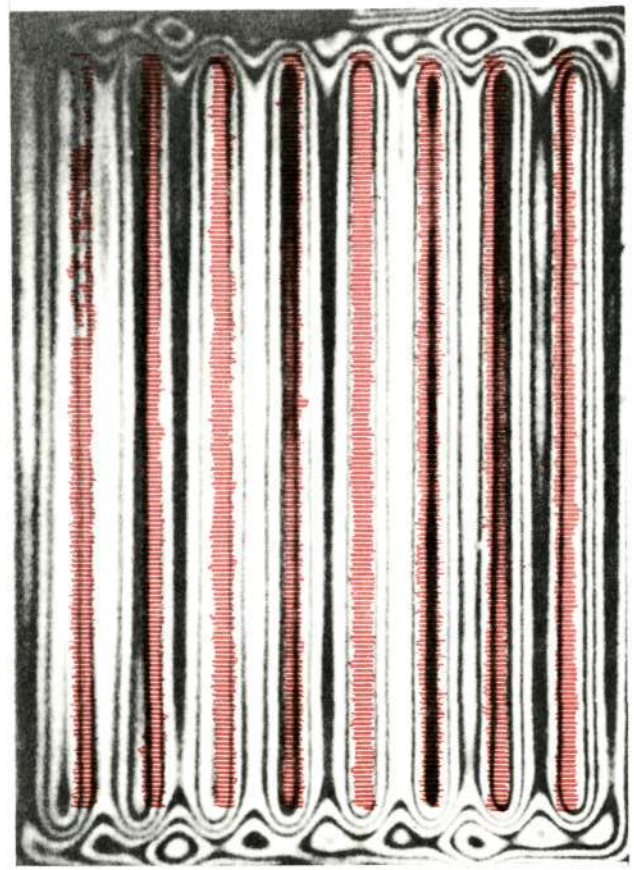

OVERLAY OF ULTRASONIC RESULT ON
HOLOGRAM FOR PANEL 34D

Figure 53

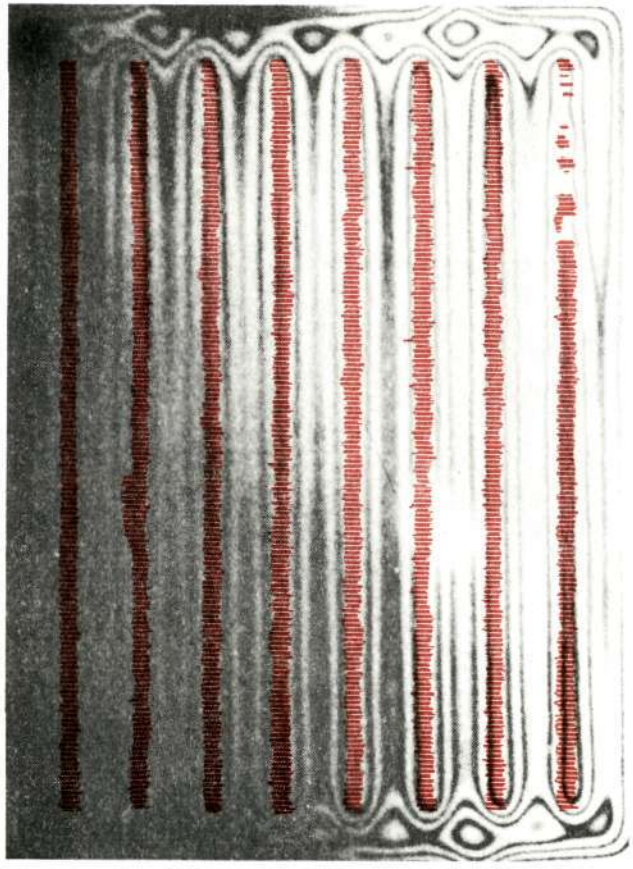

OVERLAY OF ULTRASONIC RESULT ON HOLOGRAM FOR PANEL 40D

Figure 54

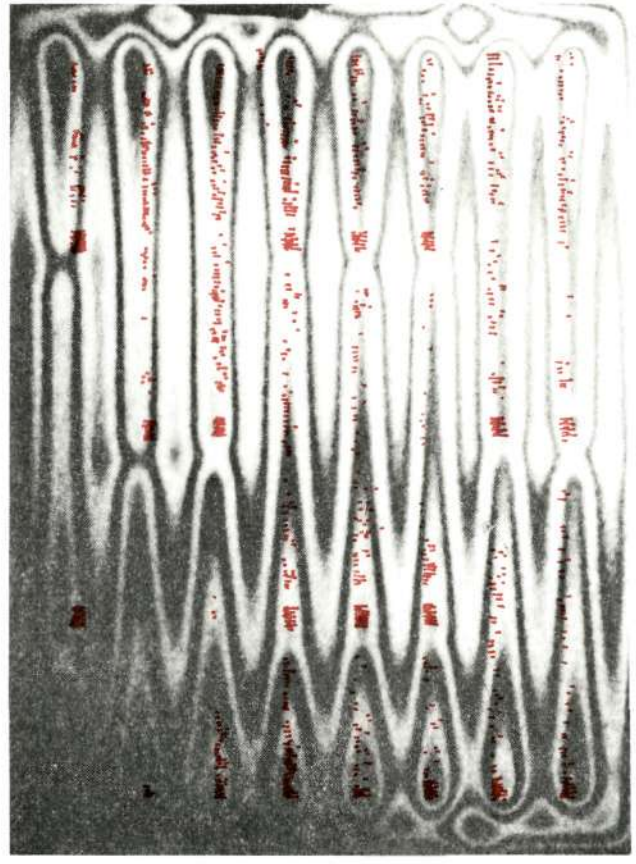

OVERLAY OF ULTRASONIC RESULT ON HOLOGRAM FOR PANEL 49D

Figure 55

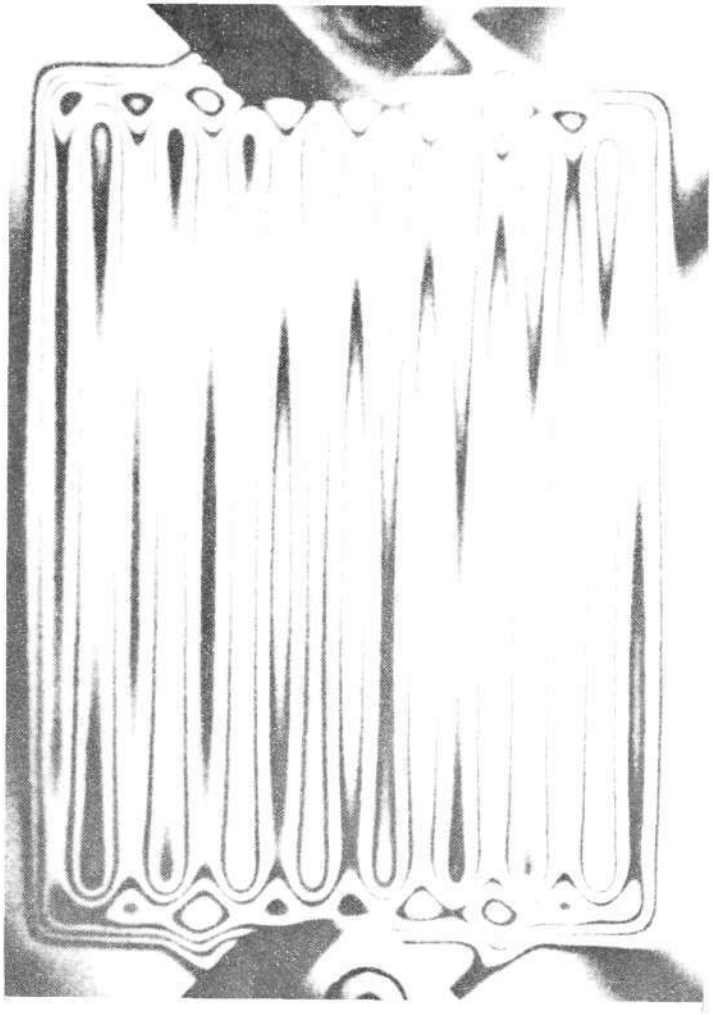

0.060 IN.
(1.524 x 10^{-3} m.)

500 PSI
(3.45 x 10^{6} N/m.^{2})

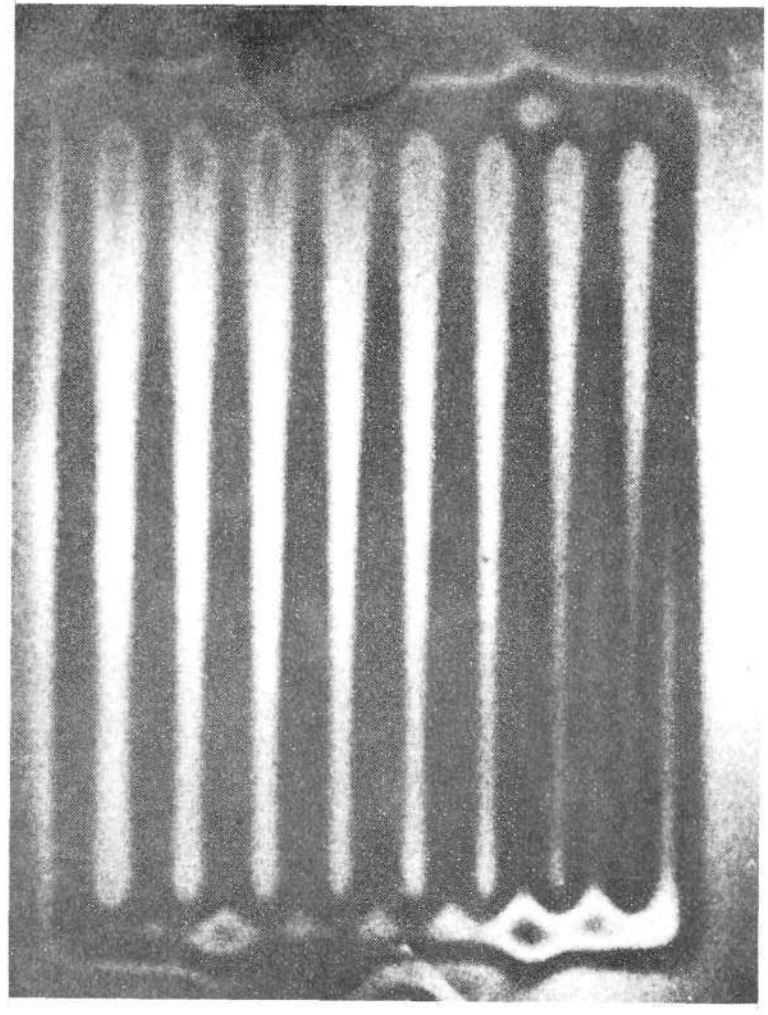

0.120 IN.
(3.048 x 10^{-3} m.)

500 PSI
(3.45 x 10^{6} N/m.^{2})

PANEL 11. EFFECT OF THICKNESS ON HOLOGRAM

Figure 56

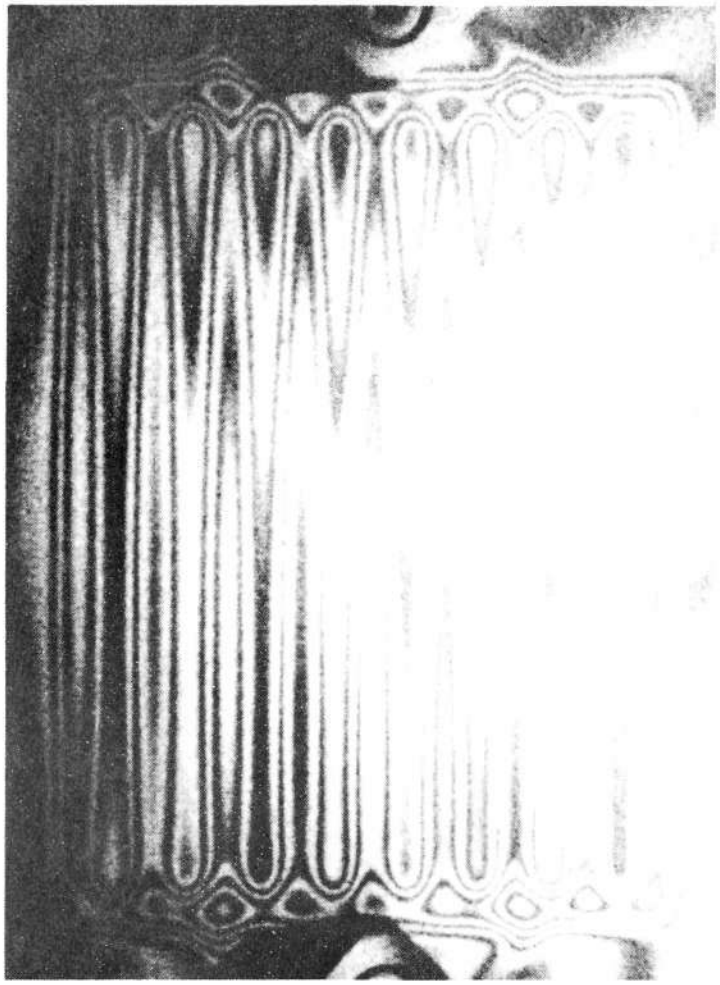

BEFORE GRINDING 500 PSI
500 PSI (3.45×10^6 N/m.^{2})

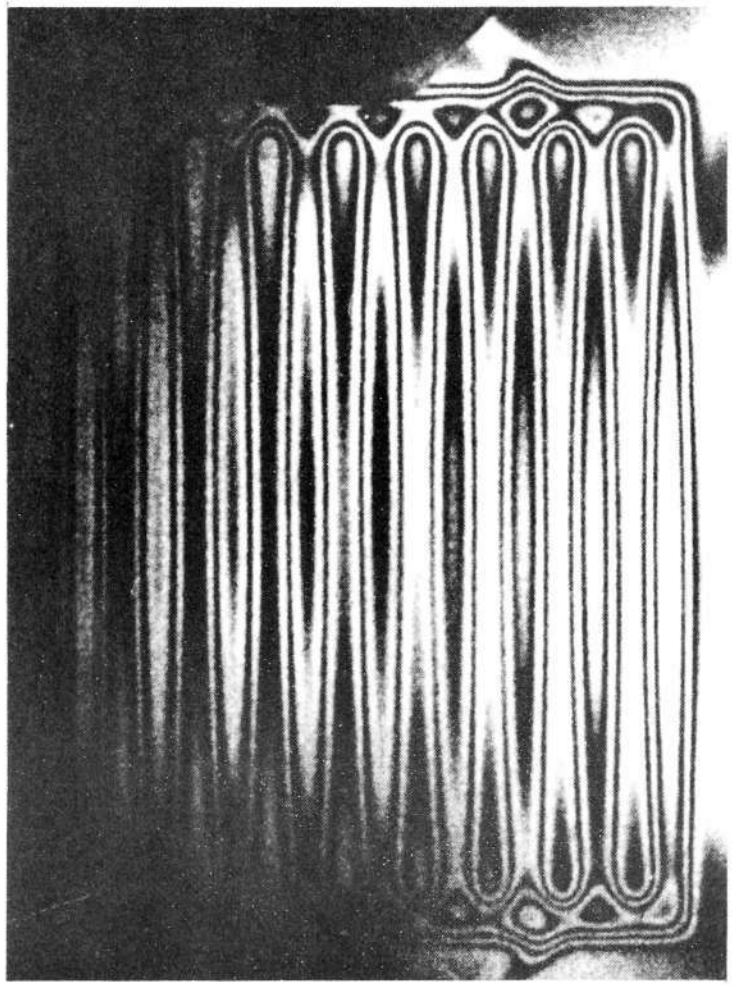

AFTER GRINDING FLAT 500 PSI
500 PSI (3.45×10^6 N/m.^{2})

PANEL 10. EFFECT OF FLATNESS ON HOLOGRAM

Figure 57

5. Spectrum Analysis

The fourth method was considerably more experimental in nature and did not show the obvious application that the other methods did. It did nevertheless show sufficient merit to have justified its inclusion in the selected methods.

The study was conducted on only two panels selected from each of the three fabrication methods. These panels were:

No.		Fabrication Method		Type
3		Electroformed		Full Bond
8		Electroformed		Weak Bond
20	△1	Brazed	△2	Full Bond
28	△1	Brazed	△2	Nonbond
37	△1	Diffusion Bonded	△2	Full Bond
49	△1	Diffusion Bonded	△2	Nonbond

△1 These panels had electroformed backing to prevent bulging during Acoustic Emission pressurization and thus limited the ultrasonic approaches.

△2 Nonbond is listed here instead of weak since the brazing and diffusion bonding process did not provide bond line variance other than full and nonbond areas.

The spectrum envelope photographs of each test are contained in the figures listed below.

(a)	Pulse-Echo Method	Figures 58 thru 81
(b)	Thru-Transmission Method	Figures 82 thru 88
(c)	Contact Pitch and Catch Method	Figures 89 thru 98

The majority of the work was conducted using the pulse-echo longitudinal wave method with 10, 15 and 25 MHz frequency transducers. In each case an envelope of the front surface reflection was obtained initially to show the transducers' characteristics and to set center frequency (Figures 58 thru 61). Subsequently, an envelope of each interface (i.e., channel, bond and back surface) was obtained where possible for comparison to the set center frequency (Figures 62 thru 81). Deviations from center were measured and designated as "actual" peak frequency. Reviewing the amount and direction of center frequency shifts reveals the following:

a. Figures 62 and 63 display an increase in frequency when gated to the channel interface where a good strong reflection is possible. Complete explanation is not evident for this other than possibly focusing was more ideal at that interface.

b. Most of the photographs depict a decrease in frequency. This was expected due to attentuation factors at each interface.

c. Figures 76 and 79 display the greatest frequency shifts on brazed Panels 20 and 28, respectively. This is understandable, since the brazing fabrication method introduced a thicker dissimilar bond interface material by using a copper sheet which creates higher impedance mismatch and attenuation.

d. Figures 76 and 79 along with Figures 69 thru 72 also indicate which transducer approached the ideal frequency for the material and thickness involved. In this case the nominal 15 MHz transducer (actually operating at 17 MHz) offered the greatest frequency shifts.

The thru-transmission method could only be gated to a composite signal representing sound transmission through all interfaces and therefore did not permit individual interface selection and hence evaluation. The test was also limited to 10 MHz which was the highest frequency available capable of sufficient sound transmittal for monitoring. In this case the setup frequency, Figure 82, was obtained with water acting as the only attenuative media. Very little frequency shift was noted, Figures 83 through 88, and no significant conclusions could be drawn.

The pitch and catch method used the back reflection from a 0.1195 in. (3.035×10^{-3} m.) thick nickel plate as its reference, Figure 89, since it is a contact test method and no sound reflection from the top surface was recordable. Review of Figures 90 thru 98 provide no conclusive trends. The only trend obvious is that where bonds exist, there is an increase in center frequency from the reference Figure 89, and where nonbond is present, there is a decrease. It is also evident that no difference is detectable between full and weak bonds. The three methods employed represent a diversified approach but should not be considered as the only possible ultrasonic approaches. Many other ultrasonic applications are possible including the "delta concept" which may provide the technology break-through in establishing spectrum analysis as a NDE tool worthy of development within its own right.

The results obtained to date offer no conclusive proof that spectrum analysis is capable of determining bond integrity.

Set-Up Pulse-Echo/Top Surface Interface/2 MHz per Div. Typ. F-16 1 Sec 3000 Speed Film (Typical)

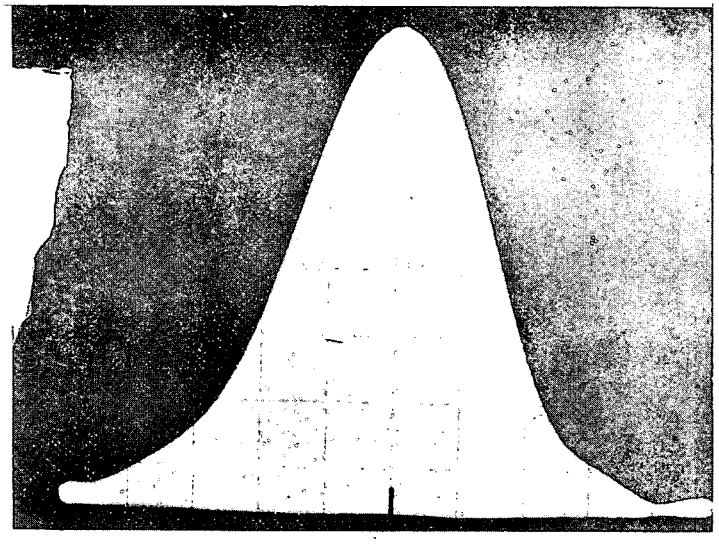

Panel No. 3 (Full) 15 MHz Transducer or Displayed
17 MHz Center Freq. 17 MHz Actual Freq.

Figure 58

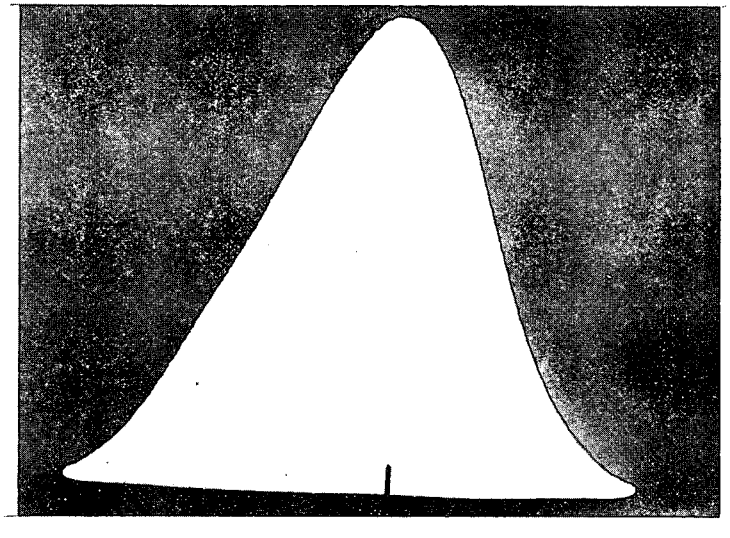

Panel No. 8 (Weak) 25 MHz Transducer
14 MHz Center Freq. 14 Actual

Figure 59

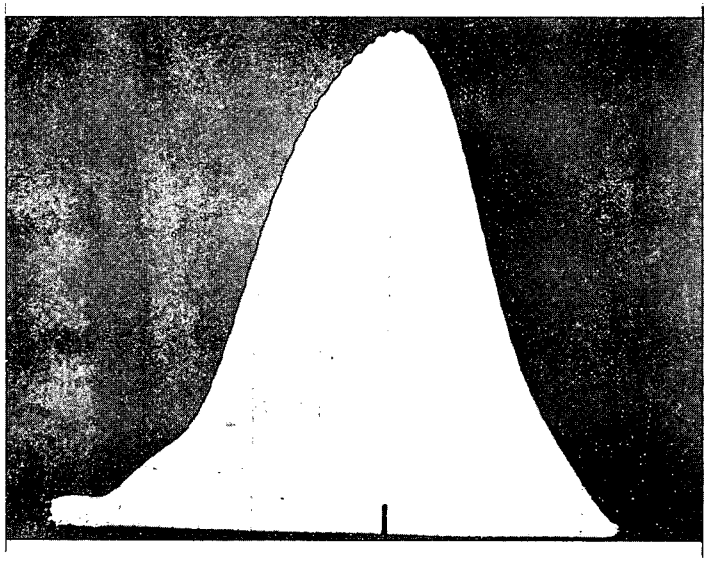

Panel No. 3 (Full) 25 MHz Transducer
15 MHz Center Freq. 15 Actual

Figure 60

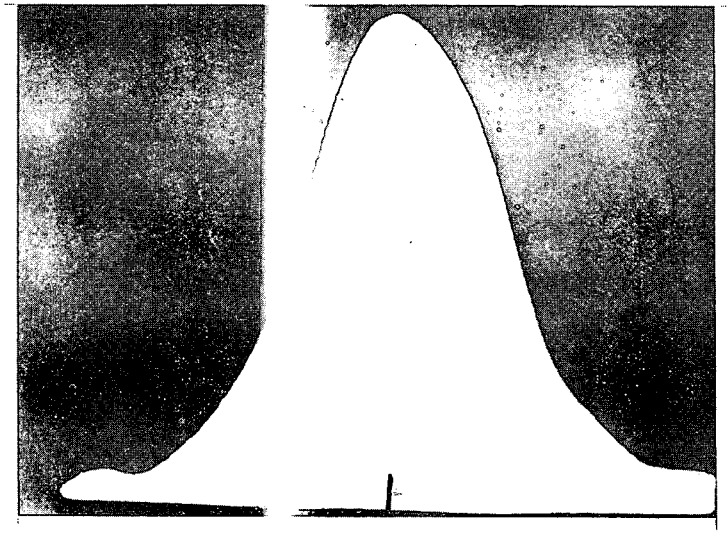

Panel No. 3 (Full) 10 MHz Transducer
10 MHz Center Freq. 10 Actual

Figure 61

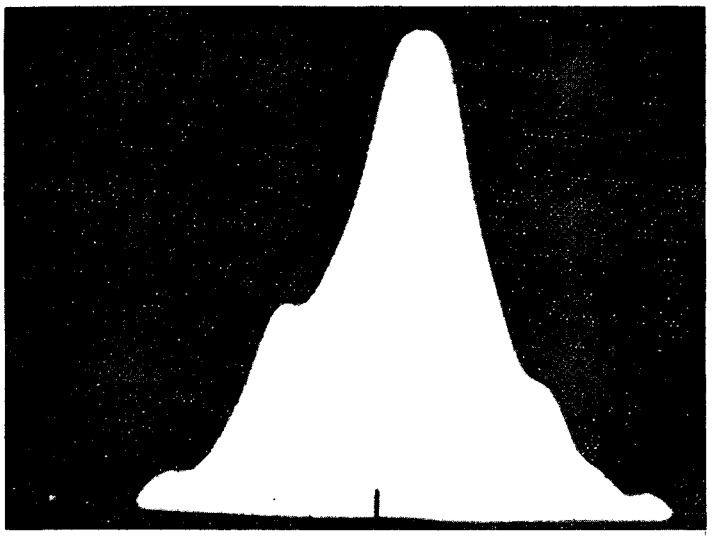

Panel No. 3 (Full)
15 MHz Center Freq
16 Actual

Figure 62

Note: Both Increase in Center Freq.

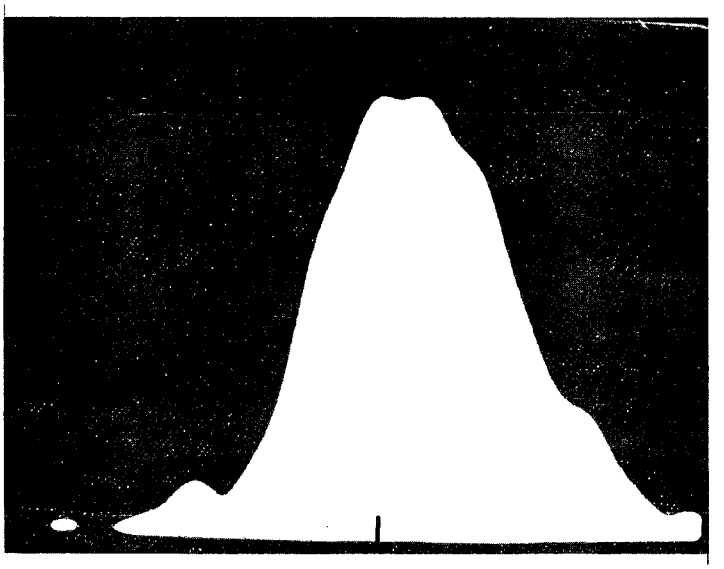

Panel No. 8 (Weak)
14 MHz Center Freq.
15 Actual

Figure 63

Pulse-Echo/Back Surface Interface Reflection/10 MHz Center Freq.

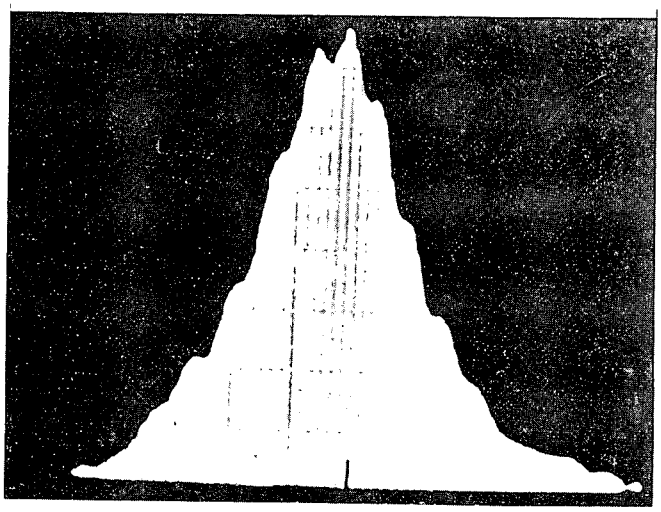

Panel No. 3 (Full)
9.75 Actual

Figure 64

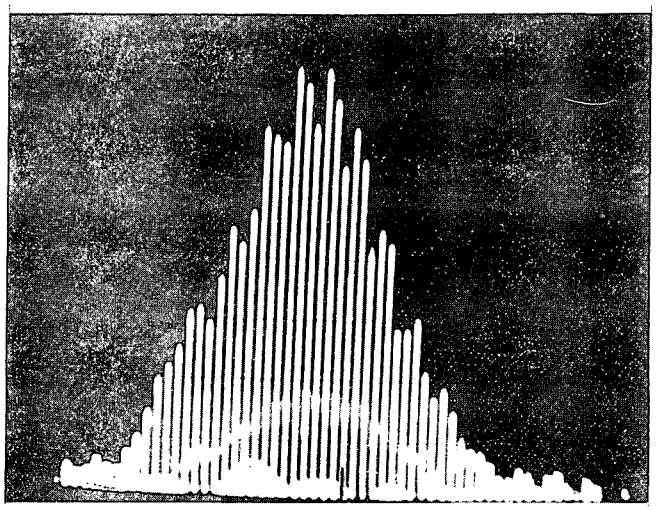

No. 37 (Full)
8 Actual

Figure 66

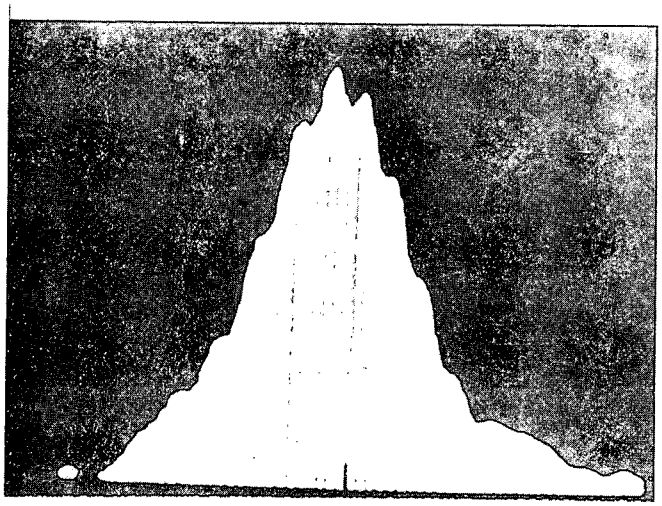

No. 8 (Weak)
9 Actual

Figure 65

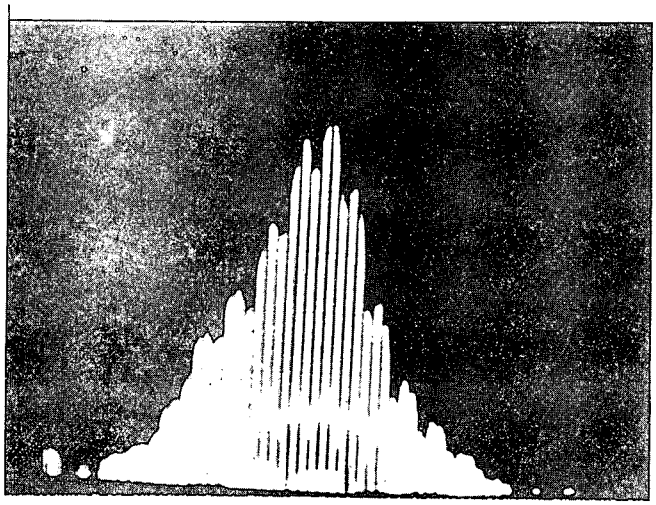

No. 49 (Non-Bond)
8 Actual

Figure 67

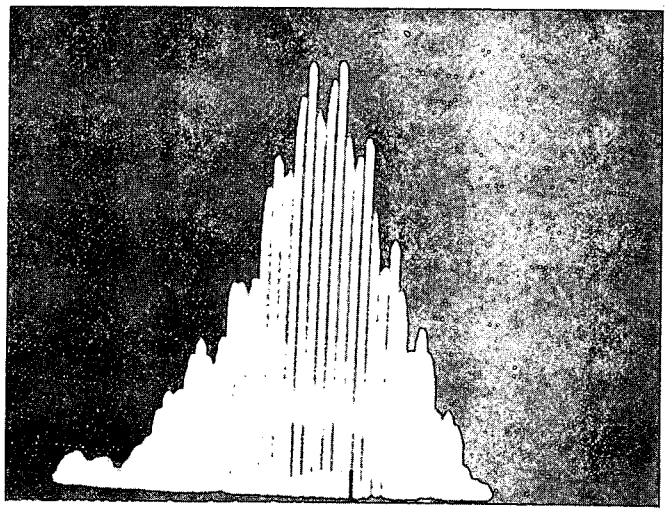

No. 20 (Full) 8 - 9 Actual

Figure 68

Note: Decrease in Center Freq.

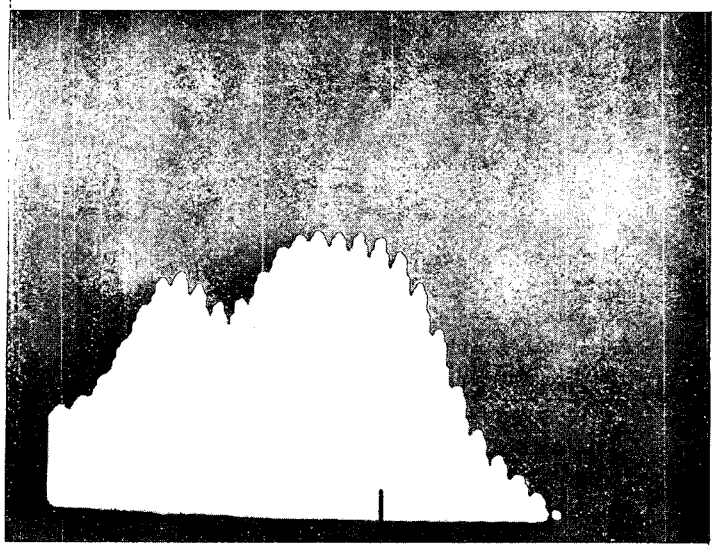

Panel No. 3 (Full)
15 Actual

Figure 69

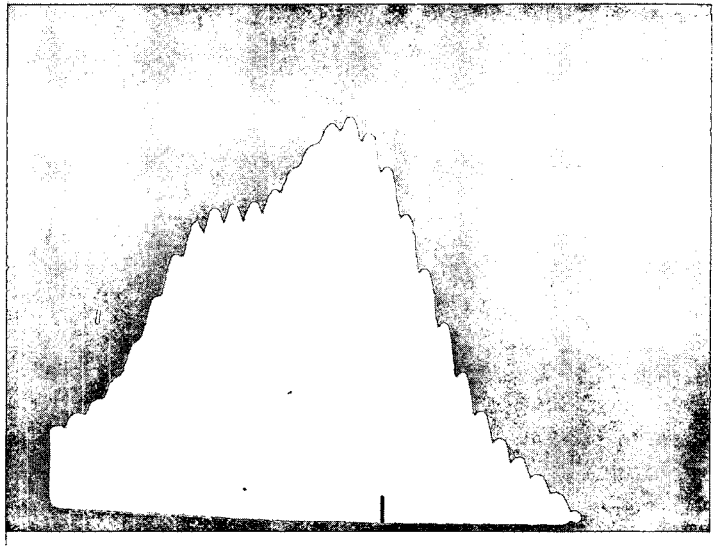

No. 8 (Weak)
16 Actual

Figure 70

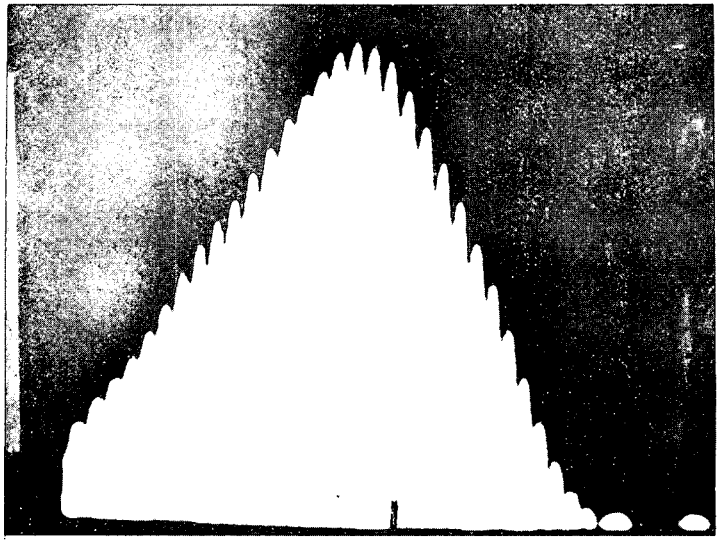

No. 37 (Full)
15.5 Actual

Figure 71

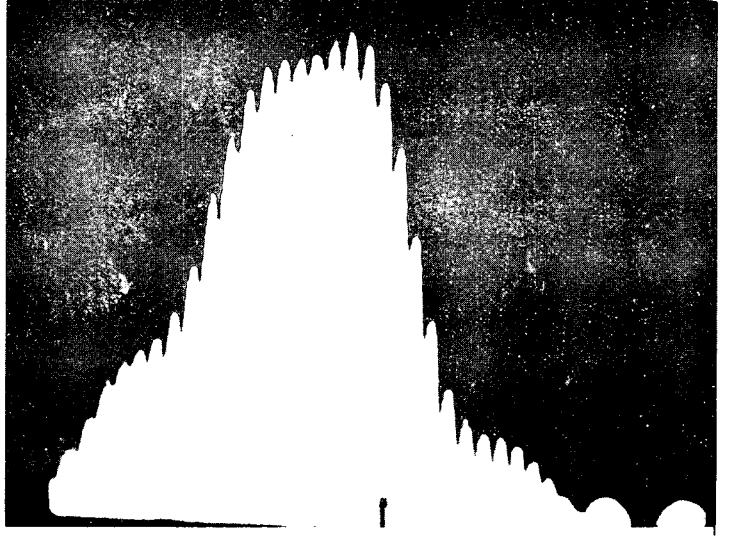

No. 49 (Non-Bond)
15 Actual

Note: Decrease in Center Freq.

Figure 72

Pulse-Echo/Back Surface Interface (Center Frequency Marked)

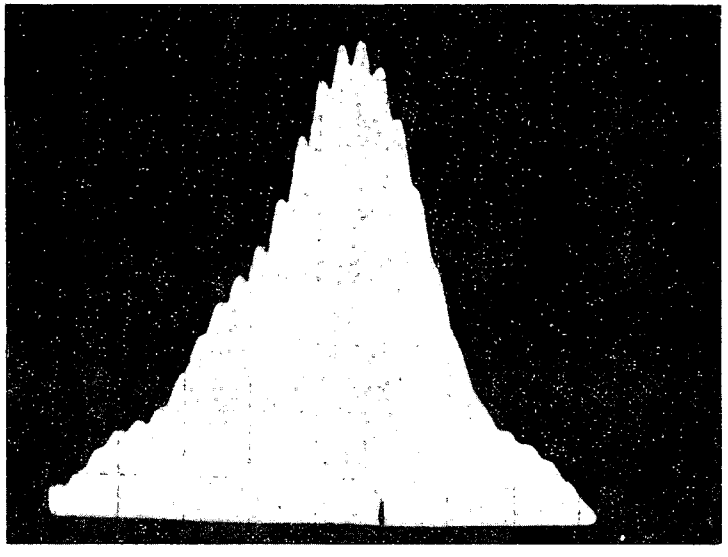

Panel No. 3 (Full)
15 MHz Center Freq.

14 Actual
Figure 73

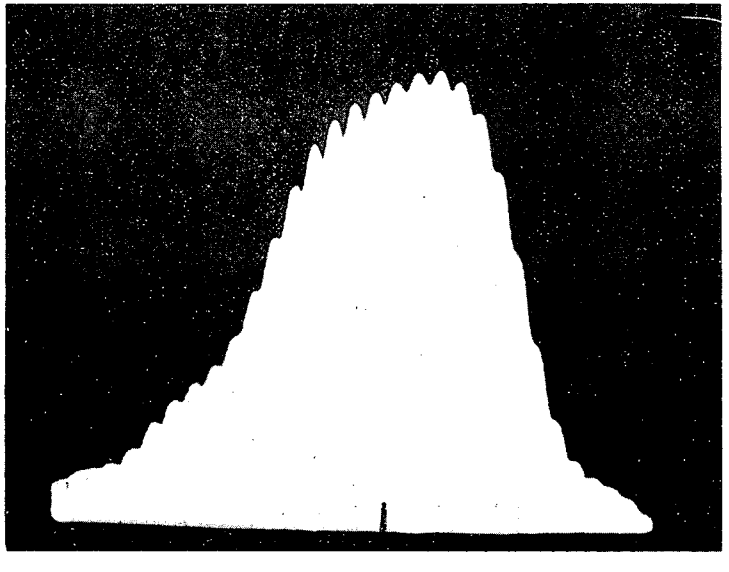

No. 8 (Weak)
14 MHz Center Fre

15 Actual
Figure 74

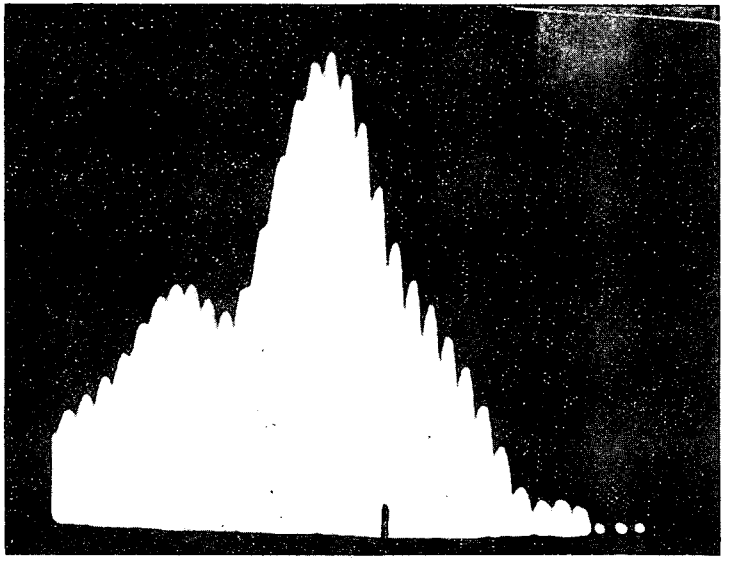

No. 37 (Full)
15 MHz Center Freq.
13 Actual

Figure 75

Pulse-Echo/Bond Interface/Panel No. 20 (Full)

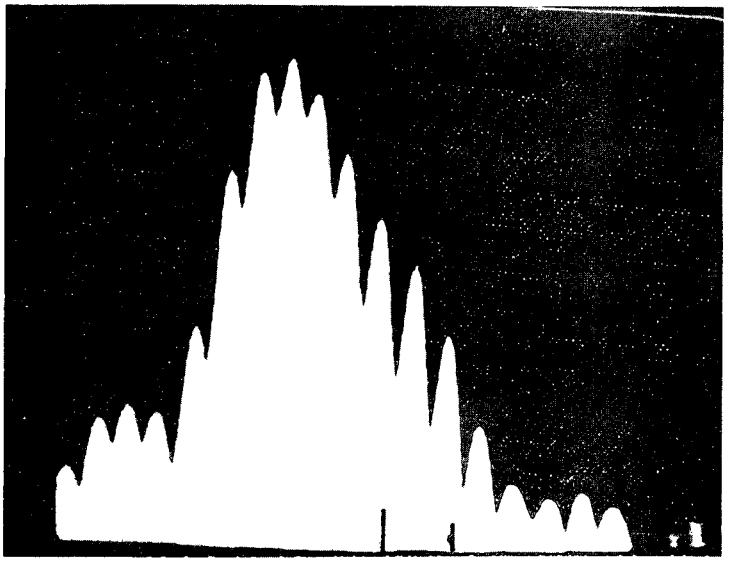

17 MHz Center Freq.
14 Actual

Figure 76

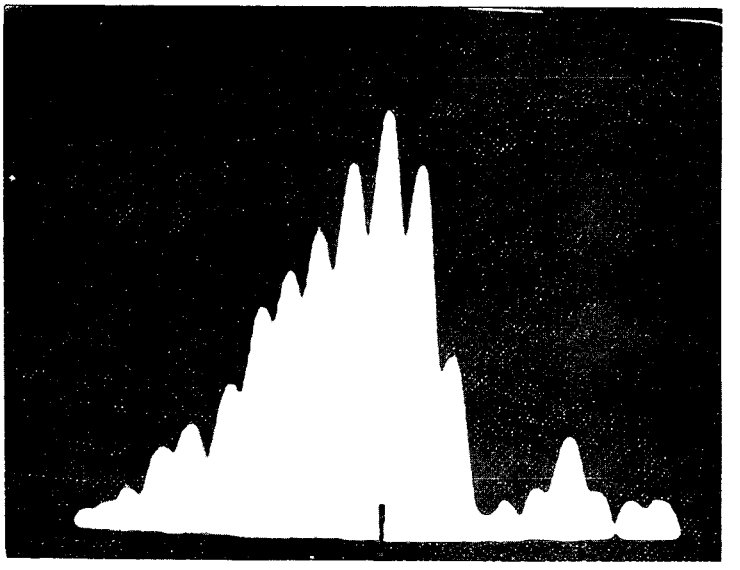

15 MHz Center Freq.
15 Actual

Figure 77

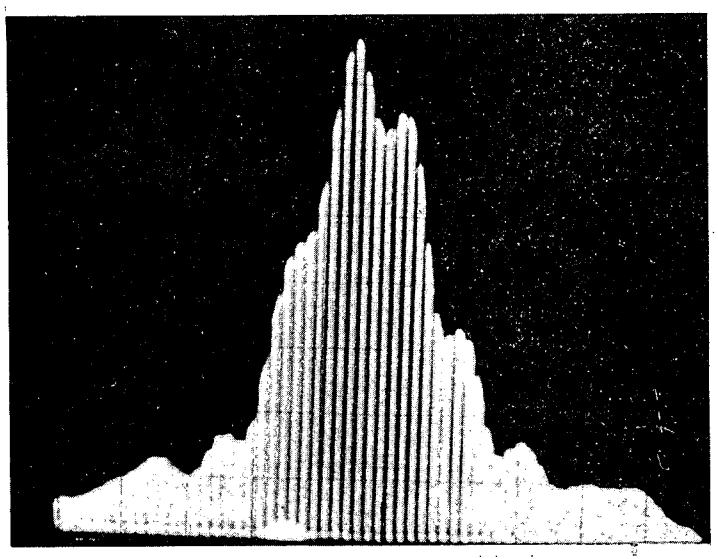

Non-Bond 10 MHz
9 Actual

Figure 78

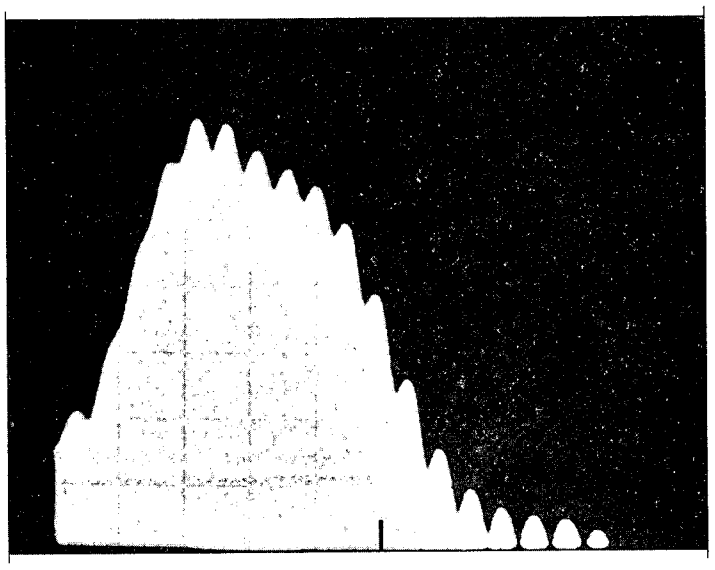

Non-Bond 17 MHz
12 Actual

Figure 79

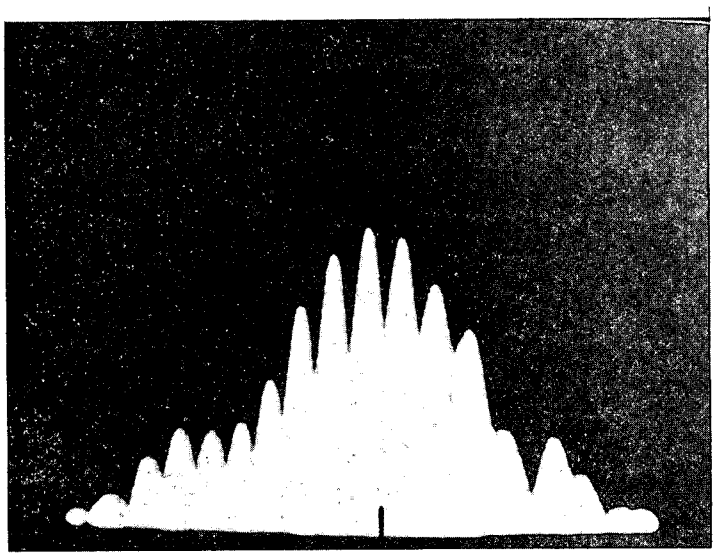

Bond 15 MHz
15 Actual

Figure 80

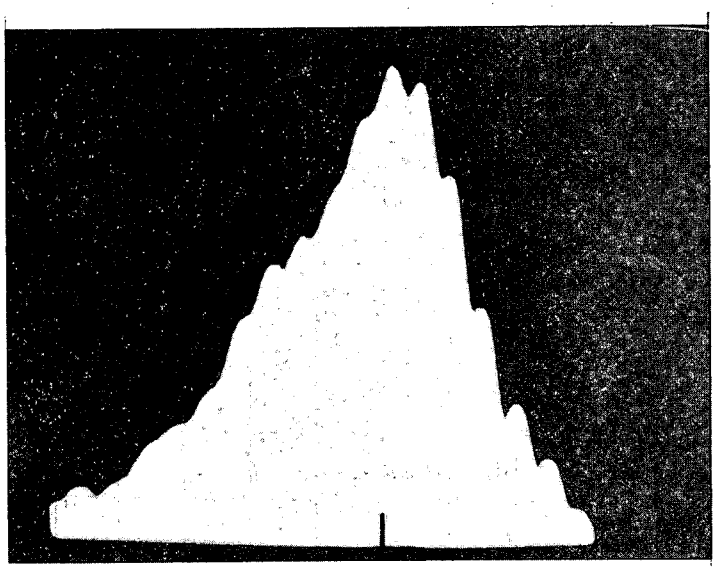

Failed Area 15 MHz
15 Actual

Figure 81

FOLDOUT FRAME 1

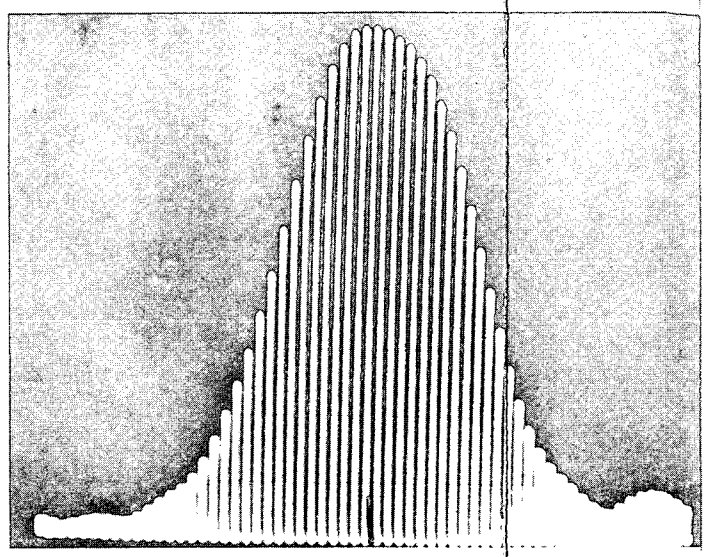

Set-UP
Transducers
2.25 in. Water Path
10 Actual

Figure 82

Through-Transmission/Land/Bond Composite/10 MHz Center Freq.

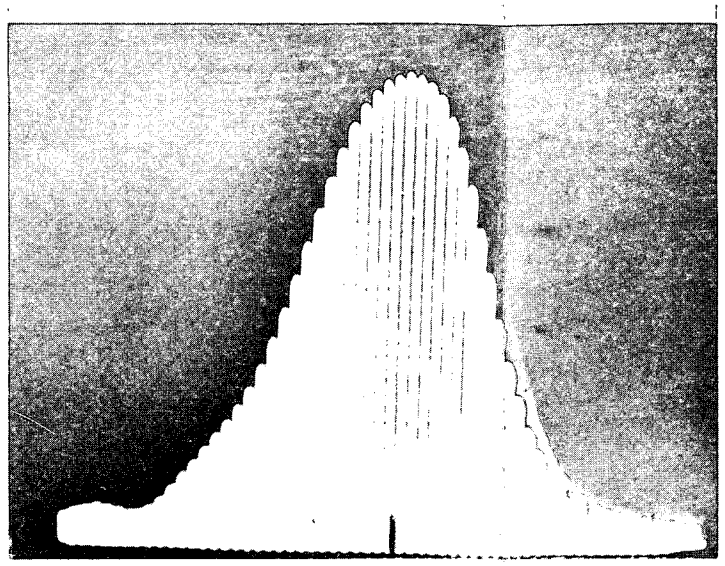

Panel No. 3 (Full)
10 Actual

Figure 83

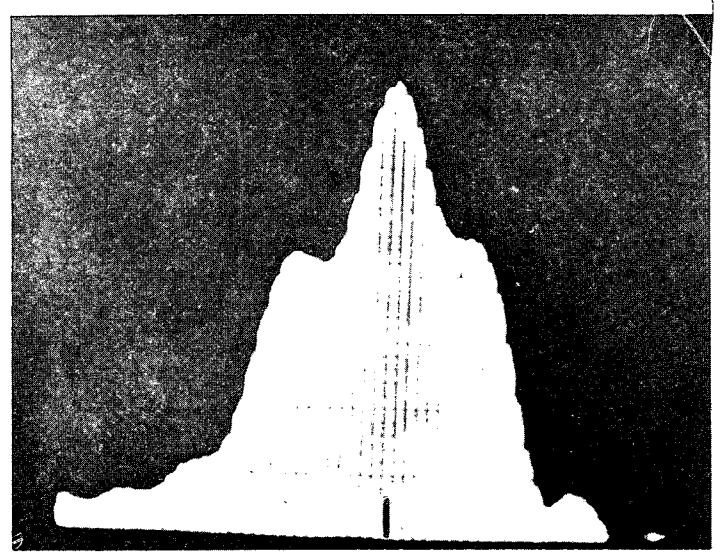

No. 8 (Weak)
10 Actual

Figure 84

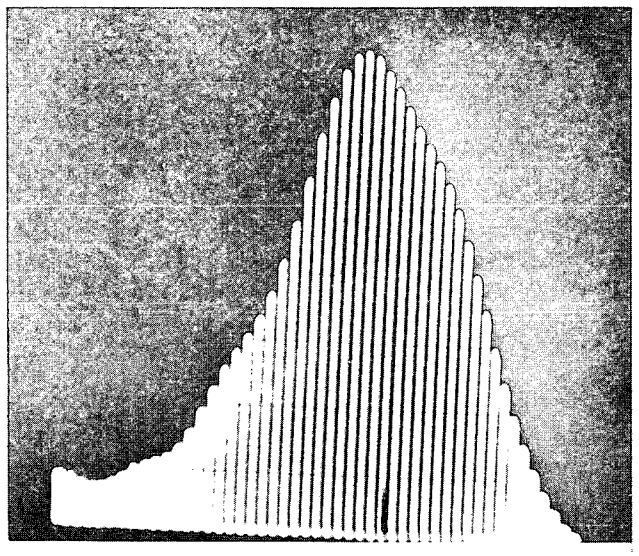

No. 20 (Full)
9 Actual

Figure 85

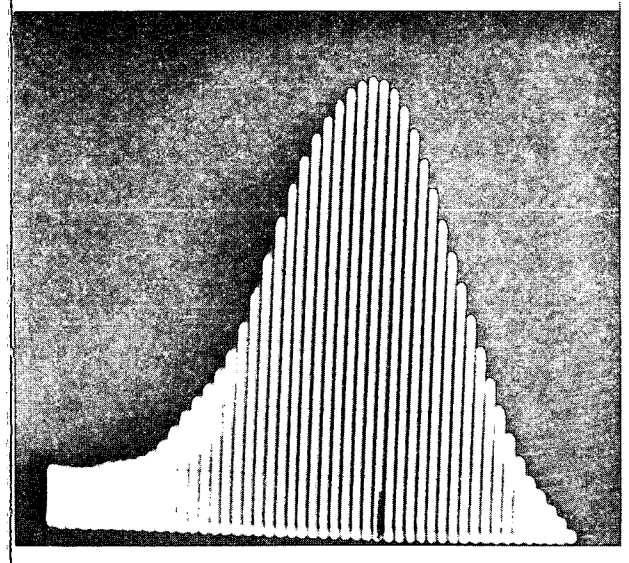

No. 28 (Non-Bond)
9 Actual

Figure 86

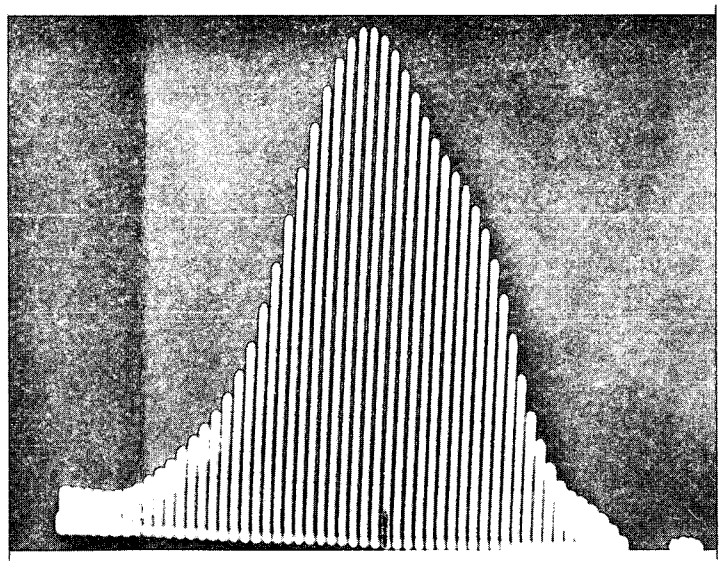

No. 37 (Full)
8 Actual

Figure 87

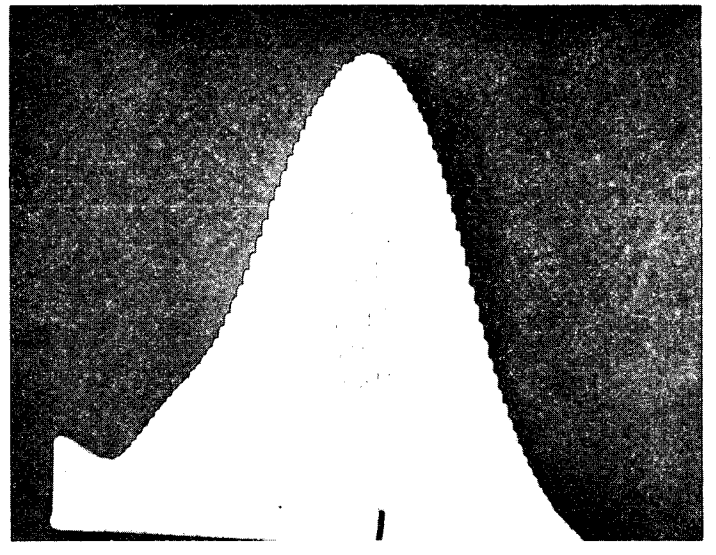

No. 49
(Non-Bond)
9 Actual

Figure 88

Pitch and Catch/5 MHz Center Freq./0.5 MHz per Div. Typ.

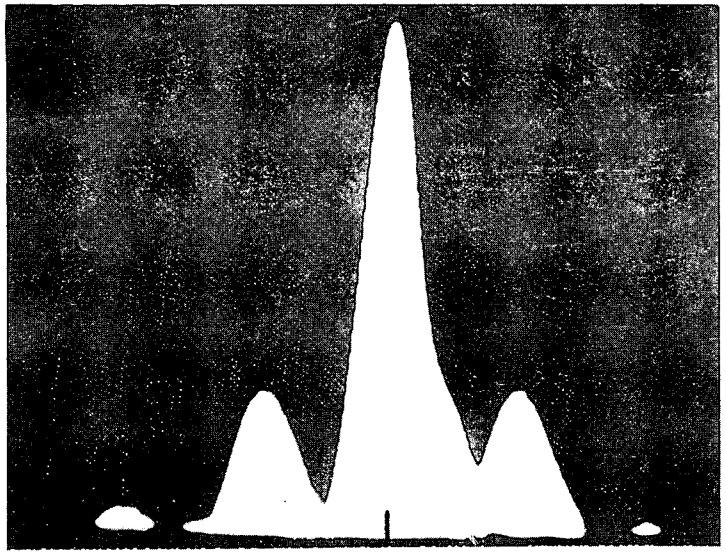

Set-UP 0.1195 N. Back Interface
5 Actual Figure 89

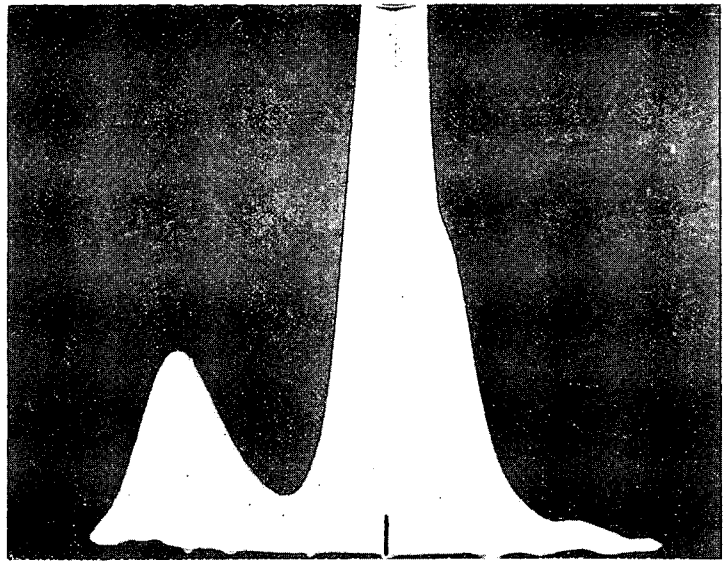

Panel No. 3 (Full) 5 Actual
Channel Interface
Figure 90

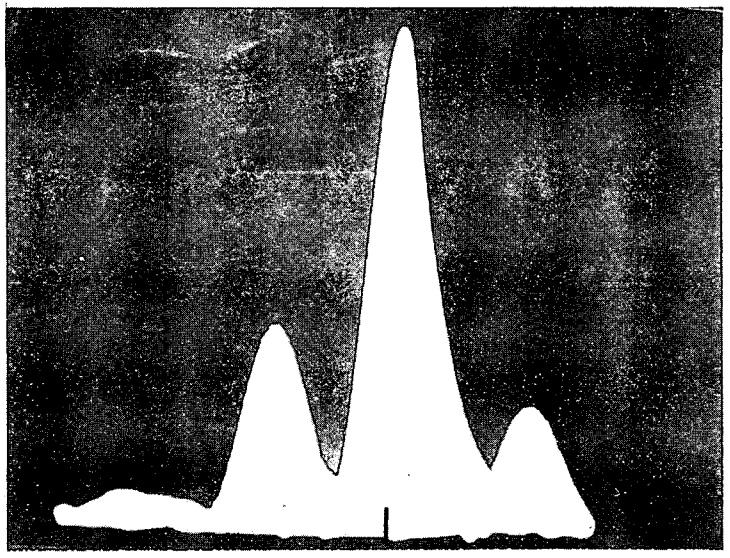

No. 20 (Full) Interface
Channel 5.25 Actual Figure 91

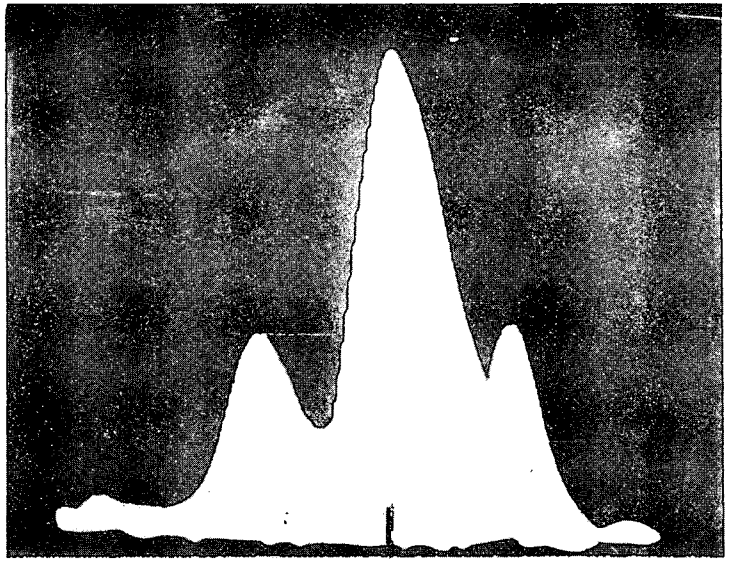

No. 28 (Non-Bond) 4.75 Actual
Non-Bond
Figure 92

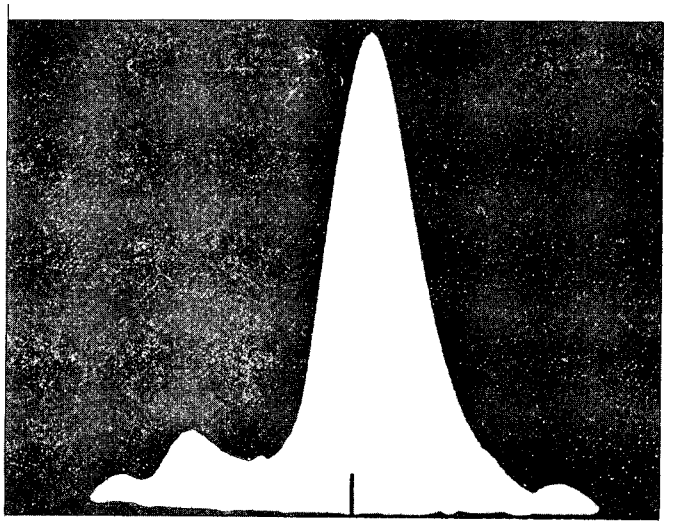

No. 3 (Full) 5.25 Actual

Figure 93

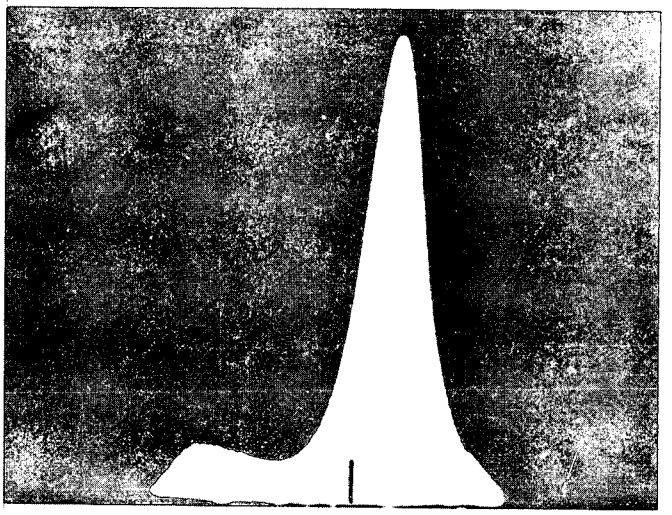

No. 8 (Weak) 5.5 Actual

Figure 94

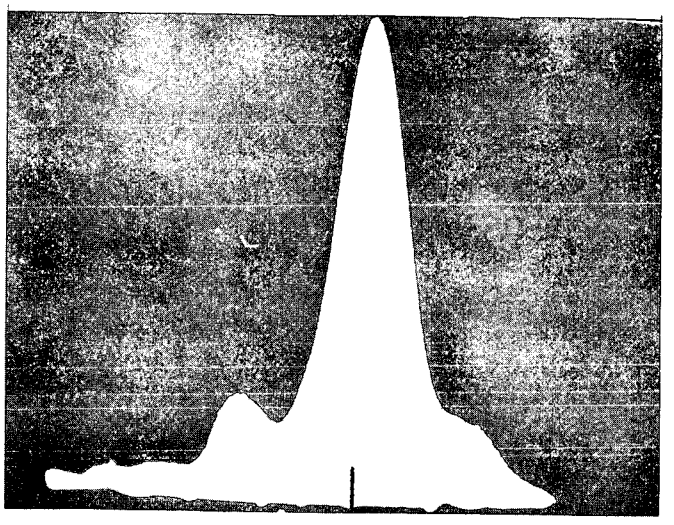

No. 20 (Full) 5.25 Actual

Figure 95

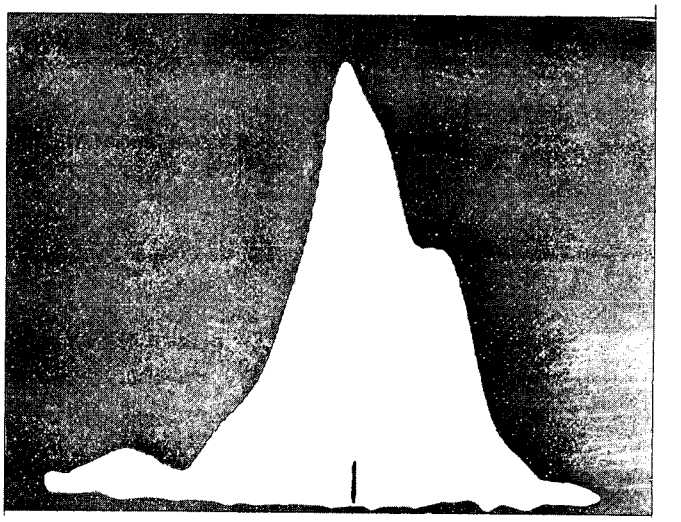

No. 28 (Non-Bond) 4.5 Actual

Figure 96

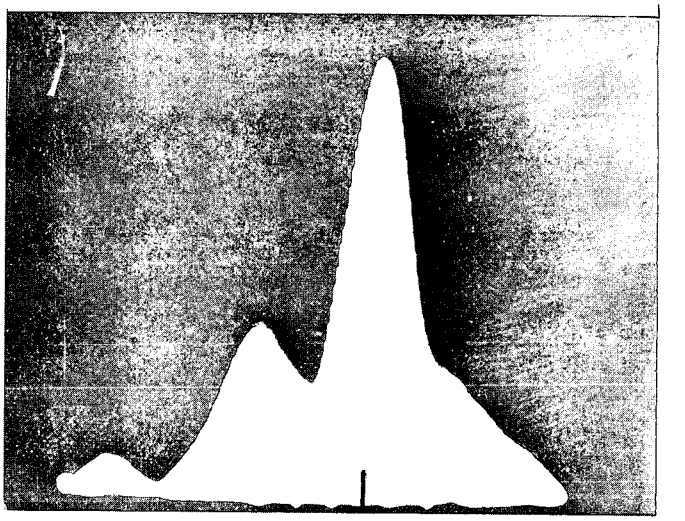

No. 37 (Full) 5.5 Actual

Figure 97

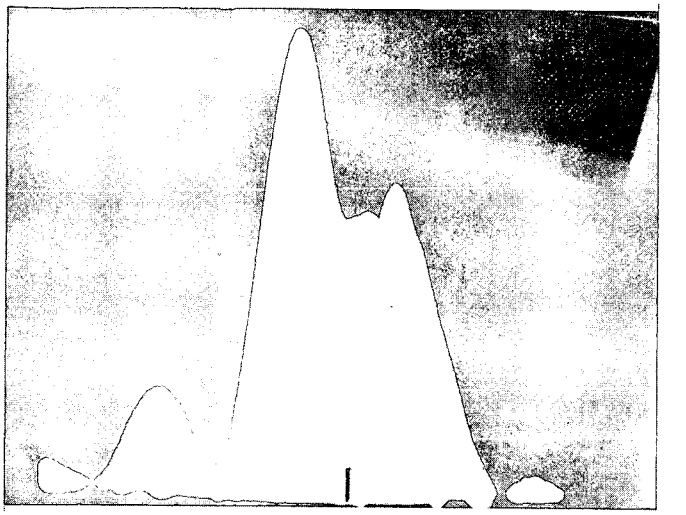

No. 49 (Non-Bond) 4 Actual

Figure 98

D. INFRARED FEASIBILITY STUDY

1. Test Methods

As stated earlier under method selection, three thin electroformed panels (0.020 in. or 5.08 x 10^{-4} m. electroform buildup) were subjected to Infrared nondestructive testing to establish if the conclusions of the literature search were correct. These tests were performed using the following equipment and techniques:

Line Scan Test

a. Liquid Nitrogen Cooled Pointing Radiometer, Model PPL 87A301.
b. Two 1000 W Bulbs with Focusing Mirror, Model HFW 87A2000.
c. Scan Table (horizontal scan - vertical index), Model TM 87A1818.
d. Recorder (X-Y).

Area Scan Test

a. Liquid Nitrogen Cooled Area Scanning Radiometer, SPM5 Camera, CR1 Recorder Control Console.

b. Heat Source

c. Scanning Table — Temp Test Area Scan System, Model TA87A280

d. Recorder.

2. Testing Techniques and Results

a. Line Scan Testing

The inspection side of the sample was painted black prior to testing. This is done to eliminate light reflection from the heat source.

The sample was then placed on the scanning stand and positioned in front of the infrared camera and the heat reflecting mirrors. The test setup is shown in Figure 99.

Several tests were performed using different scanning speeds and time delays between heating the sample and reading the surface temperature with the pointing radiometer. Slight surface temperature changes were noted only when scanning Panel 7 at 1/4 inch per second, with a monitoring delay time of 3 seconds. No temperature differences could be distinguished on the other panels submitted. Unfortunately, the temperature changes noted on Panel 7 were not of sufficient magnitude to provide any indication of the bond condition in this panel. Line scans of Panel 7 at the maximum obtainable sensitivity are shown in Figure 100. No indication of bond condition is shown on these scans.

b. Area Scan Testing

Having established what appeared to be the most sensitive test using the pointing radiometer, Panel 7 was then tested on the area scanning inspection system using these parameters. Even with changes in the scanning speed and the delay time, it was not possible to produce any recordings indicating

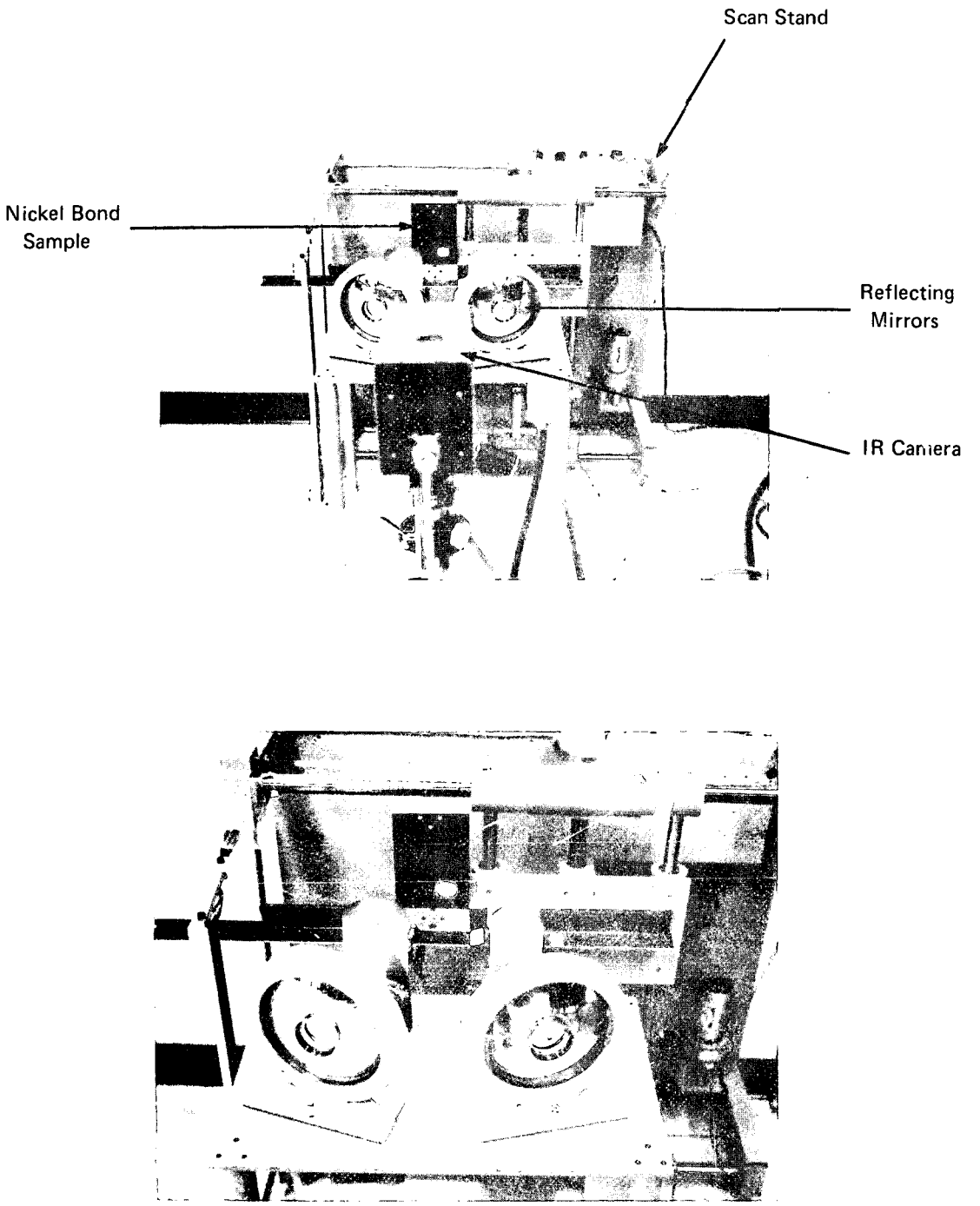

PHOTOGRAPH OF LINE SCAN INSPECTION EQUIPMENT
Figure 99

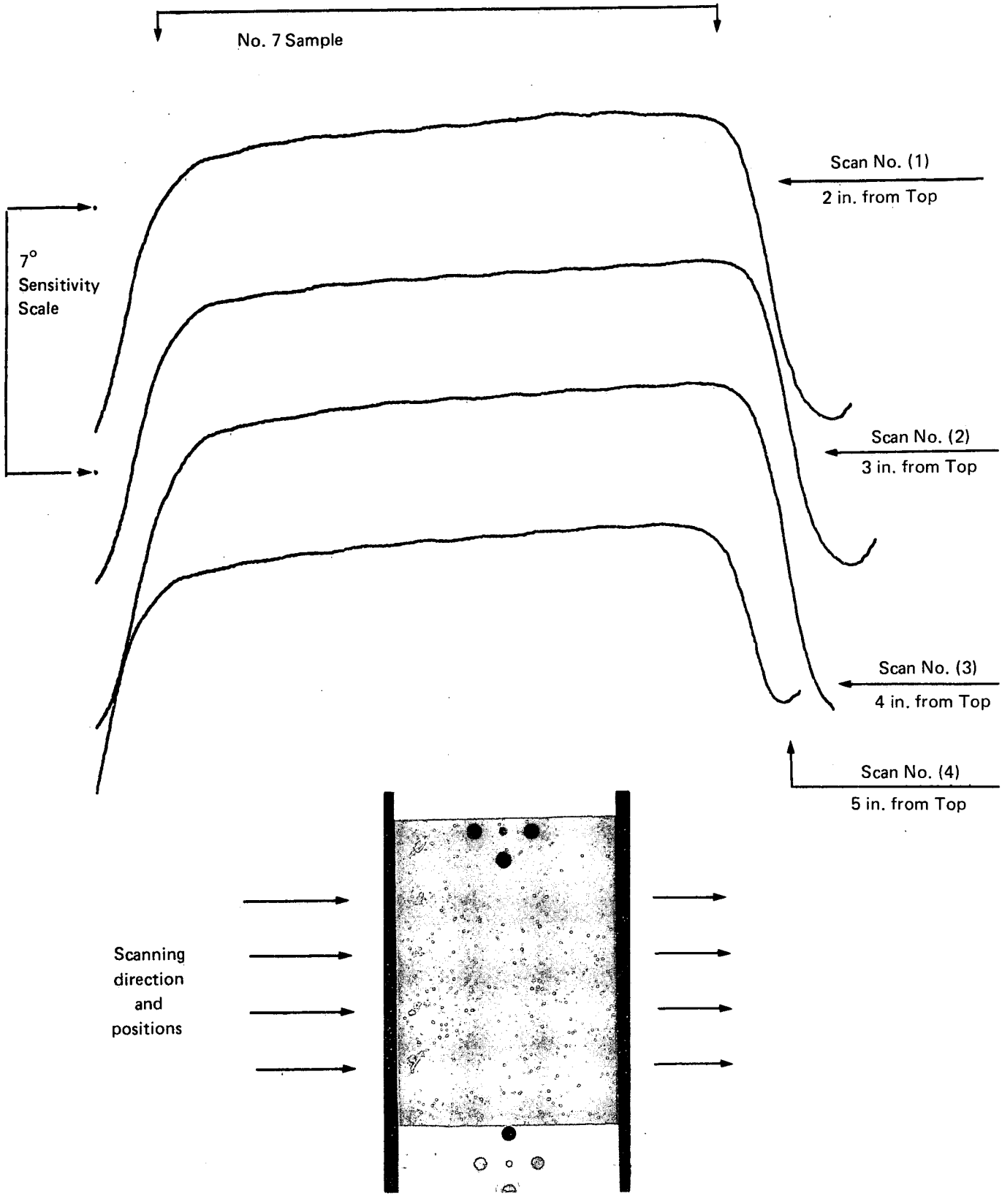

IR LINE SCAN RECORDING AND PHOTOGRAPH OF NICKEL BOND SAMPLE

Figure 100

defects. A typical example of the results obtained using the Infrared area scanning system may be seen in Figure 101.

Based on the results obtained, it must be concluded that Infrared inspection does not appear to be a feasible method of inspecting nickel bond samples of this specific process and material type for disbonds. Apparently, the heat transfer characteristics and material thickness prevent a sufficient heat buildup over an unbond to be detected with these techniques.

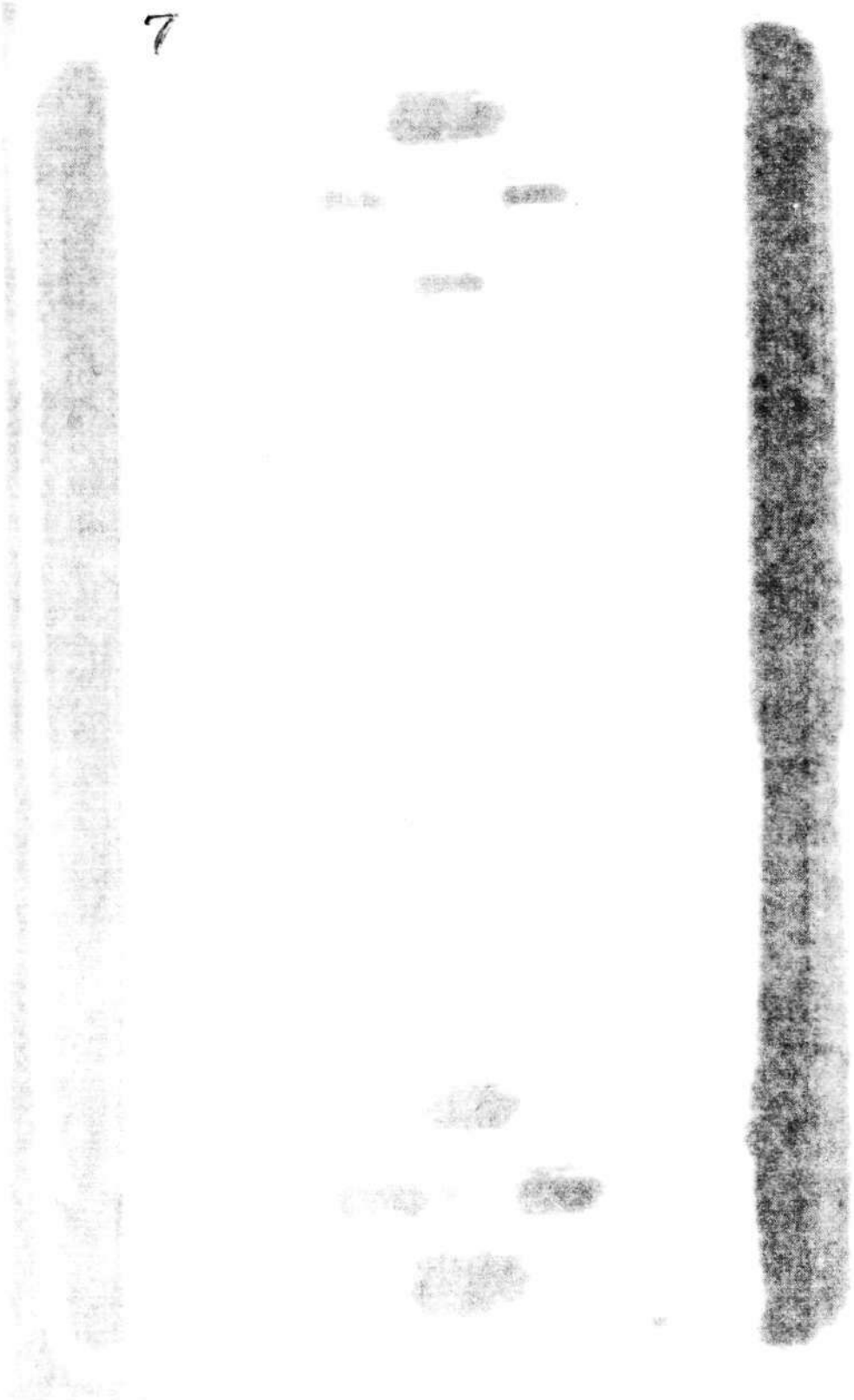

AREA SCAN RECORDING OF NICKEL BOND SAMPLE NO. 7

Figure 101

V. DESTRUCTIVE EVALUATION

A. FAILURE TESTING

After nondestructive evaluation, all test panels were subjected to destructive testing. Failure was considered to occur if: 1) the panel bulged to an extent where pressure could not be hydrostatically increased because of volume displacement due to base metal yielding, 2) visible bulging indicated bonds had fractured or were peeling, and 3) pressurization had reached the limit of the equipment (or failure of pressure seals had occurred).

Where possible the portable hydraulic handpump (Enerpak, 10,000 psig or 68.95×10^6 N/m^2 rated) was used to pressurize to destruction. Acoustic emission data was obtained on selected panels during destructive testing, but only to the maximum pressure of 10,000 psig (68.95×10^6 N/m^2). Some panels did not fail at pressures to 10,000 psig (68.95×10^6 N/m^2). These were repressurized at higher pressures in separate test facility. Pressures were recorded at which visible failure began to occur and are shown for each panel in the Appendix. The area of bulge in failure was traced for later calculation of bond strengths. This area is outlined on panel diagrams in the Appendix.

B. METALLOGRAPHIC ANALYSIS

Sections were made from each failed panel and reference panels (not subject to intentional destructive pressurization) for verification of bond integrity and comparison with results derived from nondestructive evaluation. Where possible, sections were made which illustrated the failure region (bond disturbance) and the unfailed region (each bond type which did not fail). In the Appendix, the photomicrographs are shown for each test panel, as well as the location by land number for each section. The direction of viewing is shown on the panel drawings to orient the bondline micrograph to the planned bond pattern. All photomicrographs were made at 100X magnification.

Judgment of bond type as weak, nonbond, or full bond was based on the disturbance, or lack of disturbance, of the Nickel 200 channel lands since this is the weaker of the fabrication materials. In the case of braze bond failures, disturbance of the braze alloy or Nickel 200 materials were considered in determining bond integrity. It was noted that weak and full bonding occurred in planned nonbond regions on several of the brazed and diffusion bonded panels.

Two of the electroformed panels exposed to thermal treatment for joint diffusion evaluation were sectioned and metallographically examined, Figure 102. The photomicrographs of the full bond joint of Panel No. 47 indicate segregation occurred at the bond line in the layer of electroform which bridged the channel. The bottom picture shows failure in an adjacent land bond which indicates this segregation from high temperature exposure is detrimental to bond strength.

Such segregation was not evident at the joint line on Weak Bond Panel No. 16. This was a planned weak bond which experienced diffusion after a treatment at 1800°F (1255°K). However, the bottom picture shows separation at a plating restart surface on the same panel after exposure to 1800°F (1255°K).

Some difficulty was experienced with the silver conductivizing process at the time this panel was produced. Re-conductivizing was required, and it is possible that surface contaminants were not completely removed by the cleaning process between silvering operations.

Full Bond Panel No. 47

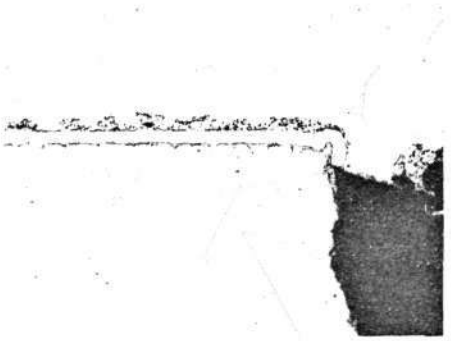

Diffusion at bond lines appear to be impeded by segregation following the thermal exposure at 1800°F (1255°K). (Magnification 100X, Reduced.)

Weak Bond Panel No. 16

Some diffusion occurred in this planned weak bond area. No segregation was evident. (Magnification 100X, Reduced).

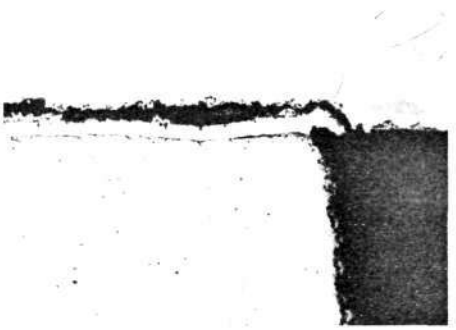

Failure of bond line in "full bond" panel after exposure to 1800°F (1255°K) and subsequent pressurization - below 1000 psig (6.89 x 10^6 N/m.^{2}). (Magnification 100X, Reduced).

Lamination occurring at electroform restart after exposure to 1800°F (1255°K). This condition existed below each blister observed after thermal treatment. (Magnification 100X, Reduced.)

Figure 102. Photogmicrographs of Electroformed-Thermally Diffused Test Panels

In the processing of both panels in Figure 102, it was necessary to surface grind for flatness during the electroform build-up. After grinding, the plates were acid etched to remove surface contaminants from the grinding process. The laminations were associated with blisters which indicates regional residues or contaminants, such as imbedded grinding material, may not have been completely removed in the acid treatment. This condition was not apparent on the other panels in the program, and bond strengths were obtained as planned.

It is evident that surface grinding may influence bond integrity of plating restarts after exposure to elevated temperature. Investigation of procedures to assure complete removal of these residues was beyond the scope of this program, but should be considered in future work where electroform diffusion is involved.

C. BOND STRENGTH CALCULATIONS

Bond strengths were determined by mapping the failure bulge of each panel at full scale and graphically integrating the effective area of pressure reaction on the channels contained in the bulge. The area of the lands within the bulge was calculated and applied to the formula:

$$\text{Bond Strength} = \frac{\text{Area of Channels x Failure Pressure}}{\text{Area of Lands}}$$

Results of these calculations are shown in Table XVII. Acoustic emission counts to failure (or to a maximum of 10,000 psig or 68.95 x 10^6 N/m.^{2} pressurization) are also shown. An examination of this data indicates the degree of success achieved in obtaining the planned bond strengths.

The electroformed weak bonds were generally stronger than planned. The high strength of the bond on Panel No. 14 was probably due to the small percent of nonbond land area and the relatively small size of flaws planned. Weak bonds produced the higher emission count during failure testing and full bonds the least count.

Brazed bond strengths were as expected. The values obtained in general reflect the percent of full bond area planned to obtain the three bond integrities. No correlation of acoustic emission data was noted. Diffusion bond strengths were as expected, except for Panel Nos. 41 and 42 which contained bond or lack of bond not planned. Acoustic emission data is not conclusive regarding bond strength during failure pressurization.

D. CORRELATION OF RESULTS

Results are correlated in the Appendix. The planned flaw patterns and fabricated patterns achieved were satisfactory with but few exceptions. These exceptions were primarily on weak and nonbond diffusion bond panels where more bonding was obtained than planned. Calculated bond strengths were relatively consistent with planned bond type with the general exception of diffusion weak and nonbonds which differed by non-bond area only. The correlation of nondestructive evaluation results and metallographic sections to verify actual bonds achieved was good.

For further information on the correlation of results, reference to Section IV, Subsection C, is suggested.

TABLE XVII
BOND STRENGTHS AND ACOUSTIC EMISSION DATA

Bonding Process	Panel No.	Bond Type	Failure Pressure		Calculated Bond Strength		Acoustic Emission		
								Pressure Range	
			psi	$N/m.^2$ (x 10^6)	psi	$N/m.^2$ (x 10^6)	Counts	psi	$N/m.^2$ (x 10^6)
Electroform	1	Full	14,000 +	96.53+	32,800 Nom.	226.16 Nom.	6,500	3500 to 9500	24.13 to 65.50
	6	Full	14,900	102.74	35,910	247.60	–	–	–
	10	Full	14,000+	96.53+	32,800 Nom.	226.16 Nom.	900	3500 to 9500	24.13 to 65.50
	11	Full	14,000+	96.53+	32,800 Nom.	226.16 Nom.	–	–	–
	5	Weak	15,000	103.42	29,520	203.54	–	–	–
	8	Weak	12,000	82.74	29,800	205.47	32,100	3500 to 9500	24.13 to 65.50
	9	Weak	8,600	59.30	19,140	131.97	–	–	–
	13	Weak	11,000	75.84	25,660	176.93	30,900	3500 to 9500	24.13 to 65.50
	4	Nonbond	8,500	58.61	15,150	104.46	10,600	3500 to 8500	24.13 to 58.61
	12	Nonbond	4,000	27.58	7,890	54.40	10,000	3500 to 4000	24.13 to 27.58
	14	Nonbond	10,200	70.33	22,950	158.24	13,900	3500 to 9500	24.13 to 65.50
	15	Nonbond	5,500	37.92	11,575	79.81	11,700	3500 to 5500	24.13 to 37.92
Braze	20	Full	9,200	63.43	23,270	160.45	219,100*	3500 to 9200	24.13 to 63.43
	21	Full	6,000	41.37	16,910	116.59	1,200	3500 to 6000	24.13 to 41.37
	31	Full	7,500	51.71	15,765	108.70	–	–	–
	35	Full	7,000	48.26	15,000	103.42	3,400	3500 to 7000	24.13 to 48.26
	45	Full	8,600	59.30	21,750	149.97	18,600	3500 to 8600	24.13 to 59.30
	18	Weak	2,300	15.86	4,820	33.23	1,800	0 to 2300	0 to 15.85
	23	Weak	2,100	14.48	5,465	37.68	1,850	0 to 2100	0 to 14.48
	24	Weak	3,500	24.13	8,310	57.30	250	0 to 3500	0 to 24.13
	28	Weak	2,500	17.24	6,030	41.58	1,800	0 to 2500	0 to 17.24
	17	Nonbond	1,900	13.10	4,155	28.65	3,600	0 to 1900	0 to 13.10
	26	Nonbond (Ref)	1,000	6.89	2,275	15.69	80	0 to 1000	0 to 6.89
	30	Nonbond	1,200	8.27	2,690	18.55	99,700	0 to 1200	0 to 8.27
	33	Nonbond	500	3.45	1,090	7.52	4,390	0 to 500	0 to 3.45
	38	Nonbond	1,000	6.89	2,296	15.83	100	0 to 1000	0 to 6.89
Diffusion	19	Full	13,200	91.01	27,825	191.85	100	3500 to 9500	24.13 to 65.50
	27	Full	12,300	84.81	29,350	202.37	500	3500 to 9500	24.13 to 65.50
	32	Full	15,400	106.18	37,100	255.80	800	3500 to 9500	24.13 to 65.50
	37	Full	14,000	96.53	32,660	225.19	400	3500 to 9500	24.13 to 65.50
	29	Weak	8,800	60.68	20,770	143.21	–	–	–
	34	Weak	7,800	53.78	22,090	152.31	–	–	–
	36	Weak	7,000	48.26	16,575	114.28	–	–	–
	43	Weak	8,000	55.16	16,000	110.32	–	–	–
	41	Nonbond	12,000	82.74	26,300	181.34	–	–	–
	42	Nonbond	400	2.76	875	6.03	4,700	0 to 400	0 to 2.76
	44	Nonbond	8,750	60.33	18,290	126.11	–	–	–
	49	Nonbond	5,500	37.92	12,830	88.46	8,000	3500 to 5000	24.13 to 37.92

*Panel 20 leaked at the pressure fitting under high pressure; this possibly contributed to the high counts recorded.

VI. CONCLUSIONS AND RECOMMENDATIONS

The overall objective of the program was to establish the feasibility of nondestructive evaluation methods to detect bond integrity in regeneratively cooled chamber walls. This was to be achieved using simulated wall sections containing bonds produced by brazing, diffusion bonding, and electroforming.

Three of the four selected nondestructive evaluation methods demonstrated feasibility. These were holography, acoustic emission, and ultrasonics. Generally, each nondestructive method was useful in providing specific information essential to complete evaluation of a bonded metallic structure.

Ultrasonics was beneficial as an initial screening approach to detect nonbonds which might prohibit use of nondestructive methods requiring pressurization. It is recommended that ultrasonics be utilized as an initial screening technique for the detection of bond from nonbond in all fabrication processes where practical. Ultrasonics was unable to detect strength differences in electroformed bonds.

Acoustic emission and holography require stressing of the test piece to produce a detectable change in the bondline. It is essential that this stress (pressure) be maintained below proof pressure for the hardware design to assure that the test remains nondestructive.

Based on results from the flat test panels, both holography and acoustic emission demonstrated a potential for detecting the weak bond condition as distinct from full or nonbond. As anticipated, holography was capable of locating the defective regions, whereas acoustic emission indicated overall condition only. Acoustic emission was unable to differentiate between emission counts from weak bonds and propagating nonbonds as explained below:

> The planned weak bond and nonbond panels contained multiple defect areas of various sizes. This complexity prevented the establishment of a fundamental data base for interpreting the full significance of emission counts for individual panel conditions.

It is suggested that an approach using a simplified panel design and defect pattern should provide the data necessary to better define the relative capabilities of holography and acoustic emission.

It is also recognized that emission source locators can be added to further define test panel flaw conditions. Displaying the test data in this manner will result in obtaining a more definitive inter-relationship of acoustic emission with the holographic and ultrasonic data.

A factor which may have influenced the holographic results was test sequence. Acoustic emission was always conducted prior to holography to minimize anticipated data loss (Kaiser-effect). The higher pressures (3500 psi) used in the acoustic emission test may have been sufficient to cause plastic deformation in some of the panels containing large non-bond areas. This permanent deformation could have enhanced the sensitivity of the holographic non-destructive test. This pre-stress may have established a new base-line condition for the holographic test. This should be considered, along with the other recommendations, in establishing the optimum test sequence for continued study.

The fourth test method investigated, spectrum analysis, did not provide the anticipated bondline characterization. Of the three bonding processes evaluated, only brazing showed any positive application.

It is significant that this bonding method was the only one to provide a dissimilar bondline material of finite thickness (relative to inspection techniques). Three ultrasonic approaches were evaluated. Other techniques are available which may provide positive results. Any future work would require an extensive development program on equipment and technique prior to application to thrust chambers.

Infrared, a method initially considered as a primary candidate, was briefly evaluated. Materials in the configuration under evaluation did not respond to this test.

Of the three bonding techniques, electroforming provided the more useful bonds for evaluation in this program. This was due to the fact that weak bonds of varying strength and size could be more easily achieved.

VII. REFERENCES

1. Guidance to Nondestructive Testing Techniques, U.S. Army Material Command, April 1970.

2. Martin, George, "Exploratory Development of Nondestructive Testing Techniques," North American Rockwell, September 1968.

3. Martin, George, Moore, John F., and Coate, F.M., "Exploratory Development of Nondestructive Testing Techniques for Diffusion Bonded Surfaces," North American Rockwell, AFML-TR-70-188, September 1970.

4. Oaks, A.E., "New and Refined Nondestructive Techniques for Graphite Billets and Shapes," General Electric Company, AFML-TR-70-212, February 1970.

5. Kraska, I.R. and Kamm, H.W., "Evaluation of Sonic Methods for Inspecting Adhesive Bonded Honeycomb Structures," General American Transportation Corporation, AFML-TR-69-283, August 1970.

6. Sessler, T.G., "The Effect of Stress Fields on Ultrasonics Energy Reflected from Discontinuities in Solids," Syracuse University Research Corporation, Syracuse, New York, June 1971.

7. Whaley, H.L. and Adler, Laszlo, "Flaw Characterization by Ultrasonic Frequency Analysis," Oakridge National Lab Metals and Ceramics Division, Materials Evaluation, August 1971.

8. Frederick, J.R., "Dislocation Mechanisms as Sources of Acoustic Emission," University of Michigan, Ann Arbor, Michigan, Army Materials and Mechanics Research Center, Watertown, Mass., June 1971.

9. Hagemaier, D.J., McFaul, H.J., and Moon, D., "Nondestructive Testing of Graphite Fiber Composite Structures," Douglas Aircraft Co., McDonnel Douglas Corporation Materials Evaluation, June 1971.

10. Dunegan, H.L., Harris, D.O., and Tetleman, A.S., "Detection of Fatigue Crack Growth by Acoustic Emission Technique," Lawrence Radiation Laboratory University of California, Livermore, California, Material Evaluation, October 1970.

11. Chambers, R.H., "Time and Frequency Domain Analysis of Acoustic Emission During Fatigue Failure," University of Arizona, Tucson, Arizona, Army Materials and Mechanics Research Center, Watertown, Massachusetts, June 1971.

12. Hartbower, C.E., "Development of a Nondestructive Testing Technique to Determine Flaw Criticality Based on Stress Wave Emission," Aerojet, Sacramento, California, Army Materials and Mechanics Research Center, Watertown, Massachusetts, June 1971.

13. Romrell, D.M. and Bunnell, L.R., "Monitoring of Crack Growth in Ceramic by Acoustic Emission," Materials Evaluation, December 1970.

14. Acoustic Emission Research/Dev., Volume 22, Number 5, Pages 20 - 24, May 1971.

15. Vest, C.M. and Sweeney, D.W., "Applications of Holographic Interferometry to Nondestructive Testing," Radar and Optics Laboratory and Department of Mechanical Engineering; The University of Michigan, Army Materials and Mechanics Research Center, June 1971.

16. Kersch, L.A., "Advanced Concepts of Holographic Nondestructive Testing," GCO Incorporated, Ann Arbor, Michigan Materials Evaluation, June 1971.

17. Harris, W.J. and Clauss, Francis J., "Inspecting Bonded Structures by Laser Holography," Metal Progress, August 1971.

18. Waters, J.P., "The Uses of Holography for NDT," United Aircraft Research Lab, East Hartford, Connecticut, June 1971.

19. Sneeringer, J.W., Hacke, K.P., and Roehrs, R.J., "Practical Problems Related to the Thermal Infrared Nondestructive Testing of a Bonded Structure," McDonnell Aircraft Company, St. Louis, Missouri, Materials Evaluation, April 1971/Volume XXIV, No. 4.

20. Inteieri, A.J., "An IR NDT Bond Inspection System for Rotor Blade Honeycomb Box Assemblies," The Boeing Company, Vertol Div., Philadelphia, Penn., Materials Evaluation, June 1970/Vol. XXVIII, No. 7.

21. Martin, George and Moore, J.F., "Research and Development of Nondestructive Testing Techniques for Composites," North American Aviation Inc., AFML-TR-68-202, June 1968.

22. Lavoie, F.J., "Acoustic Holography, A New Dimension in Seeing with Sound," Machine Design, September 1971.

23. Schneiderman, R., Nuclear Research Corporation, Brochure; Future and Termed Exciting for Nuclear NDT and Measuring Control Device, Metal Working News, October 1967.

24. Special Report/A Guide to Nondestructive Testing, Materials Engineering, June 1969.

25. Materials Evaluation
April 1970 - Vol. XXVIII, No. 4
May 1970 - Vol. XXVIII, No. 5
June 1970 - Vol. XXVIII, No. 6
July 1971 - Vol. XXIX, No. 7

26. Karplus, H.B., Semmler, R.A., and Arneson, B.E., "Evaluation of Nondestructive Testing Techniques of Diffusion Coatings," AFML-TR-67-358, May 1968.

27. Way, F.C., "Determination of the Performance of Holographic Nondestructive Testing Systems," Pratt & Whitney Aircraft, Florida Research and Development Center, West Palm Beach, Florida Materials Evaluation, July 1971.

DISTRIBUTION LIST FOR FINAL REPORT

NAS3-14376 Bell CR 120980

REPORT COPIES R	D	RECIPIENT	DESIGNEE
		National Aeronautics & Space Administration Lewis Research Center 21000 Brookpark Road Cleveland, Ohio 44135	
1		Attn: Contracting Officer, MS 500-313	
5		E.A. Bourke, MS 500-203	
1		Technical Report Control Office, MS 5-5	
1		Technology Utilization Office, MS 3-16	
2		AFSC Liaison Office, 501-3	
2		Library	
1		Office of Reliability & Quality Assurance, MS 500-111	
1		J.W. Gregory Chief, MS 500-203	
13		R.A. Duscha Project Manager, MS 500-209	
1		Alex Vary, MS 106-1	
1		R.F. Lark, MS 49-1	
1		W.E. Russell, MS 14-1	
1		Director, Shuttle Technology Office, RS Office of Aeronautics & Space Technology NASA Headquarters Washington, D.C. 20546	
2		Director Space Propulsion and Power, RP Office of Aeronautics & Space Technology NASA Headquarters Washington, D. C. 20546	
1		Director, Launch Vehicles & Propulsion, SV Office of Space Science & NASA Headquarters Washington, D. C. 20546	
1		Director, Materials & Structures Division, RW Office of Aeronautics & Space Technology NASA Headquarters Washington, D. C. 20546	
1		Director, Advanced Manned Missions, MT Office of Manned Space Flight NASA Headquarters Washington, D. C. 20546	

REPORT COPIES R	D	RECEIPIENT	DESIGNEE
20		National Technical Information Service Springfield, Virginia 22151	
1		National Aeronautics & Space Administration Ames Research Center Moffett Field, California 94035 Attn. Library	Hans M. Mark Mission Analysis Division
1		National Aeronautics & Space Administration Flight Research Center P.O. Box 273 Edwards, California 93523 Attn: Library	
1		Director, Technology Utilization Division Office of Technology Utilization NASA Headquarters Washington, D. C. 20546	
1		Office of the Director of Defense Research & Engineering Washington, D. C. 20301 Attn: Office of Asst. Dir. (Chem Technology)	
2		NASA Scientific and Technical Information Facility P.O. Box 33 College Park, Maryland 20740 Attn: NASA Representative	
1		National Aeronautics & Space Administration Goddard Space Flight Center Greenbelt, Maryland 20771 Attn: Library	Merland L. Moseson, Code 620
1		National Aeronautics & Space Administration John F. Kennedy Space Center Cocoa Beach, Florida 32931 Attn: Library	Dr. Kurt H. Debus
1		National Aeronautics & Space Administration Langley Research Center Langley Station Hampton, Virginia 23365 Attn: Library	E. Cortwright Director Lewis Thurston, Jr.
	1		

REPORT COPIES R	D	RECIPIENT	DESIGNEE
1		National Aeronautics & Space Administration Manned Spacecraft Center Houston, Texas 77001 Attn: Library	J.G. Thiobodaux, Jr. Chief, Propulsion & Power Division
1		National Aeronautics & Space Administration George C. Marshall Space Flight Center Huntsville, Alabama 35912 Attn: Library	Hans G. Paul James Thomas
1		Jet Propulsion Laboratory 4800 Oak Grove Drive Pasadena, California 91103 Attn: Library	Henry Burlage, Jr. Duane Dipprey
1		Defense Documentation Center Cameron Station Building 5 5010 Duke Street Alexandria, Virginia 22314 Attn: TISIA	
1		RTD (RTNP) Bolling Air Force Base Washington, D. C. 20332	
1		Arnold Engineering Development Center Air Force Systems Command Tullahoma, Tennessee 37389 Attn: Library	Dr. H.K. Doetsch
1		Advanced Research Projects Agency Washington, D.C. 20525 Attn: Library	
1	1	Aeronautical Systems Division Air Force Systems Command Wright-Patterson Air Force Base, Dayton, Ohio Attn: Library	D.L. Schmidt Code ARSCNC-2
1		Air Force Missile Test Center Patrick Air Force Base, Florida Attn: Library	L.J. Ullian

REPORT COPIES R	D	RECIPIENT	DESIGNEE
1		Air Force Systems Command Andrews Air Force Base Washington, D. C. 20332 Attn: Library	Capt. S.W. Bowen SCLT
1	1	Air Force Rocket Propulsion Laboratory (RPR)	Donald Penn
	1	Edwards, California 93523 Attn: Library	Robert Wiswell
1		Air Force Rocket Propulsion Laboratory (RPM) Edwards, California 93523 Attn: Library	
1		Air Force FTC (FTAT-2) Edwards Air Force Base, California 93523 Attn: Library	Donald Ross
1		Air Force Office of Scientific Research Washington, D. C. 20333 Attn: Library	SREP, Dr. J.F. Masi
1		Space & Missile Systems Organization Air Force Unit Post Office Los Angeles, California 90045 Attn: Technical Data Center	
1		Office of Research Analyses (QAR) Holloman Air Force Base, New Mexico 88330 Attn: Library RRRD	
1		U. S. Air Force Washington, D. C. Attn: Library	Col. C.K. Stambaugh, Code AFRST
1		Commanding Officer U. S. Army Research Office (Durham) Box CM, Duke Station Durham, North Carolina 27706 Attn: Library	
1		U. S. Army Missile Command Redstone Scientific Information Center Redstone Arsenal, Alabama 35808 Attn: Document Section	Dr. W. Wharton

REPORT COPIES R	D	RECIPIENT	DESIGNEE
1		Bureau of Naval Weapons Department of the Navy Washington, D. C. Attn: Library	J. Kay, Code RTMS-41
1		Commander U. S. Naval Missile Center Point Mugu, California 93041 Attn: Technical Library	
1		Commander U. S. Naval Weapons Center China Lake, California 93557 Attn: Library	
1		Commanding Officer Naval Research Branch Office 1030 E. Green Street Pasadena, California 91101 Attn: Library	
1		Director (Code 6180) U. S. Naval Research Laboratory Washington, D. C. 20390 Attn: Library	H.W. Carhart J.M. Krafft
1		Picatinny Arsenal Dover, New Jersey 07801 Attn: Library	I. Forsten
1		Air Force Aero Propulsion Laboratory Research & Technology Division Air Force Systems Command United States Air Force Wright-Patterson AFB, Ohio 45433 Attn: APRP (Library)	R. Quigley
1		Electronics Division Aerojet-General Corporation P.O. Box 296 Azusa, California 91703 Attn: Library	

REPORT COPIES R	D	RECIPIENT	DESIGNEE
1		Space Division Aerojet-General Corporation 9200 East Flair Drive El Monte, California 91734 Attn: Library	
1		Aerojet Ordance and Manufacturing Aerojet-General Corporation 11711 South Woodruff Avenue Fullerton, California 90241 Attn: Library	
1	1	Aerojet Liquid Rocket Company P.O. Box 15847 Sacramento, California 95813 Attn: Technical Library 2482-2015A	R.J. LaBotz
1		Aeronutronic Division of Philco Ford Corp. Ford Road Newport Beach, California 92663 Attn: Technical Information Department	Dr. L.H. Linder
1		Aerospace Corporation 2400 E. El Segundo Blvd. Los Angeles, California 90045 Attn: Library-Documents	J.G. Wilder
1		Arthur D. Little, Inc. 20 Acorn Park Cambridge, Massachusetts 02140 Attn: Library	A.C. Tobey
1		Astropower Laboratory McDonnell-Douglas Aircraft Company 2121 Paularino Newport Beach, California 92163 Attn: Library	
1		DCIC, Battelle Memorial Institute Columbus Lab. Room 11-9012 505 King Avenue Columbus, Ohio 43201 Attn: Library	J.F. Lynch

REPORT COPIES R	D	RECIPIENT	DESIGNEE
1		ARO, Incorporated Arnold Engineering Development Center Arnold AF Station, Tennessee 37389 Attn: Library	
1		Susquehanna Corporation Atlantic Research Division Shirley Highway & Edsall Road Alexandria, Virginia 22314 Attn: Library	
1		Beech Aircraft Corporation Boulder Facility Box 631 Boulder, Colorado Attn: Library	Douglas Pope
1		Bell Aerospace Co. Box 1 Buffalo, New York 14240 Attn: Library	
1		Instruments & Life Support Division Bendix Corporation P.O. Box 4508 Davenport, Iowa 52808 Attn: Library	John M. Brueger
1		Bellcomm 955 L'Enfant Plaza, S. W. Washington, D. C. Attn: Library	H.S. London
1		Boeing Company Space Division P.O. Box 868 Seattle, Washington 98124 Attn: Library	J.D. Alexander C.F. Tiffany
1		Boeing Company 1625 K Street, N. W. Washington, D. C. 20006	
1		Boeing Company P.O. Box 1680 Huntsville, Alabama 35801	Ted Snow

REPORT COPIES R	D	RECIPIENT	DESIGNEE
1		Chemical Propulsion Information Agency Applied Physics Laboratory 8621 Georgia Avenue Silver Spring, Maryland 20910	Tom Reedy
1		Chrysler Corporation Missile Division P.O. Box 2628 Detroit, Michigan Attn: Library	John Gates
1		Chrysler Corporation Space Division P.O. Box 29200 New Orleans, Louisiana 70129 Attn: Librarian	
1		Grumman Aircraft Engineering Corporation Bethpage, Long Island, New York Attn: Library	Joseph Gavin
1		Hercules Powder Company Allegheny Ballistics Laboratory P.O. Box 210 Cumberland, Maryland 21501 Attn: Library	
1		Honeywell Inc. Aerospace Division 2600 Ridgeway Road Minneapolis, Minnesota Attn: Library	
1		IIT Research Institute Technology Center Chicago, Illinois 60616 Attn: Library	C.K. Hersh
1		Kidde Aer-Space Division Walter Kidde & Company, Inc. 567 Main Street Bellville, New Jersey	R.J. Hanville
1		Ling-Temco-Vought Corporation P.O. Box 5907 Dallas, Texas 75222 Attn: Library	

REPORT COPIES R	D	RECIPIENT	DESIGNEE
1		Lockheed Missiles and Space Company P.O. Box 504 Sunnyvale, California 94087 Attn: Library	
1		Lockheed Propulsion Company P.O. Box 111 Redlands, California 92374 Attn: Library, Thackwell	H.L. Thackwell
1		Marquardt Corporation 16555 Saticoy Street Box 2013 - South Annex Van Nuys, California 91409	L.R. Bell, Jr.
1		Martin-Marietta Corporation (Baltimore Division) Baltimore, Maryland 21203 Attn: Library	
1		Denver Division Martin-Marietta Corporation P.O. Box 179 Denver, Colorado 80201 Attn: Library	Dr. Morganthaler F.R. Schwartzberg
1		Orlando Division Martin-Marietta Corporation Box 5827 Orlando, Florida Attn: Library	J. Fern
1		Western Division McDonnell Douglas Astronautics 5301 Bolsa Avenue Huntington Beach, California 92647 Attn: Library	R.W. Hallet G.W. Burge P. Klevatt
1		McDonnell Douglas Aircraft Corporation P.O. Box 516 Lambert Field, Missouri 63166 Attn: Library	R.A. Herzmark

REPORT COPIES R	D	RECIPIENT	DESIGNEE
1	1	Rocketdyne Division North American Rockwell Inc. 6633 Canoga Avenue Canoga Park, California 91304 Attn: Library, Department 596-306	Donald Fulton
1		Space & Information Systems Division North American Rockwell 12214 Lakewood Blvd. Downey, California Attn: Library	
1		Northrop Space Laboratories 3401 West Broadway Hawthorne, California Attn: Library	Dr. William Howard
1		Purdue University Lafayette, Indiana 47907 Attn: Library (Technical)	Dr. Bruce Reese
1		Radio Corporation of America Astro-Electronics Products Princeton, New Jersey Attn: Library	
1		Rocket Research Corporation Willow Road At 116th Street Redmond, Washington 98052 Attn: Library	F. McCullough, Jr.
1		Stanford Research Institute 333 Ravenswood Avenue Menlo Park, California 94025 Attn: Library	Dr. Gerald Marksman
1		Thiokol Chemical Corporation Redstone Division Huntsville, Alabama Attn: Library	John Goodloe
1	1	TRW Systems Inc. 1 Space Park Redondo Beach, California 90278 Attn: Tech. Lib. Doc. Acquisitions	Curtis Watts

REPORT COPIES R	D	RECIPIENT	DESIGNEE
1	1	TRW TAPCO Division 23555 Euclid Avenue Cleveland, Ohio 441117	Frank Stattler
1		United Aircraft Corporation Corporation Library 400 Main Street East Hartford, Connecticut 06108 Attn: Library	Dr. David Rix Erle Martin Frank Owen Wm. E. Taylor
1		United Aircraft Corporation Pratt & Whitney Division Florida Research & Development Center P.O. Box 2691 West Palm Beach, Florida 33402 Attn: Library	Dr. Schmitke
1		United Aircraft Corporation United Technology Center P.O. Box 358 Sunnyvale California 94038 Attn: Library	Dr. David Altman
1		Vickers Incorporated Box 302 Troy, Michigan	
1		Vought Astronautics Box 5907 Dallas, Texas Attn: Library	